The Sydney Journal of Interdisciplinary Engineering
SJIE 1(2) X-X (2025) https://doi.org/XXXX-XXXX

How Beverages Cool: Studying Heat Transfer through Concentration, Convection, and Container Material

Ilsa Khan , Jinze Li, Umar Anwar, Zhiwei Xu, Yiqiao Wang

Received 02 May 2025

Graphical Abstract

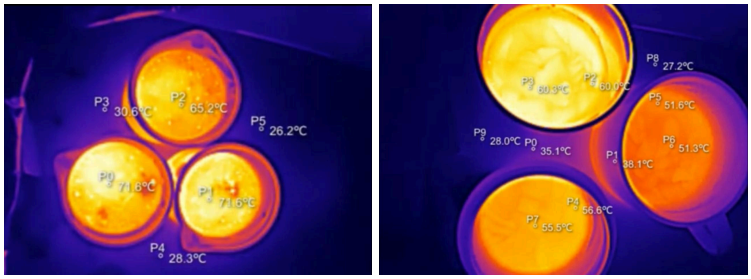

Abstract

This study investigated how concentration, stirring, container material, sugar content, particle loading and volume affect the cooling of common everyday stables Coffee, tea and oat mix suspensions were used to model fluids. Temperature changes were recorded using an InfiRay thermal camera over 180–420 seconds. Coffee trials showed that increased solute concentration reduced the cooling rate due to higher viscosity, damping natural convection. Stirring accelerated cooling, promoting forced convection and increasing the convective heat transfer coefficient. Tea experiments demonstrated that sugar addition and container material significantly altered cooling behaviour, with insulated metal cups retaining heat most effectively. The milo-oat trials showed that with increasing particle concentration, mixing within the fluid improves, leading to faster cooling. Smaller water volumes also cooled more quickly because they had lower thermal inertia, as well as, a greater surface-area-to-volume ratio. These findings were consistent with Fourier's Law of Conduction and Newton's Law of Cooling, demonstrating how these theories apply in practical situations. Furthermore, highlighting practical insights into the design of beverage containers, ready-to-drink formulations and broader applications in thermal management and food engineering. The use of experimental data along with thermal pictures and theory models is a great method for understanding how to control moving heat around hands-on situations efficiently.

Keywords: heat transfer, conduction, convection, beverage cooling, solute concentration, stirring, thermal imaging.

1. Introduction

From energy systems to food processing and consumer product design, efficient thermal management is a fundamental concern in various engineering disciplines. The rate at which heat is transferred from a hot substance to its surrounding environment determines the performance, safety and user experience of many such applications. The core of thermal energy engineering lies in the principles of conduction, convection and radiation, all of which are governed by physical laws such as Fourier's Law of heat conduction and Newton's Law of cooling. Although these two laws have been well established in the theoretical context, their application in real life and complex chemical systems is still an ongoing study.

Especially in the field of food and beverage systems, this provides a powerful analytical platform for studying convective and conductive heat transfer under nonideal conditions. Unlike pure liquids, beverages typically contain dissolved solids, such as sugar, or suspended particles, such as oats and grains, which can significantly alter the internal fluid dynamics and thermal behaviour. These constituent factors can affect viscosity, density gradient, boundary layer development and natural or forced convection. All of these factors can accelerate or slow down the efficiency of heat dissipation. In addition, the material properties of the containers for holding fluids, including their thermal conductivity, heat capacity and insulation, play a role in determining the rate of temperature loss. These elements reflect the engineering challenges faced in the design of industrial heat exchangers, slurry reactors and thermal packaging solutions.

Although the cooling of beverages is a simple and easily understandable phenomenon, it involves complex thermodynamic interactions. Previous studies have explored convection patterns and cooling rates under controlled laboratory conditions, but few have combined thermal imaging techniques with experiments involving the comparability and variable control of solute, particle and container effects. Furthermore, daily behaviours like stirring are a method to induce the formation of convection, which can be linked to macroscopic changes in heat transfer.

This research aims to systematically explore the influence of various physical and component variables on the cooling behaviour of common hot beverages, thereby filling the research gap in the field. We used the InfiRay thermal image for real time temperature tracking and analysed the temperature change curves of coffee, tea and oat liquid under different conditions. In other words, we investigated the effects of factors such as solute concentration, amount of sugar added, liquid volume, stirring or unstirring and material of containers on heat loss over time. Among them, stirring is used to simulate forced convection and changes in concentration and particle load help us understand how fluid composition regulates natural convection. The container materials are glass, ceramics and insulating metals respectively, their thermal conductivity and heat preservation performance are all within the scope of research.

By combining experimental data with theoretical heat transfer models, this research builds a bridge between principle and reality. The research results not only verified the key thermodynamics laws, but also proposed some feasible strategies that can be used in the design of beverage formulas, the improvement of packaging and optimisation of thermal equipment to enhance or delay the cooling process. Furthermore, the research also indicated that thermophysical experimental models based on the food system have potential value in industrial applications. This research provides a useful reference for extensive discussions on material selection, fluid behaviour and process optimisation in thermal engineering.

2. Materials and Methods

2.1 Experiment Setup

All experiments were conducted at an ambient laboratory temperature of 22 °C. An InfiRay thermal camera recorded fluid temperatures at 30–60 second intervals; each reported value represents the average of five independent measurements. For every trial, readings were taken at the geometric centre of the fluid. In some of the other experiments, additional measurements were made at the inside edge of the vessel wall.

2.2 Coffee Cooling Trail

2.2.1 Effect of Solute Concentration

75 mL of water was added to each of three beakers and heated to approximately 70 °C. Three different types of coffee were then added to the respective beakers. A thermal camera was used to observe the temperature changes. The initial temperature of the coffee in each beaker and the temperature surrounding the beaker were recorded. The coffee and surrounding temperatures were recorded at 60-second intervals (0 to 480 seconds). Subsequently, three new 100 mL beakers were prepared, each containing 4 g of the respective coffee types and 75 mL of water, which were again heated to approximately 70 °C. Initial temperatures were recorded, followed by temperature measurements at 60-second intervals for a total of 480 seconds. The same procedure was applied to samples containing 2 g of solute in 75 mL water to evaluate the effect of reduced concentration on cooling behaviour.

2.2.1 Effect of Stirring (Forced Convection)

75 mL of water was added to each of three beakers and heated to approximately 70 °C. Then, 4 g of three different types of coffee were added to the respective beakers. Over a period of 480 seconds, the temperature of the coffee and the surrounding environment was measured at 60-second intervals using a thermal camera. During this time, the coffee was stirred at a constant rate to simulate forced convection, in order to investigate whether enhanced convection accelerates the cooling rate. The results were compared to those from a previous step in which 4 g of coffee was added without stirring, to evaluate the effect of enhanced convection under identical solute concentration.

2.3 Container Material Comparison

2.3.1 Coffee Trail - Cup Material Comparison

100 mL of water and 2 g of the same type of coffee were added to a glass cup, a metal insulated cup, and a ceramic cup. A thermal camera was used to record the temperature over 480 seconds to evaluate the effect of different container materials on the cooling rate.

2.3.2 Tea Trail - Cup Material Comparison

To assess container-material effects without added sugar, two teabags of Twinings Camomile & Spiced Apple (4 g total) were steeped in 200 mL boiling water for 4 minutes. The infusion was then poured into a ceramic mug, a stainless-steel insulated mug and a glass beaker. Following a single stir, centre temperatures were logged every 30 seconds for 240 seconds.

2.4 Solute Addition Effects

For this trial, 5 g of sucrose was dissolved in 200 mL boiling water, then two teabags were steeped for 4 minutes. After removing the bags and stirring once, centre temperatures were recorded every 30 seconds over 240 seconds.

2.5 Particle-Induced Convection and Volume Effects

2.5.1 Effect of Oat Concentration

To determine the effect of particulate loading on cooling, milo-oat suspensions were prepared by dispersing 0.5, 1 and 2 packets of oats (17.5 g, 35 g and 70 g, respectively) into 200 mL of deionised water. After a single gentle stir to homogenise, samples were allowed to cool uncovered. Centre temperatures were logged every 30 seconds from 0 to 180 seconds.

2.5.2 Effect of Fluid Volume

The influence of fluid volume was examined by suspending one packet of oats (35 g) in 100 mL, 150 mL and 200 mL of water. For the 200 mL trial, both centre and near-wall temperatures were recorded; for the 100 mL and 150 mL trials, only centre readings were taken. All measurements were logged every 30 seconds for 180 seconds.

3. Results

3.1 Coffee Cooling Trail

3.2.1 Effect of Solute Concentration

A comparison of the cooling rates of unstirred coffee samples with identical concentrations revealed differences among the three coffee flavours (caramel latte, cappuccino and latte). According to the data in Tables 1 and 2, the caramel latte flavour exhibited a faster cooling rate than the other two types at both concentration levels. When comparing the temperature drops of the same coffee type over 480 seconds at 2 g and 4 g concentrations, the 2 g caramel latte sample cooled by 16 °C, whereas the 4 g sample cooled by only 11.7 °C over the same time. This trend was consistent across all three coffee flavours.

Table 1 – Temperature change of 2 g of three different coffee flavours in 75 mL of water for 480 seconds without stirring.

Time (sec)	Caramel Latte (℃)	Cappuccino (℃)	Latte (℃)	Surrounding temperature (℃)		
				Caramel Latte/ CL(℃)	Cappuccino/C (℃)	Latte/L (℃)
0	73.1	69.6	71.5	29.3	26.3	28.8
60	70.5	66	69.2	30.7	26.5	28.5
120	68.7	64.5	67.8	31.3	25.9	28
180	66.8	62.2	65.9	32.3	26.7	28.7
240	64.6	61.9	63.8	32.2	26.5	28.8
300	62.9	59.1	63	32.3	26.3	28.7

360	60.7	57.5	61.9	32.7	26.5	28.8
420	58.7	56.4	59.8	32.9	26.8	29.1
480	57.1	56	58.3	32.5	26.4	28.6

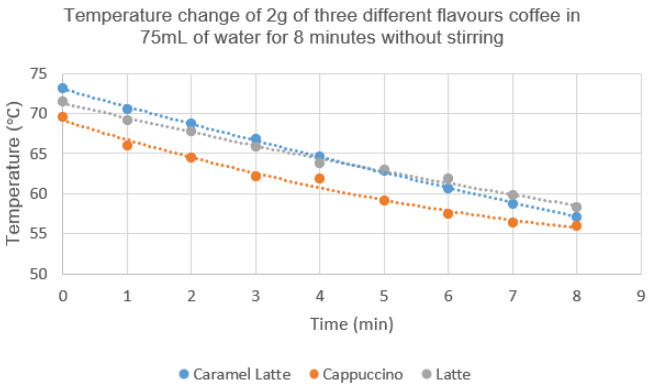

Figure 1 - Cooling Trend of 3 different flavours of coffee (2g) without stirring.

Table 2 - Temperature change of 4 g of three different coffee flavours in 75 mL of water for 480 seconds without stirring.

Time (sec)	Caramel Latte (℃)	Cappuccino (℃)	Latte (℃)	Surrounding temperature (℃)		
				CL(℃)	C(℃)	L(℃)
0	75.9	73.2	76.6	31	30	31.4
60	74.5	71.5	75.5	31.4	30.3	32
120	73.1	70.3	74.1	32.6	30.3	32.1
180	72	68.5	72	33.2	31.8	32.5
240	70.5	67.2	70.8	32.7	32.2	32.2
300	68.9	66.5	69.7	31.5	31.6	31.7
360	67.5	64.2	68.3	31	30.4	32.3
420	65.2	62.8	67	30.8	29.7	32.1
480	64.2	62	65.3	31.2	30.1	31.6

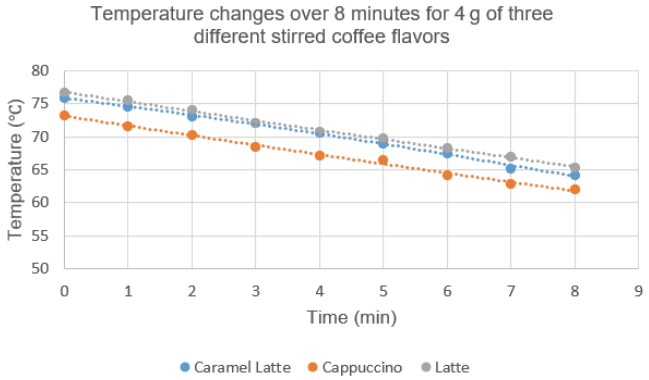

Figure 2 - Cooling trend of 3 different flavours of coffee (4g) without stirring.

2.2.1 Effect of Stirring (Forced Convection)

When the coffee samples had the same concentration (4 g of solute), under stirred conditions, the fluid cooled faster than unstirred conditions. All three coffee flavours showed a bigger temperature drop under stirring conditions.

Table 3 - Temperature changes over 480 seconds for 4 g of three different stirred coffee flavours in 75 mL of water.

Time (sec)	Caramel Latte (℃)	Cappuccino (℃)	Latte (℃)	Surrounding temperature (℃)		
				CL(℃)	C(℃)	L(℃)
0	77.2	68.9	76.4	32.8	33.2	32.7
60	76.7	66.5	75.5	33.2	33.5	33
120	72.7	64.2	73.3	34.9	33.6	33.2
180	70.9	62.5	71.1	35.3	33	33.4
240	67.1	61.7	68	36.7	33.8	34.3

300	66.3	60.2	66.2	36.7	33	33.4
360	64.5	58.7	64.9	36.9	34	34.2
420	63.7	57	63.2	35.6	32.3	32.7
480	60	56.2	62.7	36.9	33	33.6

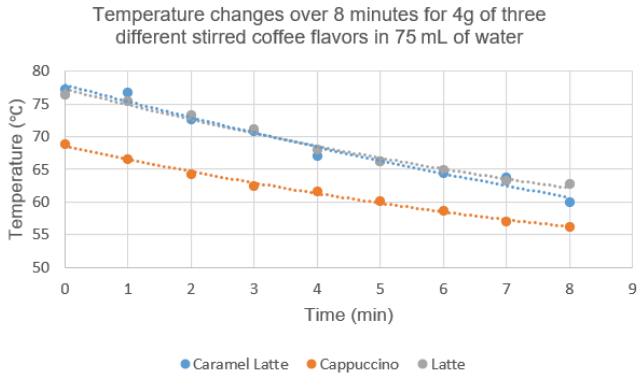

Figure 3 - Cooling trends of 3 types of coffee (4g each) dissolved in water and stirred.

3.2 Container Material Comparison

3.2.1 Coffee Trail - Cup Material Comparison

Coffee of the same flavour and concentration showed noticeable variations in temperature change over 480 seconds when placed in the three different containers. The metal insulated cup retained the most heat, while the glass cup showed the greatest temperature decrease.

Table 4 - Temperature changes over 480 seconds for coffee of the same flavour and concentration in different containers.

Time (sec)	Glass cup(℃)	metal insulated cup (℃)	ceramic cup(℃)	Surrounding temperature (℃)		
				Glass cup(℃)	metal insulated cup (℃)	ceramic cup(℃)
0	64.7	69.8	63.5	28.5	39.7	38.4
60	63.7	68.7	61.4	38.9	38.9	39.1
120	63	67.2	60.4	38.6	38.6	40.1
180	61.6	66.1	58.4	37.1	37.1	39.7
240	60.8	64.3	57.8	37	37	39.3
300	58.3	62.2	55.6	36.7	36.7	39.5
360	57.4	62.2	53.7	35.9	35.9	38.5
420	56.4	61.4	53.2	35.3	35.3	38.4
480	54.6	60.1	52	35.1	35.1	38.1

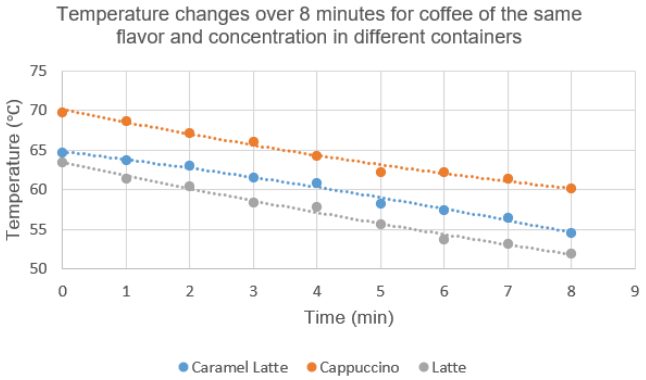

Figure 4 - Cooling trend for coffee of the same flavour and concentration in 3 different containers.

3.2.2 Tea Trail - Cup Material Comparison

Container material exerted a strong control on tea cooling. Over 240 seconds, a porcelain mug retained heat best (ΔT = 6.8 °C), glass was intermediate (8.6 °C) and stainless steel cooled fastest (12.4 °C).

Table 5 - Temperature changes over 240 seconds for tea of the same flavour and concentration in different containers.

Time (sec)	Ceramic (°C)	Stainless-Steel (°C)	Glass (°C)
0	72.7	68.1	70.1
60	70.1	61	65.7
120	68.3	59.1	64.1
180	67.9	58	63
240	65.9	55.7	61.5
ΔT	6.8	12.4	8.6

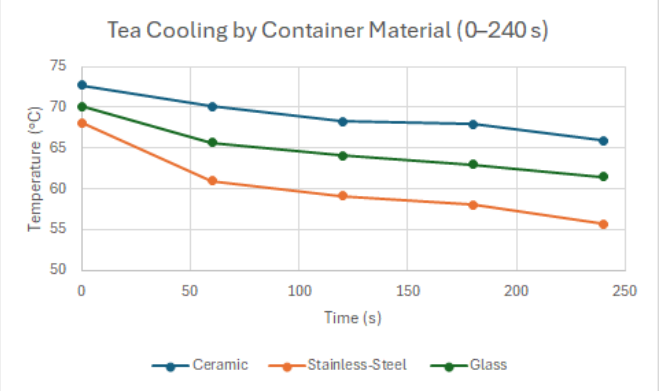

Figure 5- Cooling trend for tea of the same flavour and concentration in 3 different containers.

3.3 Solute Addition Effects

Dissolving 5 g sucrose before steeping two teabags resulted in a greater 240 s ΔT (10.3 °C) than the unsweetened infusion (8.6 °C).

Table 6 - Temperature change of tea samples with and without sucrose over 240 seconds.

Time (sec)	No Sucrose (°C)	+ 5 g Sucrose (°C)
0	70.1	68.1
30	68.4	66.7
60	65.7	64.3
90	64.9	62.9
120	64.1	61.9
150	63.4	60.7
180	63	59.8
210	62.3	58.9
240	61.5	57.8
ΔT	8.6	10.3

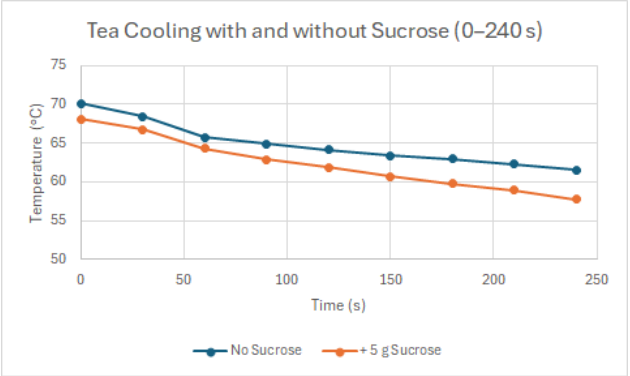

Figure 6- Cooling trend for tea samples with and without sucrose over 240 seconds.

3.4 Particle-Induced Convection and Volume Effects

3.4.1 Effect of Oat Concentration

Increasing the milo-oat concentration from 0.5 to 2 packets in a fixed 200 mL volume resulted in the 2-pack suspension losing 24.0 °C, compared with just 16.0 °C for the 0.5-pack sample over 180 seconds.

Table 7 - Temperature change of milo-oat suspensions with different oat concentrations over 180 seconds.

Time (sec)	100 mL Centre (°C)	100 mL Edge (°C)	150 mL Centre (°C)	150 mL Edge (°C)	200 mL Centre (°C)	200 mL Edge (°C)
0	71.2	69.7	67.2	65.7	67.2	65.7

30	61	59.5	64.9	63.4	65.1	63.6
60	50.7	49.2	59.3	57.8	64.3	62.8
90	49.3	47.8	57.8	56.3	63.9	62.4
120	47.9	46.4	57.3	55.8	62.2	60.7
150	47.2	45.7	55.7	54.2	61.3	59.8
180	46.5	45.1	54.2	52.6	59.3	57.7
ΔT	24.7	24.6	13	13.1	7.9	8

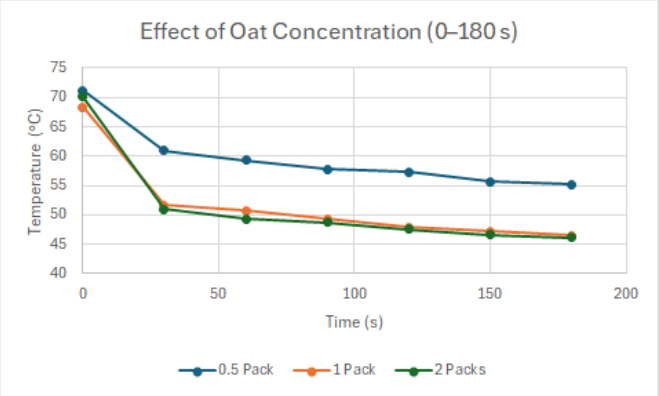

Figure 7 - Cooling trend for milo-oat suspensions at varying oat concentrations over 180 seconds.

3.4.2 Effect of Fluid Volume

Holding oat mass constant but reducing water volume caused the 100 mL suspension losing 24.7 °C at the centre (24.6 °C at the edge), whereas the 150 mL sample lost 13.0 °C (13.1 °C at the edge) and the 200 mL beaker lost only 7.9 °C at the centre (8.0 °C at the edge).

Table 8 - Temperature change of milo-oat suspensions at different fluid volumes over 180 seconds.

Time (sec)	0.5 Pack (°C)	1 Pack (°C)	2 Packs (°C)
0	71.2	68.4	70.1
30	61	51.7	51
60	59.3	50.7	49.3
90	57.8	49.3	48.7
120	57.3	47.9	47.6
150	55.7	47.2	46.6
180	55.2	46.5	46.1
ΔT	16	21.9	24

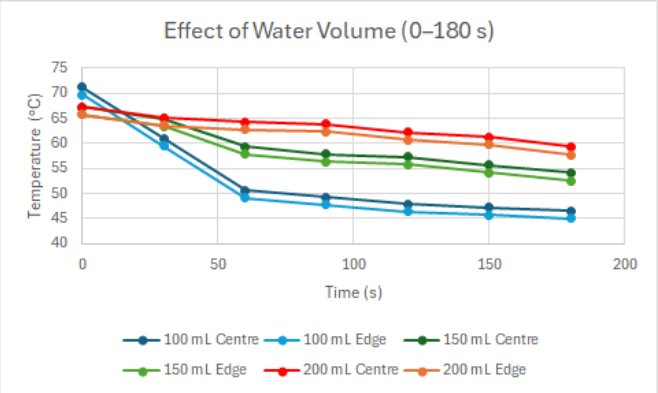

Figure 8 - Cooling trend for milo-oat suspensions at different fluid volumes over 180 seconds.

4. Discussion (need to be edited)

The experiments showed that several factors affected how fast the beverages cooled. For the coffee samples, changing the solute concentration made a noticeable difference. Tables 1 and 2 and Figures 1 and 2 showed that when the concentration increased from 2 g to 4 g, the drinks cooled more slowly. For example, in the caramel latte the 2 g sample cooled by 16 °C over 480 seconds, while the 4 g sample cooled by only 11.7 °C. This indicates that having more dissolved solids seemed to increase the viscosity of the coffee, which most likely slowed down the natural convection flow that usually helps carry heat. A similar trend was seen in the tea trial. Table 6 and Figure 6 showed that adding 5 g of sugar caused a larger temperature drop (ΔT = 10.3 °C) compared to tea without sugar (ΔT = 8.6 °C).

Stirring also had a big impact on how quickly the coffee cooled. When stirring was introduced, the cooling rate increased for all three coffee flavours. Table 3 and Figure 3 showed that caramel latte cooled by 17.2 °C under stirring conditions, compared to 11.7 °C without stirring. Stirring created forced convection, which moved the liquid around and improved heat transfer. Faster fluid flow likely increased the convective heat transfer coefficient. As a result, the Nusselt number would have increased (Nu = h * L / k), which explains why the heat left the drink more quickly.

The type of cup also made a difference. In the coffee and tea tests, the metal insulated cup and the ceramic mug kept the drinks warmer for longer, while glass allowed them to cool faster. Table 4 and Figure 4 showed that coffee in the

insulated metal cup only cooled by 9.7 °C over 480 seconds, while coffee in a glass cup cooled by 11.5 °C. To support that, in the tea trials (Table 5 and Figure 5) similar results were seen. The ceramic cup had the smallest temperature drop (6.8 °C), while the stainless steel cup cooled the fastest (12.4 °C). The insulated and ceramic cups seemed to slow down heat loss by reducing conduction through the walls. The glass cup probably allowed faster heat transfer to the air outside.

The milo-oat experiments showed that adding more oat particles made the drink cool faster. Table 7 and Figure 7 showed that the 2-pack suspension lost 24 °C over 180 seconds, while the 0.5-pack sample lost only 16 °C. The extra particles probably encouraged more movement in the fluid, which increased natural convection inside the drink and helped the heat move from the centre to the outside.

Finally, the water volume experiments (Table 8 and Figure 8) confirmed that smaller volumes cooled faster due to lower thermal inertia and a larger surface-area-to-volume ratio. The 100 mL oat suspension cooled by 24.7 °C, while the 200 mL sample cooled by only 7.9 °C at the centre. The small temperature difference between the centre and edge (≤ 0.2 °C) also showed that conduction within the liquid was not a limiting factor for heat transfer in these cases, meaning that convection remained the main way heat moved through the fluid.

Overall, the experimental results support Fourier's Law of Conduction and Newton's Law of Cooling. Firstly, Fourier's Law helped explain how the container materials affected the rate of heat transfer by conduction through the walls. While on the other hand, Newton's Law described the convective cooling from the liquid to the surrounding air. The study showed how thermophysical properties, fluid dynamics, and material conductivity influence cooling rates. These findings have practical applications for consumers and for designing beverage containers, packaging, and thermal equipment.

This study also serves as a learning point for audiences who want to manage how fast their drinks cool. For example, stirring drinks or using glass containers can speed up cooling, while using insulated or ceramic cups can keep drinks warmer for longer. The results could also be helpful for people designing drink containers and packaging. Knowing how to control cooling can also be useful in factories where food and drink products that contain dissolved solids or particles need to be heated or cooled. Changing things like stirring, concentration, and container type could help manage heat transfer in both homes and industry.

5. Conclusion

Overall, the experimental results of this study indicate that the physical composition of beverages and the characteristics of containers have a significant impact on the cooling rate. After analysis, it was found that dissolved solutes with higher concentrations, such as coffee solids, slow down the cooling process by increasing viscosity and reducing convection, while suspended particles like oats enhance convective mixing and accelerate cooling. Stirring promotes forced convection, causing the temperature to drop more rapidly. The material of the container regulates the conduction of heat loss. The insulated metal cup effectively retains heat, while the glass cup helps the drink cool down more quickly.

Smaller liquid volumes cooled faster because they had less thermal inertia and a larger surface-area-to-volume ratio. These results showed how convection and conduction worked together to control how fast heat was lost. The findings can help people choose containers and ingredients to change how fast their drinks cool. They might also be useful for designing food products and industrial systems where controlling heat transfer is important. Subsequent research may include exploring other variables, such as environmental air flow or shape and size of container, to refine these analyses.

Acknowledgements

The author(s) acknowledge the use of artificial intelligence (AI) tools to assist with editing and improving clarity, grammar, research and sentence structure. All ideas, analysis, and original writing were developed by the author(s).

References

1. Bergman, T. L., Lavine, A. S., Incropera, F. P. & DeWitt, D. P. Fundamentals of Heat and Mass Transfer, 8th ed. (John Wiley & Sons, 2017).
2. Çengel, Y. A. & Ghajar, A. J. Heat and Mass Transfer: Fundamentals and Applications, 6th ed. (McGraw-Hill, 2020).
3. Singh, R. P. Heating and Cooling Processes for Foods, 2nd ed. (CRC Press, 2006).
4. Vollmer, M. Newton's law of cooling revisited. Eur. J. Phys. 30, 1063–1084 (2009).
5. Rees, W. G. & Viney, C. On cooling tea and coffee. Am. J. Phys. 56, 434–437 (1988).
6. Ferreira, J. P. M. How a soup bowl and a coffee cup cool down. Phys. Educ. 59, 055020 (2024).
7. Mercer, N. S. G. With or without? A cooling study. Burns 14, 397–398 (1988).
8. Jamnadas-Khoda, B., See, M. S., Cubison, C. T. C. & Dheansa, B. S. How would you like your tea, vicar? Burns 36, 356–359 (2010).
9. Mawhinney, J. A. et al. Does "Prison Napalm" work? Measuring the cooling temperature of sugar solution burns in a porcine model. Burns 48, 1209–1212 (2022).

10. Warner, R. M., Wilson, Y. & Chester, D. L. Cooling properties of everyday liquids. Burns 38, 1186–1191 (2012).
11. Pastizzo, J. Analysis of Stirring Techniques and their Impact on Cooling Coffee Through Convection. (Undergraduate Thesis, California State Univ. Long Beach, 2023).
12. Ramanathan, C., Ekpenyong, L. & Stevenson, J. H. Scald burns in children caused by hot drinks — the importance of the type of cup. Burns 20, 111–114 (1994).
13. Suleman, M. & Gas, P. Analytical, experimental and computational analysis of heat released from a hot mug of tea coupled with convection, conduction, and radiation thermal energy modes. Int. J. Heat Technol. 42, 359–372 (2024).
14. Gowen, A. A., Tiwari, B. K., Cullen, P. J., McDonnell, K. & O'Donnell, C. P. Applications of thermal imaging in food quality and safety assessment. Trends Food Sci. Technol. 21, 190–200 (2010).
15. Brown, F. & Diller, K. R. Calculating the optimum temperature for serving hot beverages. Burns 32, 648–654 (2008).
16. Abraham, J. P. et al. Comprehensive method to predict and quantify scald burns from beverage spills. Int. J. Hyperthermia 32, 900–910 (2016).
17. Holman, J. P. Heat Transfer, 10th ed. (McGraw-Hill, 2010).

Investigation into Safe Kitchen Utensil Design through Conductive and Convective Heat Transfer

Saxon Krause[1], Lachlan Binnekamp[2], Cooper Ross[3], Anthony Nguyen[4], Jack Taylor[5], Minghao Zhang[6], Dr. Gobinath Rajarathnam[7]

[1] Chemical and Biomolecular Engineering, The University of Sydney, Sydney, Australia

E-mail: xxx@xxx.xx

Received xxxxxx
Accepted for publication xxxxxx
Published xxxxxx

Graphical Abstract

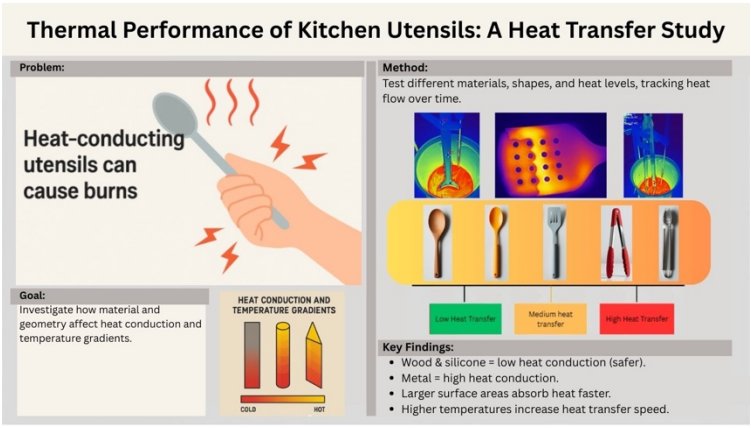

Abstract

This study investigates the thermal performance of common kitchen utensils, focusing on conduction based heat transfer, cooling rates, and insulation effectiveness. This is in order to investigate how the various properties impact the safety aspects of kitchen utensils on its users. Three experiments were conducted to assess the influence and thermal conductivity of material type, surface area, and insulation. Using a thermal imaging camera, transient temperature changes and temperature gradients were able to be recorded. Further analysis applied Fourier's Law and surface area-to-volume ratios to explain differences in heat transfer and cooling performance. Results showed how he increase in temperature increases the maximum temperature of the handle. However, made safe due to timbers exhibiting minimal heat conduction, meaning that heat does not travel up the handle presenting a hazard. Conversely, metal utensils demonstrated significantly higher heat transfer however, insulated variants reduce this significantly with the increase in surface area increases heat transfer. As a result, presenting their importance in safe utensil design. Procedural inconsistencies such as camera positioning, utensil placement, and environmental reflections were identified as key sources of error, obscuring precision and hindering repeatability. Recommendations for improved experimental setup are also discussed to increase data reliability in future studies.

Keywords: conductive heat transfer, insulation effectiveness, Fourier's Law, safety

1. Introduction

1.1 General Problem

Kitchen utensils are essential tools in the preparation and handling of food in everyday life. While their function is primarily mechanical, utensils are also expected to act as thermal barriers between the user and hot cooking environments. A failure to prevent excessive heat transfer can pose a large threat to burns, discomfort, and handling inefficiencies to the user. This is particularly relevant for utensils exposed to hot water as its high heat capacity increases the amount of energy in the system[1]. Despite design considerations often prioritising insulation or ergonomic grips, the underlying thermal safety of a utensil ultimately depends on its material conductivity and physical geometry. While anecdotal observations—such as "metal utensils get hot quickly"—are often accurate, quantitative validation through structured experimentation and known theories such as Fourier's heat transfer theory, can highlight safe material choices. This is particularly crucial for items like tongs, ladles, and spatulas, which are commonly used in high-temperature environments and are frequently made from a wide range of materials with varying thermal properties.

1.2 Previous Studies and Existing Solutions: Known Material Properties and Gaps

Previous studies on thermal conductivity have established that a material's ability to conduct heat depends on its internal structure and dominant heat carriers. In metals, such as stainless steel, electrons are the primary means of transporting thermal energy, resulting in high thermal

conductivity values whereas stainless steel with 16 W/m·K[2]. These properties highlight the effectiveness of these metals as conductors but potential hazards for utensil handles unless properly insulated.

In contrast, polymeric materials like nylon and silicone rubber conduct heat through lattice vibrations (phonons)[3]. These materials are considered thermal insulators, with conductivity values ranging from 0.2 to 0.44 W/m·K, depending on molecular structure and temperature[4] Their low conductivity and flexibility explain their widespread use in cooking utensils, especially for handles and grips where reducing burns and harm is essential.

Although these thermal properties are well-documented in material science literature, most are measured under idealised lab conditions using standard test shapes, such as thin slabs or for different kitchen appliances such as pots and pans. Few studies have experimentally examined how these material properties behave in complex geometries in common kitchen utensils. For instance, factors like handle thickness, insulation layering, and contact surface area can all affect how heat travels from the heated portion of a utensil to the user's hand.

Additionally, while Fourier's Law of heat conduction provides the theoretical framework to describe this heat flow, prior research has rarely applied it directly to utensils in domestic contexts. As such, there remains a practical gap in understanding how theoretical values translate to real-world thermal safety in consumer-grade kitchenware.

1.3 Scope and Objective of the Current Study: Focusing on Conduction with Fourier's Law.

This study aims to address the outlined gaps by conducting a targeted investigation into purely conductive heat transfer within common kitchen utensils, by breaking it down to three key questions. These key research questions are:

1. How temperature affects heat conduction within the handle of the utensil.

2. What role utensil surface area and shape play in cooling rate and heat dissipation.

3. How effective insulation is in reducing heat conduction in metal utensils.

Our experiment answered these objectives by submerging utensils into controlled-temperature water baths and recording temperature changes along their handles using a thermal imaging camera. The focus on conduction allows for a direct application of Fourier's Law of Heat Conduction, which states that the rate of heat transfer through a material is proportional to the negative gradient of temperature and the thermal conductivity of the material[5]:

$$Q = -kA\frac{dT}{dx} \qquad (1)$$

where Q is the rate of heat transfer, k is thermal conductivity, A is the cross-sectional area, T is the temperature and x is the distance along the handle.

By using this theoretical framework, the study evaluates the relative thermal performance of materials like wood, plastic, and metal. In addition, both the impact of added insulation through silicone and utensil geometry through the role of surface area-to-volume ratios on heat dissipation during cooling can be analysed. The overarching objective is to provide recommendations based on experimental data and calculations for material and design selection in kitchen utensil manufacturing, with the goal of enhancing user safety through thermal engineering principles.

2. Methodology

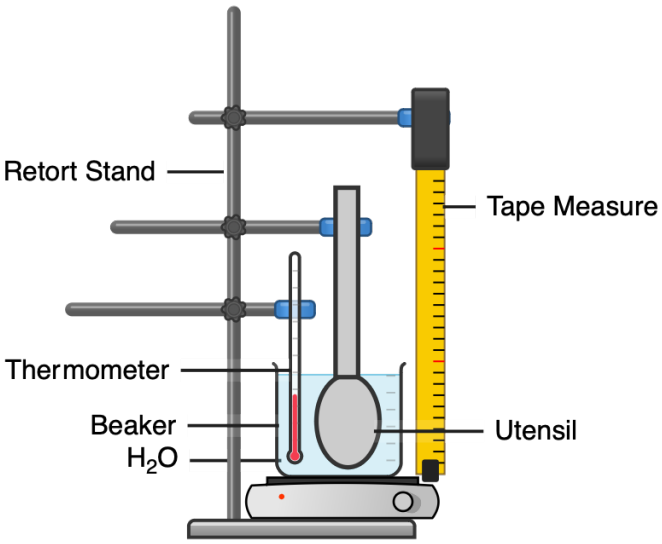

Figure 1: experimental diagram[6]

For all experiments, the experimental setup can be seen in figure 1. A 250 mL beaker was placed on a hotplate and set to specific temperatures (40°C, 60°C, or 80°C). A thermal imaging camera (InfiRay Pro 2) was used to record temperature changes in the utensils. For each measurement five readings were taken within 10-second windows around each minute to reduce random error.

Experiment 1: Effect of Temperature on Wooden Utensils

Three identical wooden spoons were submerged in water at 40°C, 60°C, and 80°C respectively. The temperature at the

base and top of the handle was recorded every minute over a five-minute period.

Experiment 2: Effect of Surface Area and Shape on Heat Transfer

Two plastic kitchen utensils, one a spatula and the other a ladle, were placed into water at 80 degrees Celsius and the rate at which the temperature changed was recorded using the camera. They were then removed and placed on the bench and had heat scans taken after approximately 20 seconds of cooling to measure the effects of different surface areas and shapes on heat distribution and cooling. Similarly, during the 5 minutes both utensils were in the hot water, measurements were gathered at the end of the respective handle with the temperature being taken on each respective handle at 10±3 second intervals with 5 separate readings each time.

Experiment 3: Effect of Insulation on Heat Distribution

Two metal tongs, one made entirely of stainless steel and another with a silicone-insulated head, were submerged in 60°C water. Temperature readings were taken along the head and handle every minute for five minutes using a thermal imaging camera. The material composition of the tongs was confirmed based on product information found online; the all-metal tongs were stainless steel, while the insulated tongs consisted of stainless steel with silicone grips and tips[7&8]. Experimental heat conductivity values were calculated using equation 1.

Key Controls and Assumptions:

Utensils assumed to be homogeneous in composition, material properties (k, C_p, ρ) sourced from literature and product data, identical beakers and thermal camera setup used across all tests. No significant air drafts or environmental temperature fluctuations. Only conductive heat transfer is considered; convective effects neglected.

3. Investigation of the effect of temperature on the rate of heat transfer and distribution

3.1 Hypothesis

1. The increase in temperature will increase the steady-state temperature.

The energy transfer from the water to the spoon is given by Newton's law of convection[9] where h is the convection constant, T is the object temperature and T_∞ is the fluid temperature:

$$Q = Ah(T - T_\infty) \quad \textbf{(2)}$$

As such, when the temperature of the water increases there will be a greater temperature differential thus, increasing the rate of energy transfer. Furthermore, as given by the formula there will continue to be a transfer of energy up until the temperature of the spoon and the temperature of the water are the same. As such, since the energy is dissipated through convection from the handle and the surface area and convection constant remain constant the temperature must increase to account for the increase in energy.

2. The low thermal conductivity of the timber allows it to remain safe to use over time when exposed to direct heat.

Thermal conduction within the spoon can be modelled by equation 1. Since there is a small thermal conductivity constant of 0.1 – 0.2 the amount of energy transferred over a given distance is quite low[10]. This results in lower temperatures along the handle. However, another competing factor in reducing the temperature along the handle would be the rate at which energy is convected away from the handle[11]. Since there is only natural convection the convection constant should be small and thus, have less of an impact on the temperature gradient through the handle[12].

3.2 Results

The data that was collected all three trials indicated that the increase in temperature over time is one of a logarithmic scale (this can be seen in the appendix). As such, to confirm this relationship the natural logs of the temperature were taken and then graphed with the corresponding times. In figure 2**,** the data conforms to a linear trend affirming with a great deal of confidence that the change in temperature over time is related by a logarithmic trend with R^2 values of 0.85, 0.98, 0.96 for 40°C, 60°C & 80°C respectfully. This affirms the accepted and theoretical understanding of transient heat conduction. This can be seen with the lumped capacitance analysis formula for the assumption of no radiation and the convection constant remaining constant over time (equation 3)[13]. Here t is the time, V is the volume, ρ is the density and c_p is the specific heat capacity.

$$T(t) = T_\infty + (T - T_\infty)e^{-\frac{hA}{\rho c_p V}t} \quad \textbf{(3)}$$
$$T \propto e^t, t \propto \ln(T)$$

However, the relevance of this formula can be argued. This is due to first the fact that some energy will be being lost to the environment by radiation simply since there is a difference in

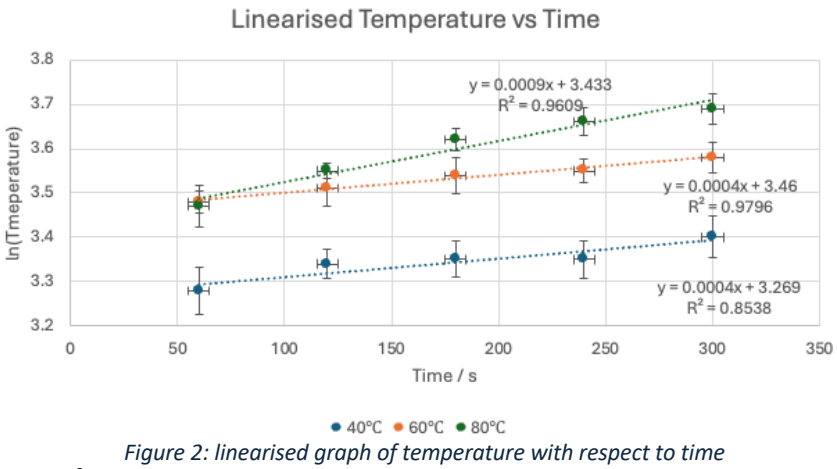

Figure 2: linearised graph of temperature with respect to time

temperatures. However, this is a somewhat reasonable assumption due to the temperature difference being small such that the energy lost will be close to negligible. Furthermore, the whole underlying assumption of general lumped capacitance is that the rate of conduction is large enough compared to the rate of convection that there is a negligible temperature gradient within the spoon. As a result, this equation is only accepted when the Biot number is less than 0.1[14]. Using the literature values for the convection constant for water we can gain a rough perspective of at least the relative order of magnitude[15]. This value, however, will be far from accurate as this is a general value not one that accounts for the wooden spoon's properties. As a result, the Biot number ranges from $4.25 \leq Bi \leq 510$ (these calculations can be found in the appendix). Hence, the assumption of lumped capacitance is not valid in this scenario and unfortunately cannot be used to model the transient temperature. However, if we compare the formula to the infinite cylinder with non-negligible temperature gradients (equation 4), we can see that the proportionality of temperature to time still holds true as the Fourier number is a function of time. As such, the data conforms with the accepted literature in forming the correct relationship between temperature and time[13].

$$T(t) = T_\infty + (T - T_\infty)\sum_{n=1}^{\infty} C_n e^{-\zeta_n^2 Fo} J_0(\zeta_n r^*), Fo = \frac{\alpha t}{r_0^2} \quad (4)$$

$$\therefore T \propto e^t, t \propto \ln(T)$$

3.3 Discussion

The heat conduction constant can be calculated by assuming that the handle is a fin that is dissipating the energy through conduction to the atmosphere. As such, the temperature can be modelled through equation 5 where P is the fin perimeter and L is the length of the fin[16].

$$\frac{T - T_\infty}{T_b - T_\infty} = \frac{\cosh m(L-x) + \left(\frac{h}{mk}\right)\sinh m(L-x)}{\cosh mL + \left(\frac{h}{mk}\right)\sinh mL} \quad (5)$$

$$m^2 = \frac{hP}{kA_c}$$

Then subbing in the temperatures and taking an average (excluding outliers which were values that are either $1.5 \times IQR$ above or below the median), we can find the average heat convection constant ($h = 0.054\ Wm^{-2}K^{-1}$) [17]. Sample calculations can be seen in the appendix with the results for all the measurements. The reason for using an average is due to the variability in the convection coefficient which had a range of 0.036 excluding outliers. Although small, when compared to the average this results in $\pm 33\%$ which is not negligible. These changes in values are most likely due to drafts and changes in the velocity of air in the room in which the experiment was taking place[18]. In addition, taking an average allows us to simplify the calculation and ignore any changes in the convection constant concerning time.

The use of the fin approximation, however, comes with some assumptions, the only one that is being violated are the steady state conditions as the measurements were taken transiently[19]. However, if we ignore the bottom of the spoon and just focus on the handle the temperature gradient should be consistent. Hence, it is relatively feasible to look at it as a fin as the observational data followed the expected trend of an exponential curve.

Using the data collected a model can be made for the transient heat conduction along the spoon. T_b can be calculated using the formula for the trendlines that come from the experimental findings. This can then be modelled in 3D to see how the temperature changes along the handle with respect to time.

Evidently even when modelling into the future the temperature along the handle will never get hot enough to be dangerous to the user. This is evident with the spoon at 80°C after 20 minutes ($T = 47$°C) only going to cause damage to the basal layer of the epidermis[20]. However, this is only when touching the very bottom of the spoon. Halfway up the spoon the temperature would be only 31°C which is not enough to cause any form of damage to the skin. Furthermore, the data clearly shows the benefits of such a small heat conduction value as the temperature gradient is incredibly steep preventing the top of the handle from getting hot. This conclusion can be approximately made due to how small the convection value is such that the energy lost is not influencing the conduction curve. This makes it a highly safe utensil as it is unrealistic to have direct contact with a water at 80°C for more than 20 minutes straight and be touching it right at the hottest point.

Although there are no specific commercial cookware safety standards, typically in commercial kitchens wooden utensils

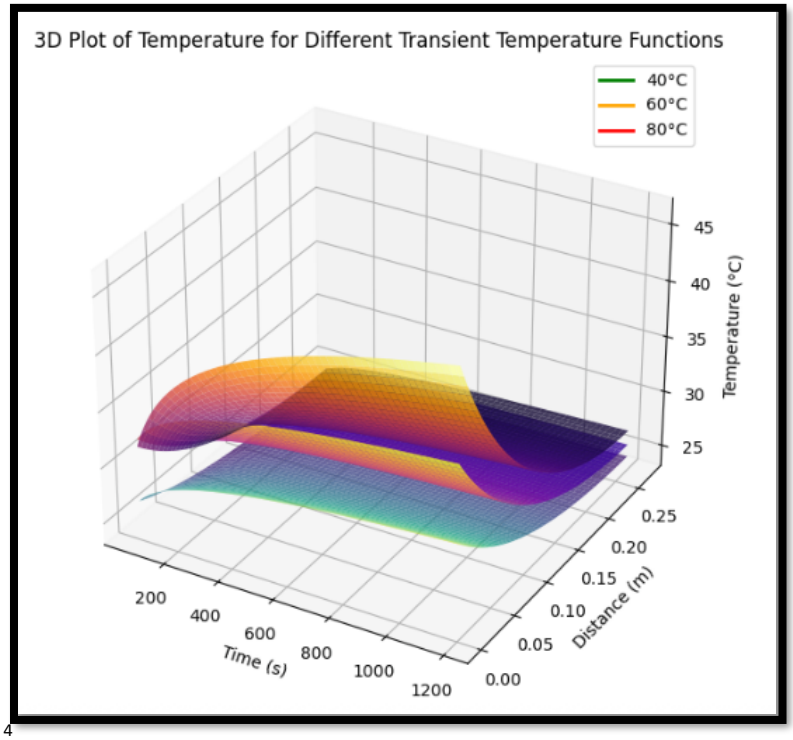

Figure 3: 3D plot of temperature, time and distance for the three different temperatures[24]

are not as common. This is due to the hygiene concerns that come with the use of timber[21]. These stem from the porous nature which allows bacteria and other pathogens to grow[22]. Since, there are extremely stringent food hygiene regulations this exacerbates the stainless-steel control over the market [23]. However, this is not to say that the findings from this experiment are worthless in a commercial environment but to say that the use of other materials with low thermal conductivities may allow for both the user to be safe and the food to maintain its hygiene. Beyond the professional environment where wooden utensils are far more common the findings conclude that they are one of the safest tools in burn prevention.

When considering other substances which can reach higher temperatures and similarly transfer heat like oil, then the temperature it will reach will be far greater increasing the energy transfer. However, oil may have a much lower convection constant ($50 - 350\ Wm^{-2}K^{-1}$) compared to water ($50 - 3000\ Wm^{-2}K^{-1}$) [16 25]. Yet again these values are most likely not correct as they are not for this specific case with timber spoons however, they serve as a comparison between their effective rates of heat transfer. As such, if taking the maximum values, it is only true when either the temperature is so high that it isn't feasible or if left in the oil for an unrealistic amount of time. However, if the convection constants are both 50 then the temperature will get considerably hotter. As such, a future area of research would be to investigate the effects of different substances.

4. Investigation into the effect of surface area and material on the rates of cooling and heat conduction

4.1.1 Hypothesis on the effects of complete insulation material on heat conduction

Both the spatula and ladle utilised in the experiment were Coles brand, however Coles does not reveal the insulation material utilised in the makeup of each product. Thus, for this experiment based on comparison to other products and the physical properties of each product compared to the properties of typical insulation plastic products to be nylon for the spatula [26] and silicone for the ladle[27]. Past academic research indicates both kitchen utensils should be good insulators of heat as each material has been found in studies to have very low heat conductivity constant with nylon ranging between 0.23-0.29W/m·k for nylon[28] and 0.2-0.44W/m·k for silicone[29], dependent on specific type of each insulating plastic utilised. These values gathered from literature reports indicate each utensil should not conduct considerable amounts of heat up the handles of each separate utensil. These values also indicate that heat conducted is expected to be found to be relatively similar amounts in each material due to similar heat conductivity constants, with silicone perhaps conducting slightly more.

4.1.2 Hypothesis on the effects of material and surface area on cooling and heat dissipation

Secondarily this experiment aimed to measure the effect of surface area, shape and material on heat distribution and cooling through taking heat scans of both the ladle and spatula 20 seconds after being removed from the hot water. Given both thermal insulating materials utilised were measured to have the same thickness it is possible to study the effects of both surface area and volume specific surface area. In general, a larger surface area leads to faster rate of cooling as a larger area allows for more contact with the cooling medium, in this case surrounding room temperature, and facilitates greater heat dissipation[30]. This would indicate the ladle head to cool much faster given the calculated surface area being $356.83cm^2$ compared to the spatula's head's calculated surface area being $177.04cm^2$. However, volume of each shape must also be considered to find a volume specific surface area(ω) as a prior study by Árpád et.at recently suggests having found ω affects Newton's law of cooling in the following way, where an increase in ω will cause an increase in cooling rate and deviation of temperature ($\Theta(\tau)$) [31].

$$\boldsymbol{\Theta(\tau) = \Theta(0) \cdot e^{-h\omega T}} \qquad \textbf{(6)}$$

This conversely indicates instead the expected outcome of the findings to be the spatula cools faster given the calculated volume specific surface area to be $10.96cm^{-1}$ compared the ladles $5.10cm^{-1}$. This also agrees with common theory that rectangular prism shaped objects generally cool faster than their spherical counterparts due to their larger surface area to volume ratio[32].

Furthermore, utilising the heat scans it will be possible to test whether the materials utilised are homogenous or if the materials are not uniform during production. Ideally homogenous plastics should have consistent heat spans that demonstrate a smooth transfer of heat during cooling with a gradual colour change being demonstrated on the heat scans[33]. However, if the materials are not homogenous, localised hot spots are more likely to be found on the heat scans.

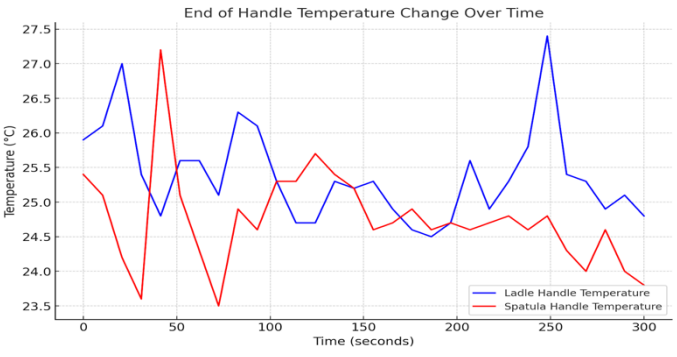

Figure 4: Line graph demonstrating the change in temperature against time at the end of the handle for both spatula and ladle

4.2 Results

4.2.1- The effects of solid insulation on heat conduction

The temperature at the end of the handle for each utensil never demonstrated a clear trend thus the data gathered can be best displayed utilising a line graph exhibiting the averages for all data points found. Averages could be taken from the 5 readings taken every 10 seconds each collection of results never exhibited major standard deviation or maximum deviation. The data collected illustrated minimal fluctuation, thus to better view variation in data the y-axis range was minimised to range between 23.5°C-27.5°C.

4.2.2 – Surface area and material heat dissipation

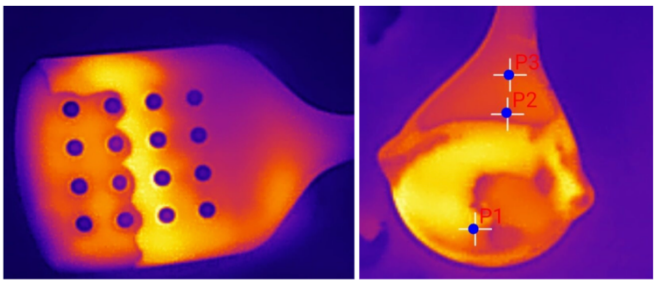

Figure 5: Heat scans taken after 20 seconds of cooling for each utensil, spatula on the left and ladle on the right.

Heat scans were taken of each utensil after 20 seconds of cooling to allow for qualitative analysis on the heat dissipation during cooling for each utensil. The spatula exhibits the central section of the utensil to be the hottest with gradual heat dissipation both the tip and back of the spatula head. The ladle also similarly demonstrates the central section of the utensil to be the hottest however its heat dissipation is slightly more irregular also with a few localised cool spots.

4.3 Discussion

4.3.1 – Solid insulation and heat conduction

The temperatures recorded at the end of both the ladle and the spatula handles evidently never displayed severe rises in temperature that could lead to them being dangerous for users. Each handle displayed initial temperature increases from room temperature of 23°C and then remained relatively stable at averages of 25.39°C for the ladle and 24.75°C for the spatula. Slight deviations in data were likely gathered from possible fluctuations within the room which lead to maximum variance from average temperature of ±1.78% for the ladle and ±1.97% for the spatula, which are relatively negligible. The gathered results support the hypothesis that each utensil should be safe for cooking at 80°C given their respective insulation materials utilised. The findings also agree to the hypothesis that silicone is a slightly better conductor of heat, hence the slightly higher average found for the lade. To further support these findings, heat flux(q) can be calculated using the Fourier law of heat conduction for a heat transfer model.

$$q = \frac{k_x A_x (\Delta T)}{L_x} \quad (7)$$

Through applying the above equation average heat flux values of 0.015W for the ladle and 0.018W for the spatula were found. These values reinforce the prior findings of the safety of each utensil and its insulating material given the gathered heat flux values for each are extremely small suggesting the amount of heat transferred through the handles is very minimal indicating the insulating materials, nylon and silicone are doing their jobs for each respective utensil[34].

4.3.2 - Surface area and material on heat dissipation

Through analysing the photos, it is evident for both utensils the central portion of each head is as expected the hottest part after being allowed to cool for 20 seconds. This is simply due to the fact that despite all sides seen on the heat scan being in contact with the atmosphere, the edges have more exposure to the atmosphere allowing it to release more heat[35]. As hypothesised the spatula appears to be cooling faster especially the edges which is likely due to the greater volume specific surface area on the rectangular prism shaped spatula then the hollowed out semi-ellipsoid shape of the ladle.

This can be quantitatively understood from the adapted Newton's laws of cooling equation displayed earlier where evidently slower cooling rates will be received for a smaller volume specific surface area value. The results shown here further prove the relatively recent discovery that volume specific heat capacity should be considered within Newton's laws of cooling as this proves the rate of cooling and heating not only heat transfer coefficient and materials characteristics but also volume specific surface area[31]. This would hence lead to the conclusion that when utilising utensils of a similar thickness and material but differing shapes those with higher volume specific surface areas will be safer to touch in a faster period. However as seen by each image each utensil head after 20 seconds still contains significant amounts of heat despite being made from insulating materials, thus it is highly recommended to not touch any part of a utensil that has come in contact with extreme heat for an extended period or until cooled by other systems[36].

The heat scans indicate some scale of uniformity within both utensils as neither display major localised hot spots and instead more gradual heat dissipation can be seen. However,

especially within the ladle small darker spots can be seen indicating those areas to be cooling faster which could be indicating small amounts of compositional non-uniformity. This would thus lead to the conclusion of the spatula being safer to cook with then the ladle as its greater amounts of uniformity throughout its heat scan indicates the spatula heating and cooling rates are more predictable throughout then the ladle. The greater predictability of the heat dissipation within the spatula means better advice can be sought on length of cooling times before it is safe to touch the utensil in comparison to the spatula, thus making the spatula head less harmful.

5. Investigation into the effect of partial insulation on heat distribution.

5.1 Hypothesis

The aim of this experiment is to investigate the effect of insulation on heat distribution within a system. Specifically, it seeks to determine how the presence of insulating materials affects the rate of heat transfer in stainless steel tongs, compared to a pair with silicone insulation to one without. The hypothesis is that the addition of silicone insulation will reduce thermal conduction, slowing the rate of temperature change and leading to a more uniform temperature distribution over time. This is due to silicon having a lower conduction constant thus, conduction less energy and reducing the overall temperature[37].

Insulating materials reduce heat transfer by providing resistance to conductive, convective, and radiative losses. Fourier's Law of Heat Conduction states that the rate of heat transfer through a material is proportional to the temperature gradient across it and its thermal conductivity[38]. Subsequently, materials with low thermal conductivity, such as silicone or even nylon, are commonly used as insulators on kitchen utensils[38]. Prior research suggests that well-insulated systems experience slower temperature changes and exhibit greater thermal efficiency compared to non-insulated systems[40].

We expect that the insulated tongs will exhibit a significantly lower rate of heat transfer than the non-insulated tongs. This will result in a slower temperature increase in the handle region and a more uniform temperature distribution across the insulated material[41]. These expectations align with transient heat conduction models, where insulation reduces temperature gradients and slows heat transfer[42]. The practical implications, suggests that insulated tongs are safer to use for handling hot objects over extended periods.

5.2 Results

The experiment measured temperature changes in two sets of Coles brand stainless-steel tongs—one with silicone insulation on the handle[7] and one without[8]—at three locations: near the bottom closest to the water, midway up the handle, and at the top of the handle. Minimal temperature change was observed at the handle for both tongs, indicating limited heat transfer along their length. The most significant temperature changes occurred at the bottom of the tongs, as shown in Figure 1. This is due to the temperature gradients discussed in section 3 of the report. The results in Figure 1 are averages from five trials per tongs type to ensure reliability, with the corresponding data and standard deviations provided in the appendix.

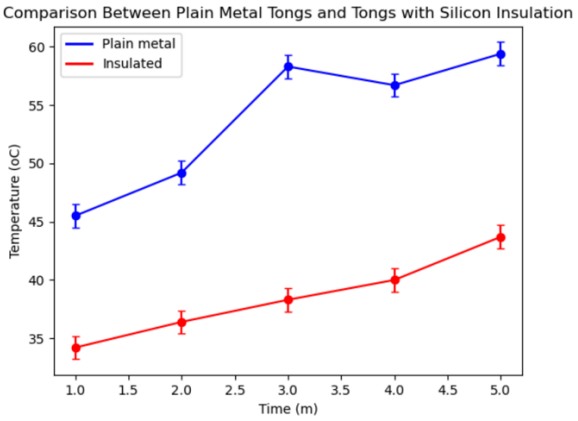

Figure 6. Temperature Change of Stainless Steel vs. -Insulated Stainless-Steel Tongs

5.3 Discussion

The results indicate that the insulated tongs conducted heat significantly less than the pure stainless-steel tongs. Based on common manufacturing standards, the stainless steel was assumed to be grade 304[43], with a thermal conductivity constant (k) of 16.2 W/m·K[44]. Its density was taken as 7930 kg/m^3, and the specific heat capacity (C_p) was identified as 490J/kg·K[45]. For the silicone insulation, the thermal conductivity constant (k) was estimated to range from 0.2 to 2.55 W/m·K, with a density of 1100 kg/m^3 and a specific heat capacity of 1050J/kg·K[37]. Since the metal core of the insulated tongs did not appear to extend deeply into the silicone tip, the submerged portion was assumed to be primarily composed of silicone.

The experimentally calculated k value for the stainless-steel tongs was 82.8 W/m·K, significantly higher than the theoretical value of 16.2 W/m·K. This discrepancy corresponds to a percentage error of 411.1% and can be attributed to multiple factors, including the simplification of the tongs' geometry. Approximating their shape as a rectangular cross-section may have led to a poor estimation of heat transfer values, as the actual geometry provides additional surface area for heat transfer not accounted for in the simplified model. Variations in temperature measurements due to shifts in the thermal imaging camera's position may have introduced minor inaccuracies.

For the insulated tongs, the experimentally determined k value was 19.93 W/m·K, which was higher than the theoretical expectation. As evident in equation 8 for the calculation of the rate of heat transfer using the total

resistance formula it is evident that *k* calculated will be an average between the stainless steel and the silicon with respect to the surface are and thickness. (Note: all values subscript one are the constants respective to the metal and subscript two for the silicon.) However, the experimentally calculated value is outside of the range indicating that the rate of heat transfer values has been underestimated, likely due to the same limitations affecting the stainless-steel tongs.

$$q = \frac{T_\infty - T_1}{R_{total}} \textbf{(8)}$$

$$R_{total} = \frac{L_1}{k_1 A_1} + \frac{L_2}{k_2 A_2} \textbf{(9)}$$

While the absolute values obtained from the experiment were inaccurate compared to theoretical values, they effectively demonstrated a comparative trend. The results consistently indicated that the insulated tongs conducted heat less effectively than the pure stainless-steel tongs. This supports the hypothesis that silicone insulation reduces heat transfer and enhances thermal safety. An additional limitation in the experiment was the estimation of the submerged portion's volume. Rather than directly measuring this volume, calculations were made using dimensional approximations, which may have introduced further error. A more precise approach, such as water displacement, would have provided more accurate data and improved the reliability of the calculated *k* values.

Overall, the insulated utensils are far superior when it comes to the safety of its user from burns. However, it is still common to see full metal utensils rather than ones with insulated grips in industry. This is due to their cost and durability which they tend to be inferior to their full metal comparision[47]. On the contrary, silicon is far more hygienic than timber presenting no real reason for insulated grips becoming more common in the industry.

6. Conclusion

6.1.1 - The effect of temperature on heat transfer

In culmination, it is clear the temperature does in fact increase the steady state temperature of the utensil. However, as seen due to the low thermal conductivity of the timber it makes the utensil incredibly safe. This is due to it preventing thermal energy from travelling up the handle and thus, maintaining the end of the handle at practically room temperature no matter how long it is supposed to heat. This was evident with the model indicating that even at 80℃ for 20 mins the end of the handle reached a temperature of 25℃. This was similarly cooperated with the base of the handle only reaching 47℃ which was barely enough to cause harm.

6.1.2 - Investigation into the effect of surface area and material on the rates of cooling and heat conduction

To summarise, the key findings illustrated both the Coles brand spatula and ladle, which are believed to have utilised nylon and silicon respectively, to successfully maintain a safe temperature for holding whilst cooking at 80°C. Each utensil only saw slight immediate increases when placed in the water to move above room temperature and then the ends of the handles remained in between 23.5-27.5°C each. Therefore, indicating the vital role of including the conduction constant into utensil design as it limits how much energy enters the spoon.

The heat dissipation of each material exhibited the spatula to cool faster than the ladle due to its smaller volume specific surface area. This hence points towards validating Árpád et.al study recommending the addition of volume specific surface area to Newtons law of cooling. Furthermore, the slightly more irregular shape of heat dissipation in the ladle with localised cool spots, indicates the spatula was made more uniform and thus safer as its rate of cooling is more predictable.

6.1.3 - Insulation effect on heat distribution.

This experiment demonstrated that even partial insulation significantly affects rates of conduction. Thus, in utensil design it is not necessary to be made completely out of an insulated material whilst keeping the safety a priority. By reducing the rate of heat transfer, the insulation promoted a more gradual temperature change and contributed to a more uniform temperature distribution. These findings align with Fourier's Law and support the hypothesis that insulation enhances thermal efficiency by resisting conductive, convective, and radiative heat losses. The trends seen in the experimental results matching expectations, confirming that insulated materials lowered the overall temperature. While errors and external factors may have influenced the results, the overall trends were consistent with theoretical predictions.

6.2 – Summary

To conclude, this article has successfully investigated and summarised various possible sources of harm through heat conduction of an array of different kitchen utensils through a range of forms, including the effect of temperature, surface area, material and insulation. Further studies could examine how changes in liquid utilised could affect the rates of heat transfer in each investigation and further investigate the role of convection in heat transfer for kitchen utensils. Addressing potential sources of error, such as ambient temperature fluctuations, movement of the position of the thermal camera and geometric modelling assumptions, could further improve experimental reliability. Additionally, employing direct measurement techniques for submerged volume would enhance the precision of heat transfer calculations.

Acknowledgements

Thankyou to the University of Sydney for their facilities and the lab team in providing the appropriate equipment to carry out our investigation. In addition, thankyou to Gobinath

Rajarathnam and Minghao Zhang for continuous feedback during the drafting process.

References

1. Qazi, S. Chapter 7 - Solar Thermal Electricity and Solar Insolation. ScienceDirect 203–237 https://www.sciencedirect.com/science/article/abs/pii/B9780128030226000071 (2017).
2. de Naoum, K. & Schadegg, J. 316 Stainless Steel: Uses, Composition, Properties. www.xometry.com https://www.xometry.com/resources/materials/316-stainless-steel/ (2023).
3. Uher, C. Thermal Conductivity of Metals. Thermal Conductivity 21–91 (2004) doi:https://doi.org/10.1007/0-387-26017-x_2.
4. Baetens, R. High performance thermal insulation materials for buildings. Nanotechnology in Eco-Efficient Construction 188–206 (2013) doi:https://doi.org/10.1533/9780857098832.2.188.
5. Matsuno, K. & Nemoto, A. Quantum as a heat engine—the physics of intensities unique to the origins of life. Physics of Life Reviews 2, 227–250 (2005).
6. Chemix. Chemix - Draw Lab Diagrams. Simply. Chemix.org https://chemix.org (2019).
7. Coles. Cook & Dine Tongs 30cm | 1 Each. Coles https://www.coles.com.au/product/cook-and-dine-tongs-30cm-1-each-3116330?srsltid=AfmBOort0zg0761jt52r_jpW0ECnDV7_ (2025).
8. Coles. Cook & Dine Silicone Tongs | 1 Each. Coles https://www.coles.com.au/product/cook-and-dine-silicone-tongs-1-each-7071346 (2025).
9. Vollmer, M. Newton's Law of Cooling Revisited. European Journal of Physics 30, 1063–1084 (2009).
10. Pásztory, Z., Fehér, S. & Börcsök, Z. The effect of heat treatment on thermal conductivity of paulownia wood. European Journal of Wood and Wood Products 78, 205–207 (2019).
11. Swierczyna, R., Sobiski, P. & Fisher, D. Revised heat gain rates from typical commercial cooking appliances from RP-1362. ASHRAE Transactions 115, 138–161 (2009).
12. Ostrach, S. Natural Convection in Enclosures. Advances in heat transfer 161–227 (1972) doi:https://doi.org/10.1016/s0065-2717(08)70039-x.
13. P Koštial et al. Lumped Capacitance Model in Thermal Analysis of Solid Materials. Journal of physics. Conference series 588, 012006–012006 (2015).
14. Jungbauer, A. & Hahn, R. Large Scale Separations. Journal of chromatography library 561–599 (2003) doi:https://doi.org/10.1016/s0301-4770(03)80038-6.
15. Engineering Toolbox. Overall Heat Transfer Coefficient. Engineeringtoolbox.com https://www.engineeringtoolbox.com/overall-heat-transfer-coefficient-d_434.html (2019).
16. Engineers Edge. Convective Heat Transfer Coefficients Table Chart | Engineers Edge | www.engineersedge.com. Engineersedge.com https://www.engineersedge.com/heat_transfer/convective_heat_transfer_coefficients__13378.htm (2015).
17. Fundamentals of Heat and Mass Transfer. Google Books (John Wiley & Sons, 2011).
18. PennState Eberly College of Science. 3.2 - Identifying Outliers: IQR Method | STAT 200. PennState: Statistics Online Courses https://online.stat.psu.edu/stat200/lesson/3/3.2 (2024).
19. Louisiana Tech University. ME 354 - Lab 5 - Fin Experiment. Latech.edu https://www2.latech.edu/~hhegab/pages/me354/Lab5/Lab5_fin_Sp99.htm (2024).
20. Camci, M., Karakoyun, Y., Acikgoz, O. & Dalkilic, A. S. A comparative study on convective heat transfer in indoor applications. Energy and Buildings 242, 110985 (2021).
21. Martin, N. A. & Falder, S. A review of the evidence for threshold of burn injury. Burns 43, 1624–1639 (2017).
22. Toggerson, B. & Philbin, A. Uncertainty for natural logarithms. openbooks.library.umass.edu 132, (2020).
23. McDonald, E. Wood vs plastic chopping boards: which is better? delicious.com.au https://www.delicious.com.au/food-files/health/article/wood-vs-plastic-chopping-boards-which-better/i2pjec8n# (2024).
24. Food Standards Australia New Zealand Safe Food Australia. Standard 3.2.3 Food Premises and Equipment. https://www.foodstandards.gov.au/sites/default/files/publications/SiteAssets/Pages/safefoodaustralia3rd16/Standard%203.2.3%20Food%20Premises%20and%20Equipment.pdf.
25. Python Software Foundation. Welcome to Python.org. Python.org https://www.python.org (2019).
26. de Naoum, K. 7 Properties of Nylon: Everything you Need to Know. *Xometry* https://www.xometry.com/resources/materials/properties-of-nylon/ (2022).
27. Mullins, M. J., Liu, D. & Sue, H.-J. . Mechanical properties of thermosets. *Thermosets* 28–61 (2014) doi:https://doi.org/10.1533/9780857097637.1.28.
28. Xie, K., He, Y., Cai, J. & Hu, W. Thermal conductivity of Nylon 46, Nylon 66 and Nylon 610 characterized by Flash DSC measurement. *Thermochimica Acta* **683**, (2019).
29. Sahu, G., Gaba, V., Panda, S., Acharya, B. & Mahapatra, S. Thermal conductivity, thermal

diffusivity, and volumetric heat capacity of silicone elastomer nanocomposites. *High Performance Polymers* **30**, 365–374 (2017).
30. Plasquy, E., Garcia, J. M., Florido, M. C. & Sola-Guirado, R. R. Estimation of the Cooling Rate of Six Olive Cultivars Using Thermal Imaging. *Agriculture* **11**, 164–164 (2021).
31. Árpád, I. W., Kiss, J. T. & Kocsis, D. Role of the volume-specific surface area in heat transfer objects: A critical thinking-based investigation of Newton's law of cooling. *International Journal of Heat and Mass Transfer/International journal of heat and mass transfer* **227**, 125535–125535 (2024).
32. Luu, T. Impact of Surface Area and Porosity on the Cooling Performance of Evaporative Cooling Devices. (2020).
33. Chen, X., Cheng, L., Gu, J., Yuan, H. & Chen, Y. Chemical recycling of plastic wastes via homogeneous catalysis: A review. *Chemical Engineering Journal* **479**, (2023).
34. What is Heat Flux? (Thermal Flux) | SimWiki. *SimScale* https://www.simscale.com/docs/simwiki/heat-transfer-thermal-analysis/what-is-heat-flux/ (2023).
35. Posselt, B. & Pavlov, G. G. The Cooling of the Central Compact Object in Cas A from 2006 to 2020. *Astrophysical journal/□The □Astrophysical journal* **932**, 83–83 (2022).
36. Comcare. Kitchen appliances - Comcare, Australia. *Office Safety tool* https://www.comcare.gov.au/office-safety-tool/spaces/kitchens/kitchen-appliances (2021).
37. AZO Materials. Properties: Silicone Rubber. *AZoM.com* https://www.azom.com/properties.aspx?ArticleID=920 (2019).
38. Bahrami, M. *Steady Heat Conduction*. https://www.sfu.ca/~mbahrami/ENSC%20388/Notes/Staedy%20Conduction%20Heat%20Transfer.pdf.
39. Jingsourcing. 11 Materials of Kitchen Utensils: How to Choose the Right One? *jingsourcing* https://jingsourcing.com/p/b23-kitchen-utensils-materials/
40. Knauf. The Science of Insulation Explained | Knauf Insulation Australia. *Knauf* https://knauf.com/en-AU/knauf-insulation/competencies/expertise/energy-efficiency/tips-to-keep-warm/science-of-insulation-explained (2024).
41. Sahin, A. Z. & Kalyon, M. Maintaining uniform surface temperature along pipes by insulation. *Energy* 30, 637–647 (2004).
42. Ji, X. L., Zhang, H. H. & Han, S. Y. Transient heat conduction modeling in continuous and discontinuous anisotropic materials with the numerical manifold method. *Engineering Analysis with Boundary Elements* **155**, 518–527 (2023).
43. U.S Department of Energy. Insulation. *Energy.gov* https://www.energy.gov/energysaver/insulation.
44. de Naoum, K. & Conniff, M. Comparing 18/8, 18/10, and 18/0 Stainless Steels. *Xometry.com* https://www.xometry.com/resources/materials/18-8-vs-18-10-vs-18-0-stainless-steel/ (2024).
45. Metals Cut 4U. 304 Vs 316 Stainless Steel: Know The Real Difference. *metalscut4u.com* https://metalscut4u.com/blog/post/304-stainless-steel-vs-316-stainless-steel.html.
46. AZO Materials. Properties: Stainless Steel - Grade 304 (UNS S30400). *AZoM.com* https://www.azom.com/properties.aspx?ArticleID=965
47. *Payne, B. Exploring the Different Types of Tongs for Cooking. Misen https://misen.com/blogs/news/exploring-the-different-types-of-tongs-for-cooking (2024).*

Appendix

Table 1: 40℃ change in temperature over time at the bottom of the handle

Time ± 5s	Trial 1 / ±0.1℃	Trial 2 / ±0.1℃	Trial 3 / ±0.1℃	Trial 4 / ±0.1℃	Trial 5 / ±0.1℃	Average / ℃	Error / ±	Standard Deviation	Ln(Temperature)	ln(T) Error / ±
60	25.4	27.1	27.9	25.1	27.5	26.6	1.4	1.35	3.28	0.05
120	29.1	27.3	27.8	27.7	28.6	28.1	0.9	0.780	3.34	0.03
180	28.1	27.0	29.3	28.6	29.0	28.4	1.2	0.968	3.35	0.04
240	27.3	28.9	28.3	29.7	27.8	28.4	1.2	1.01	3.35	0.04
300	29.0	30.2	28.7	31.5	30.1	29.9	1.4	1.28	3.40	0.05

Table 2: 60℃ change in temperature over time at the bottom of the handle

Time ± 5s	Trial 1 / ±0.1℃	Trial 2 / ±0.1℃	Trial 3 / ±0.1℃	Trial 4 / ±0.1℃	Trial 5 / ±0.1℃	Average / ℃	Error / ±	Standard Deviation	Ln(Temperature)	ln(T) Error / ±
60	33.1	31.8	32.9	31.5	32.2	32.3	0.8	0.793	3.48	0.02
120	32.2	34.8	32.8	33.9	34.3	33.6	1.3	1.16	3.51	0.04
180	33.0	34.8	35.8	35.6	33.8	34.6	1.4	1.28	3.54	0.04
240	33.7	34.5	35.2	35.1	35.5	34.8	0.9	0.690	3.55	0.03
300	35.4	36.7	34.6	37.1	36.2	36.0	1.3	1.16	3.58	0.03

Table 3: 80℃ change in temperature over time at the bottom of the handle

Time ± 5s	Trial 1 / ±0.1℃	Trial 2 / ±0.1℃	Trial 3 / ±0.1℃	Trial 4 / ±0.1℃	Trial 5 / ±0.1℃	Average / ℃	Error / ±	Standard Deviation	Ln(Temperature)	ln(T) Error / ±
60	30.7	32.7	30.9	33.7	32.5	32.1	1.5	1.27	3.47	0.05
120	34.7	34.3	35.6	34.9	35.0	34.9	0.7	0.47	3.55	0.02
180	38.0	36.5	37.6	36.1	37.8	37.2	0.9	0.846	3.62	0.03
240	37.4	39.8	39.5	38.0	39.8	38.9	1.2	1.12	3.66	0.03
300	40.1	38.1	40.6	40.8	39.9	39.9	1.4	1.07	3.69	0.03

Table 4: 40℃ change in temperature over time at the bottom of the handle

Time ± 5s	Trial 1 / ±0.1℃	Trial 2 / ±0.1℃	Trial 3 / ±0.1℃	Trial 4 / ±0.1℃	Trial 5 / ±0.1℃	Average / ℃	Error / ±	Standard Deviation
60	23.0	23.9	22.8	24.1	23.7	23.5	0.7	0.650
120	23.9	23.7	24.8	25.4	25.2	24.6	0.9	0.780
180	23.2	23.9	25.1	24.6	23.2	24.0	1.0	0.829
240	24.1	23.7	25.1	24.8	24.3	24.4	0.7	0.640
300	23.2	24.1	25.2	24.9	23.1	24.1	1.1	0.900

Table 5: 60℃ change in temperature over time at the bottom of the handle

Time ± 5s	Trial 1 / ±0.1℃	Trial 2 / ±0.1℃	Trial 3 / ±0.1℃	Trial 4 / ±0.1℃	Trial 5 / ±0.1℃	Average / ℃	Error / ±	Standard Deviation
60	24.9	25.2	23.8	23.6	23.5	24.2	0.9	0.793
120	24.1	23.7	24.3	24.9	24.0	24.2	0.6	0.500
180	22.9	23.5	23.9	23.1	23.1	23.3	0.5	0.440
240	24.7	25.4	25.5	24.9	25.5	25.2	0.4	0.386
300	23.2	24.4	24.5	23.8	23.6	23.9	0.7	0.600

Table 6: 80℃ change in temperature over time at the bottom of the handle

Time ± 5s	Trial 1 / ±0.1℃	Trial 2 / ±0.1℃	Trial 3 / ±0.1℃	Trial 4 / ±0.1℃	Trial 5 / ±0.1℃	Average / ℃	Error / ±	Standard Deviation
60	24.1	25.1	24.9	24.0	24.9	24.6	0.6	0.510
120	25.1	25.5	26.1	26.0	25.3	25.6	0.5	0.440
180	24.6	24.3	25.7	25.1	24.8	24.9	0.7	0.534
240	25.3	24.7	24.6	25.9	25.0	25.1	0.6	0.520
300	23.9	24.3	25.0	24.8	23.5	24.3	0.8	0.620

Sample calculations for calculating the convection constant

$$\frac{T-T_\infty}{T_b-T_\infty}=\frac{\cosh m(L-x)+\left(\frac{h}{mk}\right)\sinh m(L-x)}{\cosh mL\ +\left(\frac{h}{mk}\right)\sinh mL}, m^2=\frac{hP}{kA_c}$$

$$P=\pi D=\frac{1.7\pi}{100}, k=0.15, A_c=\pi\left(\frac{D}{2}\right)^2=\pi\left(\frac{1.7}{2\times 100}\right)^2, L=0.269, T_\infty=23℃, x=0.269$$

$$\frac{T-23}{T_b-23}=\frac{\cosh m(0.269-0.269)+\left(\frac{h}{0.15m}\right)\sinh m(0.269-0.269)}{\cosh 0.269m\ +\left(\frac{h}{0.15m}\right)\sinh 0.269m}, m^2=\frac{h\pi\left(\frac{1.7}{100}\right)}{0.15\pi\left(\frac{1.7}{2\times 100}\right)^2}$$

For the 40 degrees 60s calculation using the temperature at the top of the spoon and the temperature at the base.

$$T=23.5, T_b=26.6$$

$$\frac{23.5-23}{26.6-23}=\frac{1}{\cosh 0.269m\ +\left(\frac{h}{0.15m}\right)\sinh 0.269m}, m^2=\frac{h\pi\left(\frac{1.7}{100}\right)}{0.15\pi\left(\frac{1.7}{2\times 100}\right)^2}$$

$$h=0.061$$

Table 7: value of the respective convection constants (Note: those underlined and italicised are outliers and were not counted towards the average)

Time / s	**40**℃	**60**℃	**80**℃
60	0.061	0.064	0.051
120	*0.029*	0.071	0.039
180	0.048	*0.16*	0.063
240	0.035	0.048	0.063
300	0.055	*0.097*	*0.091*

Biot number calculations

$$L_c=0.017$$

$$50<h<3000, 0.1, k<0.2$$

$$Bi=\frac{hL_c}{k}$$

$$4.25\leq Bi\leq 510$$

Uncertainty calculations for ln [15]

$$\delta ln(T)=\frac{error}{average}$$

Example calculation for 40 degrees at 60s

$$\delta ln(T)=\frac{1.4}{26.6}=\pm 0.05$$

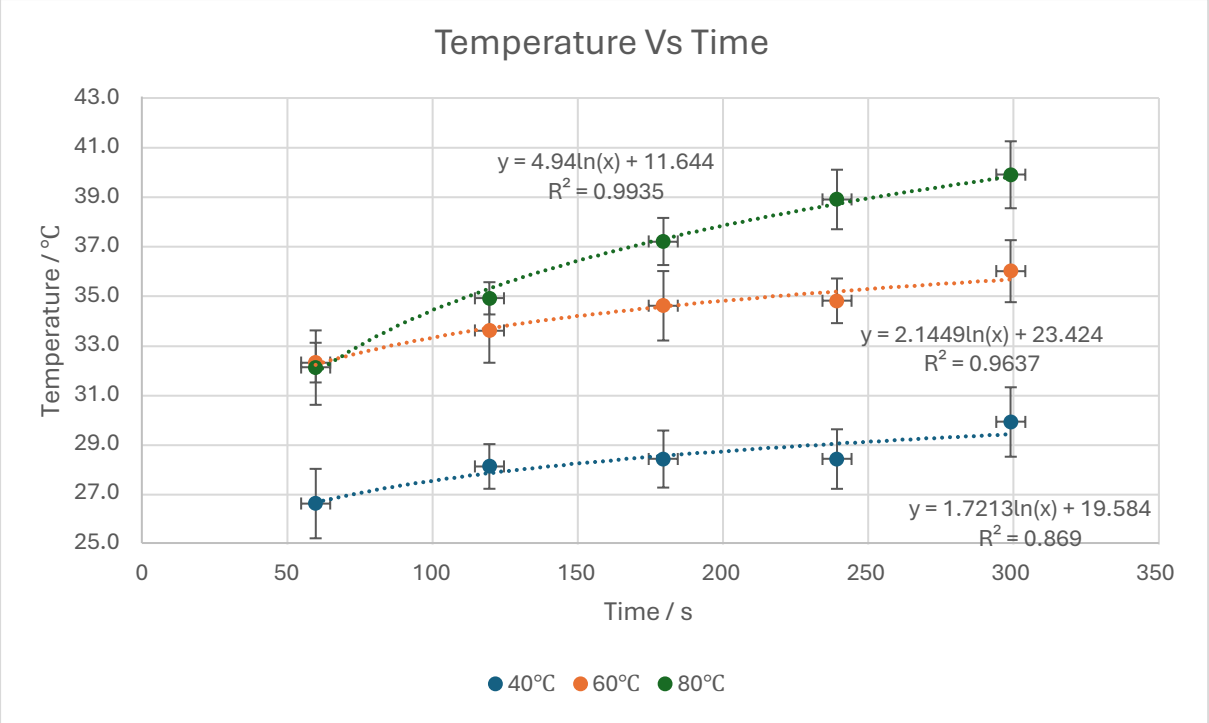

Figure 7: non linearised graph of the transient heat at the base of the handle of the wooden spoons for different temperatures of water

Table 8: Change in temperature at end of ladle handle

Time(s) ±3	Reading 1 / ±0.1℃	Reading 2 / ±0.1℃	Reading 3 / ±0.1℃	Reading 4 / ±0.1℃	Reading 5 / ±0.1℃	Mean / ℃	Error / ±	Standard deviation
0	25.9	26	26	25.9	25.7	25.9	0.15	0.012
10	26.1	26.2	26.1	26.3	25.9	26.1	0.2	0.018
20	27.3	26.9	27.2	27	26.6	27	0.35	0.06
30	25.4	25.7	25.1	25.2	25.6	25.4	0.3	0.052
40	24.5	25	25	25	24.5	24.8	0.25	0.06
50	25.9	25.8	25.6	25.8	25	25.6	0.45	0.106
60	25.4	25.7	25.4	25.9	25.7	25.6	0.25	0.038
70	25.1	25	25	25.3	25.1	25.1	0.15	0.012
80	26.3	26.3	26	26.4	26.5	26.3	0.25	0.028
90	26.2	26.2	26.4	26.2	25.6	26.1	0.4	0.074
100	25.2	25.3	25.4	25	25.6	25.3	0.3	0.04
110	24.8	24.8	24.5	24.5	24.9	24.7	0.2	0.028
120	24.6	24.6	24.7	24.7	24.9	24.7	0.15	0.012
130	25.6	25.1	25.1	25.1	25.6	25.3	0.25	0.06
140	25.3	25.1	25.2	25	25.4	25.2	0.2	0.02
150	25.1	25.1	25.4	25.1	25.9	25.3	0.4	0.098
160	24.7	24.8	25.1	24.7	25.2	24.9	0.25	0.044
170	24.8	24.4	24.9	24.6	24.4	24.6	0.25	0.042
180	24.8	24.6	24.6	24.2	24.3	24.5	0.3	0.048
190	24.6	24.5	24.6	24.5	25.4	24.7	0.45	0.118
200	25.5	25.5	25.3	25.7	25.9	25.6	0.3	0.042
210	24.9	24.8	24.9	24.7	25.2	24.9	0.25	0.028
220	25.3	25.6	25.2	25.4	25	25.3	0.3	0.04
230	25.6	25.9	25.7	25.6	26.2	25.8	0.3	0.052
240	27.5	27.1	27.6	27.1	27.7	27.4	0.3	0.064
250	25.5	25.3	25.5	25.7	25	25.4	0.35	0.056
260	25.1	25.3	25.4	25.3	25.3	25.3	0.15	0.01
270	24.7	25.2	24.9	25.1	24.6	24.9	0.3	0.052
280	25.2	25	25.3	25	25	25.1	0.15	0.016
290	25	24.8	25	24.9	24.2	24.8	0.4	0.09
300	24.9	24.8	25.1	24.9	24.3	24.8	0.4	0.072

Table 9: Change in temperature at end of spatula handle

Time (s) ±3	Reading 1 / ±0.1℃	Reading 2 / ±0.1℃	Reading 3 / ±0.1℃	Reading 4 / ±0.1℃	Reading 5 / ±0.1℃	Mean / ℃	Error / ±	Standard deviation
0	25.5	25.3	25.4	25.2	25.5	25.4	0.15	0.014
10	24.9	25.1	25	25.4	25.1	25.1	0.25	0.028
20	24.4	24.3	24.4	24	23.9	24.2	0.25	0.044
30	23.6	23.7	23.9	23.5	23.4	23.6	0.25	0.03
40	27	27	26.9	27.5	27.6	27.2	0.35	0.084
50	25.2	25.3	25	25.2	24.9	25.1	0.2	0.022
60	24	24.3	24.6	24.5	24.1	24.3	0.3	0.052
70	23.4	23.8	23.3	23.8	23.2	23.5	0.3	0.064
80	25.2	25.1	25	25.1	24.2	24.9	0.5	0.134
90	24.5	24.8	24.7	24.3	24.7	24.6	0.25	0.032
100	25.2	25.1	25.6	25.3	25.3	25.3	0.25	0.028
110	25.3	25.4	25.2	25.1	25.5	25.3	0.2	0.02
120	25.9	25.5	25.7	25.5	25.9	25.7	0.2	0.032
130	25.2	25.6	25.7	25.7	24.9	25.4	0.4	0.102
140	25.4	25.4	25.1	24.9	25.1	25.2	0.25	0.038
150	24.5	24.4	24.4	24.3	25.3	24.6	0.5	0.134
160	24.8	24.4	24.9	24.5	24.9	24.7	0.25	0.044
170	24.6	24.7	25	24.7	25.4	24.9	0.4	0.086
180	24.6	24.6	24.8	24.7	24.3	24.6	0.25	0.028
190	24.6	24.5	24.4	24.6	25.4	24.7	0.5	0.128
200	24.5	24.6	24.7	24.7	24.5	24.6	0.1	0.008
210	24.6	24.6	24.5	24.9	24.9	24.7	0.2	0.028
220	24.5	24.9	25	25	24.6	24.8	0.25	0.044
230	24.5	24.5	24.7	24.5	24.9	24.6	0.2	0.026
240	24.7	24.6	24.8	24.5	25.4	24.8	0.45	0.1
250	24.5	24	24.3	24.2	24.5	24.3	0.25	0.036
260	24	24.3	24.1	23.7	23.9	24	0.3	0.04
270	24.6	24.6	24.6	24.7	24.5	24.6	0.1	0.004
280	23.9	23.8	23.9	24.3	24.1	24	0.25	0.032
290	23.6	24	23.8	23.8	23.7	23.8	0.2	0.018
300	23.5	23.8	23.9	23.7	24.1	23.8	0.3	0.04

Surface area for spatula

Dimensions of head:

Width(w) = 8.9cm
Length(l) = 9.8cm
Thickness(t) = 0.2cm
Radius of holes(r_h) = 0.35cm

Front and Back surface area of spatula head:

$$A_f = wl = 8.9cm * 9.8cm = 87.42cm^2$$

$$A_B = A_f = 87.42cm^2$$

Surface area of side of spatula head:

$$A_s = 2wt + 2lt = 2 * 8.9cm * 0.2cm + 2 * 9.8cm * 0.2cm = 7.48cm^2$$

Area of one hole:

$$A_h = \pi r^2 = \pi 0.35^2 = 0.385cm^2$$

Surface area of inner edge of one hole

$$A_I = 2\pi rt = 2 * \pi * 0.35cm * 0.2cm = 0.44cm^2$$

Total surface area of spatula head:

$$A_{spat} = \left(A_f - 16A_h\right) + (A_B - 16A_h) + A_S + 16A_I = 177.04cm^2$$

Surface area of Ladle:

Dimensions of head:

Depth(D) = 5.9cm
Left to right radius(r_s) = 5.05cm
Front to back radius (r_l) = $5.2cm$

Outer surface area of ladle head:

$$A_O = 2\pi\left(\frac{(r_s \times r_l)^{1.6075} + (r_s \times D)^{1.6075} + (r_l \times D)^{1.6075}}{3}\right)^{\frac{1}{1.6075}} = 181.90cm^2$$

Inner surface area of ladle head:

$$A_I = 2\pi\left(\frac{((r_s - 0.2) \times (r_l - 0.2))^{1.6075} + ((r_s - 0.2) \times (D - 0.2))^{1.6075} + ((r_l - 0.2) \times (D - 0.2))^{1.6075}}{3}\right)^{\frac{1}{1.6075}} = 168.62cm^2$$

Surface area of side of ladle:

$$A_s = \Pi\pi r_l - \pi(r_s - 0.2)(r_l - 0.2) = 6.31cm^2$$

Total surface area of ladle head:

$$A_{lad} = A_O + A_I + A_S = 356.83cm^2$$

Volume of spatula head:

Volume of spatula head, not accounting for holes:

$$V_{rect} = wlt = 8.9cm \times 9.8cm \times 0.2cm = 17.44cm^3$$

Volume of one cylindrical hole:

$$V_{hole} = \pi r^2 t = \pi \times (0.35cm)^2 \times 0.2cm = 0.08cm^3$$

Total volume of spatula head:

$$V_{spat} = V_{rect} - 16V_{hole} = 16.16cm^3$$

Volume of ladle head:

Volume of a semi ellipsoid:

$$V_{full} = \frac{4}{3}\pi r_s r_l D = \frac{4}{3}\pi \times 5.05cm \times 5.2cm \times 5.9cm = 648.99cm^3$$

Volume of inner semi ellipsoid:

$$V_{inner} = \frac{4}{3}\pi(r_s - t)(r_l - t)(D - t) = \frac{4}{3}\pi \times 4.85cm \times 5cm \times 5.7cm = 579.00cm^3$$

Total volume of ladle head:

$$V_{lad} = V_{full} - V_{inner} = 69.99cm^3$$

Volume specific surface area of spatula head:

$$\omega_{spat} = \frac{A_{spat}}{V_{spat}} = \frac{177.04cm^2}{16.16cm^3} = 10.96cm^{-1}$$

Volume specific surface area of ladle head:

$$\omega_{lad} = \frac{A_{lad}}{V_{lad}} = \frac{177.04cm^2}{69.99cm^3} = 5.10cm^{-1}$$

Heat Flux calculation for ladle

$$\boldsymbol{q} = \frac{\boldsymbol{k_x A_x}(\Delta \boldsymbol{T})}{\boldsymbol{L_x}}$$

K_{lad} = 0.32W/m·k, $A_{lad} = \pi(\frac{d}{2})^2 = \pi(\frac{0.025}{2})^2 = 4.91 \times 10^{-4}m^2, L_{lad} = 0.227m$

$$\boldsymbol{q} = \frac{0.32 * 4.91 \times 10^{-4}(\Delta \boldsymbol{T})}{0.227}$$

$$q_{avg} = 0.015W$$

Heat flux calculation for spatula

$$\boldsymbol{q} = \frac{\boldsymbol{k_x A_x (\Delta T)}}{\boldsymbol{L_x}}$$

K_{spat} = 0.26W/m·k, $A_{spat} = \pi(\frac{0.028}{2})^2 = 6.16 \times 10^{-4} m^2$, $L_{spat} = 0.273m$

$$\boldsymbol{q} = \frac{0.26 * 6.16 \times 10^{-4} (\Delta \boldsymbol{T})}{0.227}$$

$$q_{avg} = 0.015W$$

Table 10: 60°C change in temperature over time at bottom of handle of stainless steel tongs

Time ± 5s	Trial 1 / ± 0.1℃	Trial 2 / ± 0.1℃	Trial 3 / ± 0.1℃	Trial 4 / ± 0.1℃	Trial 5 / ± 0.1℃	Average / °C	Error / ±	Standard deviation
60	44.2	43.6	46.1	47.5	46.1	45.5	2	1.583
120	49.3	48.1	50.1	49.5	49	49.2	1.1	0.735
180	57.9	57.4	58.1	58.9	59.2	58.3	0.9	0.738
240	54.7	56.2	56.8	58.6	57.2	56.7	2	1.425
300	58.7	58.9	60.2	59.7	59.5	59.4	0.8	0.608

Table 11: 60°C change in temperature over time at bottom of handle of insulated stainless steel tongs

Time ± 5s	Trial 1 / ± 0.1℃	Trial 2 / ± 0.1℃	Trial 3 / ± 0.1℃	Trial 4 / ± 0.1℃	Trial 5 / ± 0.1℃	Average / ± 0.1℃	Error / ±	Standard deviation
60	33	34.1	35.4	34.9	33.6	34.2	1.2	0.967
120	36.1	35.8	37.2	36.9	36	36.4	0.8	0.612
180	38.3	37.9	38.8	38.5	38	38.3	0.5	0.367
240	40.4	40.4	40.1	39.8	39.3	40	0.7	0.464
300	43.3	44.1	43.2	43.4	44.5	43.7	0.8	0.570

Insulated stainless steel tongs heat conduction constant calculations:

$$m = \rho_{Silicone} V = \rho_{Silicone} \times (L \times w \times T_h) = 1100 \frac{kg}{m^3} \times (0.02m \times 0.029m \times 0.006m)$$
$$= 3.828 \times 10^{-3} kg$$

$$\frac{dT}{dt} = \frac{T_{Final} - T_{Initial}}{t} = \frac{43.7°\boldsymbol{C} - 23°\boldsymbol{C}}{300s} = 0.069 \frac{K}{s}$$

$$q = m \times c_{p-s} \times \frac{dT}{dt} = (3.828 \times 10^{-3} kg) \times (1050 \frac{J}{kg \cdot K}) \times (0.069 \frac{K}{s}) = 0.2773 \frac{J}{s}$$

$$\frac{dT}{dx} = \frac{T_{Final} - T_{Initial}}{d} = \frac{43.7°\boldsymbol{C} - \boldsymbol{23°C}}{0.269m} = 79.95\frac{K}{m}$$

$$k = \frac{q}{A} \times \frac{dT}{dx} = \frac{0.2773\frac{J}{s}}{0.006m \times 0.029m} \times \frac{1}{79.95\frac{K}{m}} = 19.93\frac{W}{m \cdot K}$$

Stainless steel tongs heat conduction constant calculations:

$$m = \rho_{SS}V = \rho_{SS} \times (L \times w \times T_h) = 7930\frac{kg}{m^3} \times (0.02m \times 0.031m \times 0.001m)$$
$$= 4.9166 \times 10^{-3}kg$$

$$\frac{dT}{dt} = \frac{T_{Final} - T_{Initial}}{t} = \frac{59.4°\boldsymbol{C} - \boldsymbol{23°C}}{300s} = 0.1213\frac{K}{s}$$

$$q = m \times c_{p-s} \times \frac{dT}{dt} = (4.9166 \times 10^{-3}kg) \times (490\frac{J}{kg \cdot K}) \times (0.1213\frac{K}{s}) = 0.292\frac{J}{s}$$

$$\frac{dT}{dx} = \frac{T_{Final} - T_{Initial}}{d} = \frac{59.4°\boldsymbol{C} - \boldsymbol{23°C}}{0.32m} = 113.75\frac{K}{m}$$

$$k = \frac{q}{A} \times \frac{dT}{dx} = \frac{0.292\frac{J}{s}}{0.001m \times 0.031m} \times \frac{1}{113.75\frac{K}{m}} = 82.8\frac{W}{m \cdot K}$$

Stainless steel tongs heat conduction constant percent error calculation:

$$PE = \left| \frac{82.8\frac{W}{m \cdot K} - 16.2\frac{W}{m \cdot K}}{16.2\frac{W}{m \cdot K}} \right| \times 100\% = 411.1\%\ error$$

The Sydney Journal of Interdisciplinary Engineering
SJIE 1(2) X–X (2025) https://doi.org/XXXX/XXXX

Investigating the rate of heat transfer through chocolate varieties

Toby Downes[1], Douglas Cameron[1], Braden Raffo[1], Hamyung Jang[1], Sebastian D. Flores[1], Juanita S. Perez[1], Minghao Zhang[1] , David Alam[1] and Gobinath Rajarathnam[1]

[1] School of Chemical and Biomolecular Engineering, University of Sydney, Sydney, Australia

E-mail: dcam0225@uni.sydney.edu.au

Received 4/4/25
Accepted for publication xxxxxx
Published xxxxxx

Abstract

This study investigates the effect of different chocolate fillings on the rate of conductive heat transfer through various chocolate bars. Using four varieties from Cadbury's 'Favourites'; Dairy Milk, Caramilk, Cherry Ripe, and Crunchie, the experiment used hotplates set to 70 °C to heat the chocolates, and IR cameras to measure both inner and surface temperatures as the chocolates were heated. The setup was designed to mimic a squat rectangular fin in order to allow for analysis based on Fourier's law in order to estimate the heat flux through the chocolates. Data was collected through manual repositioning of the IR camera, however technical limitations in the IR camera software necessitated the use of linear interpolation to recover data. This encompassed both the Dairy Milk and Crunchie datasets, but only Dairy Milk could be successfully recovered. While limited, the results indicate that Cherry Ripe exhibits delayed heat conduction compared to chocolates with no filling such as Dairy Milk and Caramilk. Despite the uncertainties introduced by measurement variability, convective heat losses that were not accounted for, and the destruction of the Crunchie thermal data, the findings indicate that further research should be done into the thermal performance of filled versus non-filled chocolates in order to optimise manufacturing processes and improve the thermal resistance of chocolate products in warm environments.

1. Introduction

While the mechanics and rate of heat transfer through chocolate may seem an irrelevant field of study, it is highly relevant to globalised chocolate manufacturers such as Cadbury and Hershey, where any melting or softening of their products can cost millions of dollars. This is especially relevant in warm climates such as Australia, where summer temperatures can regularly exceed 33.8 °C, the temperature at which chocolate generally melts as the solid cocoa butter transitions to liquid [1]. It is therefore critical in these environments to consider the thermal properties of chocolate in order to provide guidelines on refrigeration, maximum environmental exposure times and, if these guidelines prove to be too restrictive or inefficient, potential additives to increase the melting point of the chocolate.

1.1 Literature review

Due to the industrial relevance of the subject matter, this field has been researched extensively, with particular focus on various techniques for adjusting thermal properties, as well as how they affect manufacturing viability and consumer sentiment. D. Bikos et al. [2] highlights how micro-aeration can be used to increase specific heat capacity by 10%, as well as decrease thermal conductivity by 20%, however, this technique can affect both the flavour profile and the texture of the chocolate. H. Tewkesbury et al. [3] demonstrates how different polymorphic forms of chocolate have different properties, with Form V possessing the most desirable confectionery. Unfortunately, Form V is difficult to achieve through simple cooling, and specialised 'cooling tunnels' must be used in order to achieve specific temperature control [3]. While temperature is highly controlled during

manufacturing, it is almost impossible to maintain a similar level of control during shipping and sale, and as such, many heat-related issues can present. These are investigated by both R.E. Timms [4] and P. Figoni [5], and include seizing [5] as well as sugar and fat bloom [4]. They elucidate how heat can contribute to seizure of chocolate, where molten chocolate is vulnerable to small amounts of water or polyols incorporating into it and causing it to become an unusable solid-like chocolate mass [5]. They also discuss the blooming of sugar and fat, where sugar is recrystallised on the surface of the chocolate and the solid fat phase grows [4]. These defects create highly undesirable properties in the chocolate, and as such, attempts are made to avoid them, mostly through storage at 18-20 °C and less than 50% humidity [1]. Attempts are also made through manipulation of chocolate's thermal properties, via the micro-aeration mentioned earlier in [2], or through Ethylcellulose, Interesterification of Cocoa Butter and Water-in-Oil Emulsion-Based Chocolate techniques evaluated in [1]. Unfortunately, none of these techniques achieve simple, cost-effective and highly heat-resistant results while maintaining the taste profile and mouthfeel of the chocolate. While further research should be done on the manufacture of heat-resistant chocolates, it is also industrially relevant to consider the effects on heat transfer that common chocolate fillings have. This is in order to determine whether certain varieties of chocolate should use current techniques for manufacturing of heat-resistant chocolate that have greater costs and produce a less desirable product for consumers. This is the area which this paper seeks to investigate, as despite the breadth of research on the thermal properties of chocolate in general, there is a large focus on the performance of pure milk chocolate, with little to no consideration of how fillings affect these properties.

1.2 Objectives

As indicated briefly in the literature review, this article will investigate the effects of chocolate fillings on heat transfer, specifically conduction, as due to the position of the filling inside the chocolate, it is the only method of heat transfer that is directly relevant to the thermal effects of the filling. While it is not directly related, convection will also be addressed briefly in relation to the experimental conditions and limitations. This research is relevant due to the current lack of fully effective heat resistant chocolate manufacturing techniques [1]. It is therefore desirable to evaluate how fillings affect the heat resistance of chocolate, in order to determine if specific confections can avoid utilising production methods that increase cost or reduce the consumer appeal of the product.

2. Methods

2.1 Experimental setup

In order to examine how chocolate fillings affect heat transfer through conduction, hotplates set to 70 °C were used to provide heat to the chocolates, while InfiRay Pro 2 IR cameras were used to measure the temperatures of the chocolates. Hotplates were set up with a small water-filled beaker for calibration and a thin piece of wax paper on which three identical chocolates were placed. This experimental setup can be found in Figure 1. The chocolates were placed on wax paper on top of the hotplate in order to protect the hotplates from melting chocolate while having minimal impact on heat transfer due to the thinness of the paper sheets (<1mm). As the precise melting point of the chocolates was unknown, and the aim of the experiment was focussed on the rate of heat transfer rather than any specific changes in the material properties of the chocolate as it heated, the chocolates were heated to 55 °C surface temperature rather than the melting point.

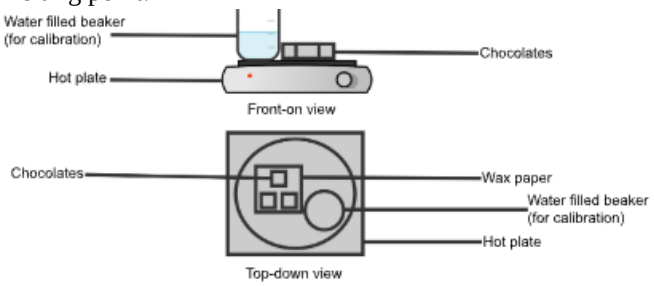

Figure 1: Experimental Setup

2.2 Chocolate selection and preparation

In selection for the chocolate varieties we would test, we chose four types of Cadbury chocolates that are all found in 'Favourites', and all chocolates were sourced from the same box for standardisation of age. The chocolates chosen were: Dairy Milk, as a control with no filling; Caramilk, to determine how a different variety of chocolate affects heat transfer (although this choice may have been a mistake, as it would be more beneficial to specialize the experiment for chocolate filling only); Cherry Ripe, to test how the viscous liquid cherry filling affects heat transfer; and Crunchie, to determine how solid honeycomb affects heat transfer. Before the chocolates were heated, they were bisected, measured for the cross sectional area of the bottom, and weighed. This was done in order to allow for standardisation in the data.

2.3 Data collection and analysis

Due to limitations in the IR camera software, only three points could be used to measure temperature. In order to circumvent this limitation, the cameras were handheld and the points were periodically moved from the center of the chocolates to the top surface in order to obtain measurements for both inner and surface temperature. Unfortunately, this

movement introduced a large amount of variability in the data as the points were not taken in the exact same location each time.

2.4 Converting RGB values to temperature

Data from some of the videos was unfortunately obscured due to technical errors. However, the first half of the videos was able to collect data, which enabled the use of linear interpolation to predict the temperatures, given the RGB values of the video. This technique was effective in capturing the data for the Dairy Milk temperatures, however it failed on the Crunchie, as there was not enough data to form an accurate linear interpolation. The RGB values matched the predicted structure following the color spectrum, where the blue values were highest at the lowest temperature, green values were highest at the median temperature, and red values were highest at the highest temperature. This can be seen in Figure 2 below, where as the temperature increases, the RGB units of blue decrease, units for green reach its peak at the middle, and the units for red increase.

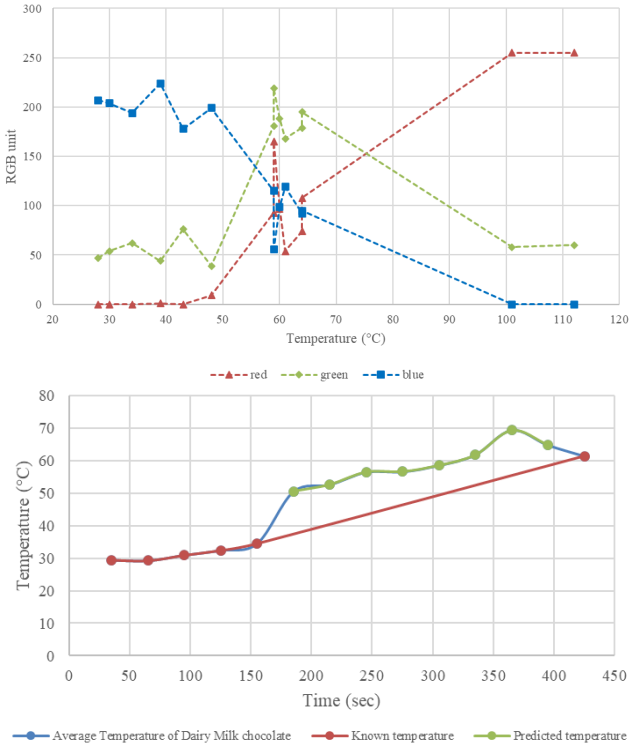

Figure 2: (top) Relationship between RGB values and temperature. (bottom) Relationship of the known temperature and the predicted temperature of the Dairy Milk chocolate

Although the scale differs, the correlation between RGB values and temperature aligns with the color space. This alignment supports the validity of employing linear interpolation to estimate temperature based on RGB values. However, due to the missing data for the range of 30 °C to 60 °C, the linear interpolation was not as accurate. As shown in the bottom graph of Figure 2, the predicted temperatures exhibit noticeable deviations from the known temperatures. The nature of linear interpolation requires the linear prediction of the two nearest data points. Thus, as seen in the bottom graph of Figure 2, the predicted temperatures at the ranges 30 °C to 60 °C were not as accurate.

3. Results and Discussion

In order to conduct analysis on the effect of various chocolate fillings on the melting characteristics and thermal conductivity, thermal camera data was collected to measure the internal and surface temperatures of the chocolates over time. Thermal shots of the sides of the chocolates were also taken to observe how the heat transferred through the chocolate from the bottom in contact with the hotplate, through the centre where the side shots measured the temperatures, to the surface where the temperature was also monitored. This data collection was completed for the Cherry Ripe, Caramilk, and Dairy Milk varieties from Cadbury's favorites range. The full tabulated data can be found in the supplementary and is also shown in Figures 3, 4 and 5 below, error bars were also added and calibrated to the standard deviations of the gathered data.

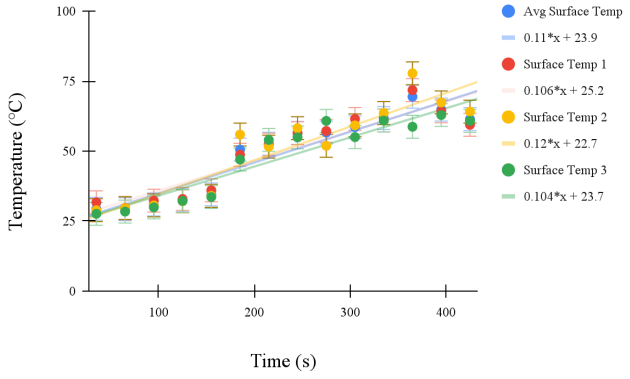

Figure 3: Temperature versus time for Dairy Milk

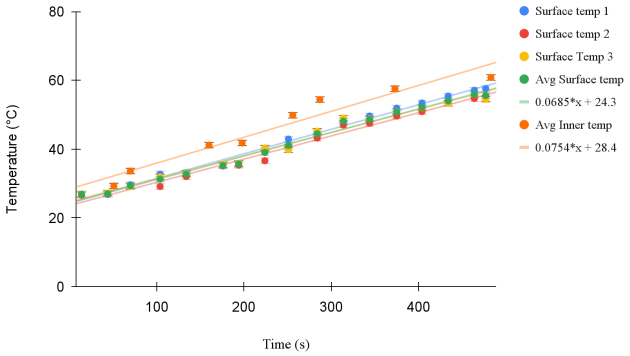

Figure 4: Temperature versus time for Cherry Ripe

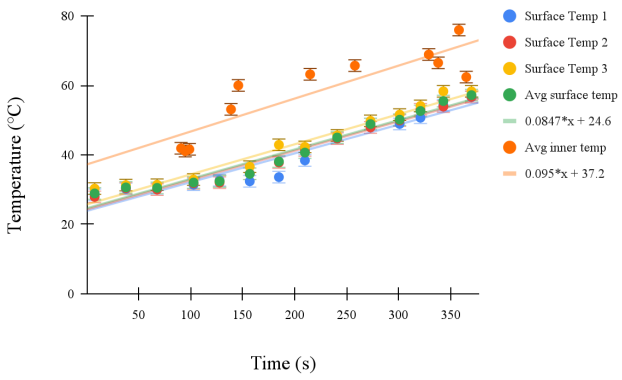

Figure 5: Temperature versus time for Caramilk

3.1 Appropriate modelling of heat transfers occurring

In order to analyse these results correctly, we must first consider the types of heat transfer acting within the melting chocolate model system, as well as the points at which these occur and how changing the type of chocolate could potentially affect the heat transfer throughout the system. When considering the physical situation of the chocolate sitting on top of the hotplate, it can be considered analogous to a rectangular fin, except where fins are typically long and thin in order to maximise surface area for heat dissipation, the chocolate is wide and short. Nevertheless, the heat transfer principles can be applied in the same way. This means that there is conductive heat transfer moving from the hot plate through the chocolate, where it eventually reaches the surface of the chocolate and then convective heat transfer occurs from the surface of the chocolate. It is important to note that all convection within the experimental design was natural convection rather than forced convection. See Figure 6 for a visual representation of the model.

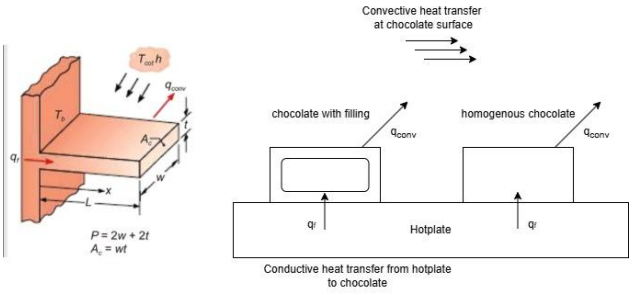

Figure 6: Rectangular fin heat transfer diagram to model heat transfer components present within our experimental design [6]

Once these concepts are established, it is clear that our data is investigating the differences in the heat distribution as well as the rate of heat distribution caused by differences in composition between chocolates. The utilisation of this fin model to analogise chocolate melting on a hotplate was inspired by M. M. Dreger et al's work in [7]. While the fin model is accurate to model our experiment, as mentioned earlier in the objectives of the experimental design, the primary focus of the experiment was on the inner thermal conductivities of the chocolate rather than the convective heat transfer. Therefore, the convection heat transfer element was left out completely in order to focus more fully on the conductive properties of chocolate. While applying Newton's law of cooling in order to account for convective heat transfer as well as taking into account the transient conditions of the temperature distribution within the chocolate would allow for a more accurate analysis, it is simply not feasible for the scope of this experiment. This is a considerable limitation within the experimental design, however potential error margins due to omitting this are discussed and quantified in 3.4.

3.2 Qualitative analysis of data

Figures 4 and 5 show that, using the Caramilk data as a baseline for homogenous chocolates, the coconut centre filling within the Cherry Ripe has caused it to conduct heat through it much slower. This is indicated by the 370 second experiment runtime for the Caramilk to reach a surface temperature of 57°C, whereas the Cherry Ripe took 477 seconds to reach a similar surface temperature of 55°C. This means the Cherry Ripe took approximately 29% longer to reach the same surface temperature as the Caramilk despite the relatively smaller distance the heat had to travel through the Cherry Ripe. The Cherry Ripe's 1.2cm height being characteristically shorter than the standard height of the Cadbury Dairy Milk or Caramilk share size bars [8] (This height was obtained by assuming that the width of a standard size Cherry Ripe and the share size Cherry Ripe are the same, which is reasonable as they appear to differ in only length, not width or height). Further, Dairy Milk was the fastest to reach the same temperature at 245 seconds, indicating that the homogenous Dairy Milk chocolate composition has the highest thermal conductivity. This is not certain however, as the Dairy Milk data is far less reliable due to the method of obtaining data values via linear interpolation of RGB values rather than direct temperature measurements. This difference in time to reach the same temperature indicates that the Cherry Ripe has a lower thermal conductivity, likely due to the different composition of the dark chocolate layers and/or from the coconut cherry filling. These layers also likely hold different thermal resistivities due to their different composition compared to the Dairy Milk and Caramilk which also impede its ability to conduct heat. The faster heating rate of the Dairy Milk comparatively to the Caramilk indicates that its composition must lend itself to conduct heat better as they both have the exact same dimensions. Furthermore, the difference between the inner and outer temperature

measurements on the Cherry Ripe data is much less than that of the Caramilk as observed in Figure 4 by the difference in the trendline intercept point differences. Where the Cherry Ripe inner to surface temperature difference was 28.4-24.3 = 4.1 °C, the Caramilk had a difference of 37.2-24.6 = 12.6 °C (roughly a 3x difference). This may seem to indicate a higher thermal conductivity for the Cherry Ripe, but it is quite possible that this large difference is simply due to the thickness difference between the chocolates.

3.3 Compositions of chocolate

According to [9], the main differences in composition between dark, milk and white chocolate are the ratios between sugar, cocoa liquor, cocoa butter and full cream milk powder used when creating the product. This is in agreement with the ingredient information on the official Cadbury websites for product information for the Cherry Ripe and Caramilk [10],[11]. The Cherry Ripe is advertised as composed of a dark chocolate outer coating with a centre filling, a mix of coconut and glace cherries (cherries mixed with wheat glucose syrup) as the main components. The Caramilk is advertised as a 'Caramelised White Chocolate' [11] and so is presumably of a similar composition to white chocolate. This means that the Caramilk is composed of around 47% sugar, 31% cocoa butter and 21.5% full cream milk powder and the Cherry Ripe dark chocolate component is 39.52% sugar, 53% cocoa liquor and 7% cocoa butter[9]. These differences in compositions affect the physical properties of each chocolate and so it is important to be aware of them.

3.4 Calculating experimental thermal conductivity

While the effect of convection will be disregarded in calculations of thermal resistance for simplicity, the effect that the convective heat transfer has on the results can be estimated by observing the differences in the gradient of the inner vs outer temperature trendlines. This is because in a system where there is no convective heat transfer present, they would have the same gradient as the two points should theoretically heat at the same rate. The only difference being one lagging behind the other due to distance from the source of heat. However, since there was convective heat transfer present within the obtained experimental data, we can attribute the differences in gradient to this and use the difference to estimate the relative error throughout our results for thermal conductivity data via purely conductive calculations. By taking a percentage difference between the trendline gradients, we get a relative error of 1 - 0.0847/0.095 = 10.8% for the Caramilk values and a relative error of 1 - 0.0685/0.0754 = 9.2% for the Cherry Ripe values. The inability to account for the convective heat transfer within our experimental design is a considerable limitation, however, since the focus of the experiment is to investigate the effect of fillings within the chocolates on the conductive heat transfer, it is acceptable.

To calculate the heat flux through the chocolates, we can use Fourier's Law (1).

$$q = k\frac{dT}{dx} = k\frac{T_{Inner} - T_s}{L} \quad (1)$$

Where k = 0.26W/K.m is the thermal conductivity of the chocolate[12], T_s is the surface temperature of the chocolate, T_{inner} is the inner temperature of the chocolate and for Cherry Ripe L = 0.012/2 = 0.006m, and for Caramilk L = 0.015/2 = 0.0075m [13] (closest available measurements) (halved since measurements were taken roughly halfway through the chocolate). We will use documented values from literature to find k [7] and then calculate the heat flux. Using the heat flux the total thermal resistivity can be determined (2) and then the thermal resistivity split into its component parts (3). [14]

$$q = \frac{T_H - T_s}{R_T} \quad (2)$$

Where T_H = 90 C^o and is the temperature of the hotplate

It is important to note that since the experimental heat flux value was not measured it is not possible to calculate the experimental thermal conductivity of any of the chocolates or component fillings. To get around this, a standard thermal conductivity value of chocolate was taken from available literature [12] which falls within the expected range among other sources available. However the calculations conducted are not of an extremely high accuracy due to this fact as some data had to be supplemented from outside sources. As a result, the values obtained may not be accurate but they are still comparatively useful as any error is systematic, so the chocolates can still all be compared to each other effectively.

$$R_T = R_1 + R_2 + R_3 = \frac{L_1}{k_1} + \frac{L_2}{k_2} + \frac{L_3}{k_3} \quad (3)$$

Since a single unit area is used, the A term is omitted. Using literature values for k value of the cherry filling we can find their specific thermal resistivity. Knowing that the cherry filling is a mix of cherries, coconut and sugar it is expected that its thermal conductivity is somewhere from 0.3-0.49 as it would fall between a sugar heavy composition and water heavy composition [15]. However, after isolating the cherry filling thermal conductivity value, it was back calculated as k=0.0676W/K.m which aligns with the experimental results as it took much longer for the Cherry Ripe to reach its final temperature. The length of dark chocolate coating was estimated at 1mmx2 for each side.

Table 1: Calculated thermal resistivity for different chocolate layers via approximated thermal conductivity using (3) and total thermal resistivity

Layer	Dairy Milk	Caramilk	Cherry Ripe
	K.m/W	K.m/W	K.m/W
R_T	0.0769	0.120	0.156
Dark Choc	N/A	N/A	0.00769
Cherry Filling	N/A	N/A	0.148

These thermal resistivity values are valuable as they are inversely proportional to the thermal conductivity of their components. Figure 7 shows a diagram for how the thermal resistivity circuit would appear within the Cherry Ripe. The Dairy Milk and Caramilk diagrams would be the same except only one layer as they are homogenous, hence why they only have one resistivity value in Table 1.

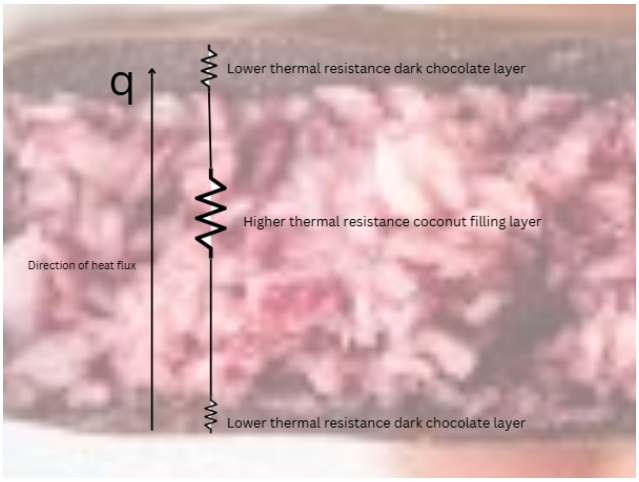

Figure 7: Thermal resistivity diagram for Cherry Ripe layers

The results in Table 1 make sense within the context of this investigation as the calculated values, while not very accurate, are of enough quality to compare to other values within this experiment. The thermal resistivity of the Cherry Ripe filling being higher than that of either Caramilk or Dairy Milk corresponds with the long time for the Cherry Ripe chocolate to transfer heat to the surface. The total calculated resistivity values explain why the Dairy Milk was the fastest to heat up and why the Cherry Ripe took so long since its internal layers are more resistive than that of standard chocolate. This can even explain why, despite the runtime taking so long, there was such a little instantaneous difference between the inner and outer surface temperatures of the Cherry Ripe. It was due to all the heat accruing in the centre with the higher resistance filling and as it slowly heats up as expected the lower resistance thin dark chocolate layer was able to heat quickly by comparison. This is in contrast to the data of the Dairy Milk and Caramilk data which had higher instantaneous

temperature differences between the inside and surface despite heating up faster overall.

3.5 Thermal gradients of chocolates over time

Figures 8a, 8b and 8c below contain both regular and thermal images of the chocolates on the hotplates at time intervals of 0 seconds, 2 minutes and 5 minutes (the empty slots did not have an available image).

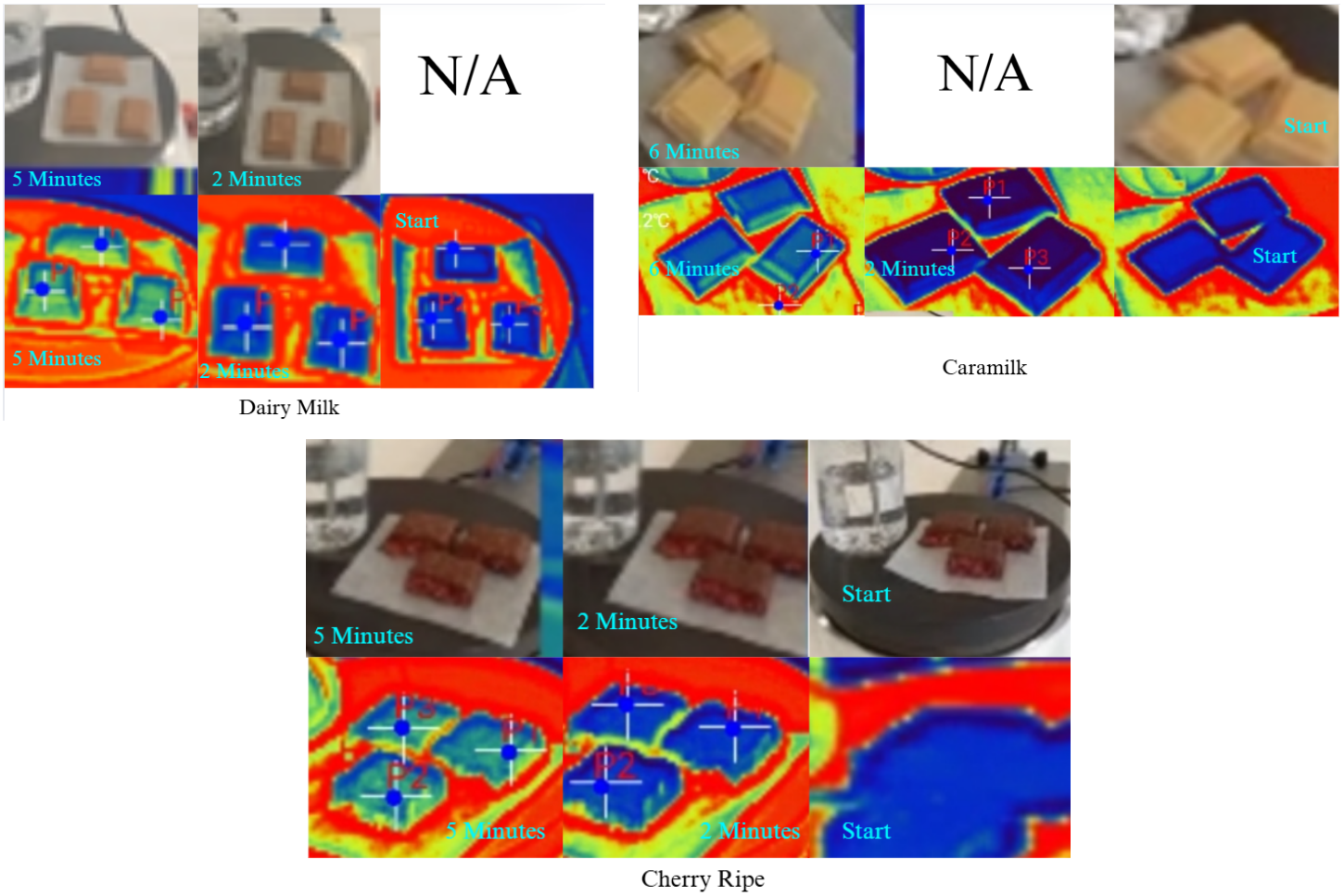

Figure 8 a) Dairy Milk thermal images, b) Caramilk thermal images, c) Cherry Ripe thermal image

3.6 Applications to industrial uses

While it is clear that the thermal properties of chocolate are essential to industrial manufacture, transport, and storage of confectionery in order to ensure that it retains desirable qualities for consumers and avoids potentially damaging effects such as melting or fat and sugar bloom, there are also less obvious benefits to this research from the perspective of the consumer. If the thermal effects of chocolate fillings are made more clear, it may inform how purchased chocolates are treated, such as allowing more thermally resistive chocolates to remain in hot environments for longer without melting, or the opposite, reducing heat exposure time of chocolates that are more likely to melt.

In another vein, global chocolate consumption is consistently trending upward. In particular, the consumption of chocolate and cacao products in Asia is increasing at a very high rate compared to the rest of the world [16] [17]. Traditionally, Europe and North America represent the overwhelming majority of this consumption [18], but as demand in Asia increases, companies may seek to gain footholds in what could be a lucrative market due to the large population. As discussed in the literature review section, temperature throughout the distribution from manufacture to the point of sale is an important consideration in maintaining product quality. The average temperature of many countries in Asia is quite high [19], and so research into the rate of heat transfer through different chocolate varieties would be significant in the

production of chocolate products for sale. As seen in the data, chocolates with fillings/different compositions tended to conduct heat much slower, and so such products may be prioritised in asian marketplaces.

While not directly connected to this research, further consideration is that of the supply of cocoa. Both constraints such as climate change, disease and falling nutrient quality in cocoa production, along with global demand constantly increasing [17] creates a situation where chocolate suppliers may need to increase the production of other products instead. As chocolate bars with fillings can take the space of a chocolate product while using significantly less cocoa, producers may look to the thermal data of such fillings as one consideration of manufacturing selection.

3.7 Error analysis

Errors in collecting data proved to be a serious limiting factor for the investigation, as errors were both significant and numerous throughout this phase. The existence of such errors greatly reduced the quality and quantity of data available, and perhaps presents the need for further trials. Of most importance was the utilisation of a thermal (IR) camera connected to a mobile device for temperature readings. Inexperience in utilising this equipment led to the recordings of data for the Crunchie being rendered unusable, representing approximately one quarter of the total data. Furthermore, the use of an IR camera means that our measurements for the 'inside' temperature are not truly inside the solid; rather, they are measurements of the exposed filling on the side of the chocolate. In terms of the recording of data, random errors existed from numerous sources. As discussed briefly, software limitations allowed only for three points of data to be collected, requiring the cameras to be handheld. The imprecision of human measurement leads to inconsistencies in the data points recorded. The positioning of each chocolate on the hotplates was different by some unmeasured amount, which may vary the heat flow supplied for each. Furthermore, the proximity of the chocolates on the hotplate would impact the air flow around each other. We know that the convection coefficient between a solid and fluid is affected by air flows, and as such, each chocolate would have different, unquantifiable heat loss rates at the surface due to convection.

3.8 Quantitative errors/uncertainty

The loss of data from the use of the IR camera necessitated the use of a linear interpolation model in order to complete and compare datasets. The effect of errors on data would be significant due to both the lack of repetitions and the quality of such repetitions. With such a small number of repetitions, the effect of errors is much more difficult to observe. In terms of quality, as the repetitions were carried out simultaneously within the same system, any such errors in the system would apply to each repetition, allowing them to carry into the final data. Thus, the value is significantly diminished. For further study into this area, the quality of data can be improved quite readily. Increasing the allotted time to the testing phase is key. By allowing more time to take an increased number of repetitions of higher quality, the amount and effect of errors on data would be greatly reduced. Furthermore, improving the method of temperature measurement, be it by changing the device used or improving the current thermal camera use. Combining this with an increased variety in samples would allow a much more detailed analysis of the rate of heat transfer through chocolate varieties.

4. Conclusion

Unfortunately, this experiment did not achieve its aim of accurately quantifying the thermal effects of fillings in chocolate, this was due to several limitations in the experimental method, including the lack of proper mounts for the thermal cameras, the inability to properly insulate the chocolate from heat loss through convection and radiation in order to increase the accuracy of the calculations. The most impactful error was the loss of the data for Crunchie, which limited the scope of the experiment to Dairy Milk, Caramilk, and Cherry Ripe. These flaws could be remedied by further pre-planning before the experiment, potentially including custom-made insulation rigs and mounts, as well as improved software for the thermal cameras that allow for a wider selection of test points and more accurate point-setting methods. As stated in the discussion, increasing both the repetition of tests as well as the variability of the chocolates tested would also improve the reliability and validity of this study. It may also be beneficial to vary heating sources in order to more accurately model the thermal conditions in the real world. Despite the lack of complete success in this case, there is still some value in the data produced as it was able to be internally compared to determine the thermal properties of the Cherry Ripe filling. This field of study remains relevant to the industry and should be more properly explored in future due to its applications and impact on the storage and transport of chocolate confectionery.

5. Acknowledgements

The authors acknowledge the use of ChatGPT for assistance in clarifying text and cleaning up grammar throughout the paper.

Toby Downes, Douglas Cameron, Braden Raffo and Hamyung Jang designed the experiment and recorded and collected data; Toby Downes gathered and prepared data for the Caramilk and Cherry Ripe chocolates as well as conducting analysis and calculations of all sets of data, as well as writing the article from point 3 to point 3.5 inclusive and all associated figures and diagrams; Douglas Cameron completed the abstract, introduction, materials and methods,

and conclusion, as well as assisting with section 3.6 and finalising the formatting and editing the article; Braden Raffo wrote section 3.6 with assistance, along with sections 3.7-3.8 and further formatting and editing; Hamyung Jang gathered and performed the preparation of data for the Dairy Milk chocolate and the linear interpolation analysis, as well as contributing in the writing, formatting, and editing of the article; Minghao Zhang, Sebastian Dominguez and Juanita Suarez provided task direction and project assistance, and Dr. Gobinath Rajarathnam provided conceptual direction, research and writing guiding frameworks, facilitated project resources, and directed project supervision.

6. References

1. Stortz, T. A. & Marangoni, A. G. Heat resistant chocolate. *Trends in Food Science & Technology* **22**, 201–214 (2011).
2. Bikos, D. et al. Experimental and numerical evaluation of the effect of micro-aeration on the thermal properties of chocolate. Food & Function 13, 4993–5010 (2022).
3. Tewkesbury, H., Stapley, A. G. F. & Fryer, P. J. Modelling temperature distributions in cooling chocolate moulds. Chemical Engineering Science 55, 3123–3132 (2000).
4. Timms, R. E. Confectionery fats handbook : properties, production and application. (Oily Press, 2003).
5. Figoni, P. How baking works : exploring the fundamentals of baking science. (John Wiley & Sons, 2011).
6. Hemanth, J. Experimental, Mathematical and Finite Element Analysis (FEA) of Temperature Distribution through Rectangular Fin with Circular Perforations. Modeling and Numerical Simulation of Material Science 07, 19–32 (2017).
7. Dreger, M. M. The experimental determination of the thermal conductivity of melting chocolate: thermal resistance analogies and free convection boundary conditions. Advanced Computational Methods and Experiments in Heat Transfer XIII (2014) doi:https://doi.org/10.2495/ht140431.
8. Cadbury Cherry Ripe Bar, 48 x 52 Grams : Amazon.com.au: Pantry Food & Drinks. Amazon.com.au https://www.amazon.com.au/Cadbury-Cherry-Ripe-Bar-Grams/dp/B07GJJXSP2 (2025).
9. Glicerina, V., Balestra, F., Dalla Rosa, M. & Romani, S. Microstructural and rheological characteristics of dark, milk and white chocolate: A comparative study. Journal of Food Engineering 169, 165–171 (2016).
10. Cadbury Cherry Ripe Sharepack 12 Pack 180g. Cadbury.com.au https://www.cadbury.com.au/products/cadburycherryripesharepack12pack180g/ (2025).
11. Cadbury Dairy Milk & Caramilk Share Pack 18pcs 216g. Cadbury.com.au https://www.cadbury.com.au/products/cadburydairymilkandcaramilksharepack18pcs216g/ (2025)
12. Beckett, S. T., Fowler, M. S. & Ziegler, G. R. Useful Physical Constants. 667–668 (2008) doi:https://doi.org/10.1002/9781444301588.oth1..
13. Cadbury Milk Chocolate Bar 50g. Officeworks.com.au https://www.officeworks.com.au/shop/officeworks/p/cadbury-milk-chocolate-bar-50g-td324927#specifications (2024).
14. 16.4 Thermal Resistance Circuits. Mit.edu https://web.mit.edu/16.unified/www/FALL/thermodynamics/notes/node118.html (2020).
15. C-Therm, C.-T. Characterizing the Thermal Conductivity of Fruits & Honey. *C-Therm Technologies Ltd.* https://ctherm.com/resources/newsroom/blog/characterizing-thermal-conductivity-fruit-honey/ (2020).
16. Beg, M. S., Ahmad, S., Jan, K., & Bashir, K. (2017). Status, supply chain and processing of cocoa - A review. Trends in Food Science & Technology, 66, 108–116. https://doi.org/10.1016/j.tifs.2017.06.007
17. Kongor, J. E., Owusu, M., & Oduro-Yeboah, C. (2024). Cocoa production in the 2020s: challenges and solutions. CABI Agriculture and Bioscience, 5(1). https://doi.org/10.1186/s43170-024-00310-6
18. Global Market Report: Cocoa Cocoa on JSTOR. (2024). Jstor.org. https://doi.org/10.2307/resrep22025
19. Average Temperature by Country | Asia. (n.d.). Tradingeconomics.com. https://tradingeconomics.com/country-list/temperature?continent=asia

7. Supplementary:

Table 2: Cherry Ripe surface temperature values

Time(s)	Surface temp 1	Surface temp 2	Surface Temp 3	Avg Surface temp
14	26.9	26.6	26.9	26.8
44	26.8	26.9	27.2	26.96666667
70	29.6	N/A	29.1	29.35
104	32.7	29.1	31.9	31.23333333
134	33.1	32	32.9	32.66666667
176	35.1	35.1	35.4	35.2
194	35.8	35.3	35.8	35.63333333
224	40.1	36.6	40.3	39
251	42.9	40.5	39.8	41.06666667
284	44.9	43.2	45.2	44.43333333
314	48.2	47	49	48.06666667
344	49.6	47.5	48.8	48.63333333
375	51.9	49.6	50.9	50.8
404	53.4	50.9	52	52.1
434	55.4	53.3	53.3	54
464	57.1	54.7	55.9	55.9
477	57.6	54.7	54.5	55.6

Table 3: Cherry Ripe inner temperatures values

Time (s)	Inner temp 1	Inner temp 2	Inner temp 3	Avg Inner temp
51	28.7	31.5	27.6	29.26666667
70	N/A	33.6	N/A	33.6
160	41.7	41.2	40.5	41.13333333
198	41.4	41.3	42.6	41.76666667
256	47.4	55.3	46.8	49.83333333
287	53.9	58.8	50.5	54.4
373	58.6	57.1	57	57.56666667
483	61.8	60.1	60.6	60.83333333

Table 4: Caramilk surface temperature values

Time (s)	Surface Temp 1	Surface Temp 2	Surface Temp 3	Avg surface temp
8	28.5	27.9	30.3	28.9
38	30.2	30.4	31.3	30.63333333
68	30.1	30	31.4	30.5
103	31.4	31.8	32.9	32.03333333
128	32.7	32	32.4	32.36666667
157	32.4	34.6	36.6	34.53333333
185	33.6	37.8	42.9	38.1
210	38.4	41.3	42.3	40.66666667
241	44.7	44.7	45.6	45
273	48.9	47.9	49.8	48.86666667
301	48.9	49.9	51.6	50.13333333
321	50.7	53.1	54.1	52.63333333
343	54.3	53.9	58.3	55.5
370	56.6	56.7	58.3	57.2

Table 5: *Caramilk inner temperature values*

Time (s)	Inner temp 1	Inner temp 2	Inner temp 3	Avg inner temp
91	N/A	N/A	41.9	41.9
95	N/A	41.1	N/A	41.1
99	41.6	N/A	N/A	41.6
139	N/A	N/A	53.1	53.1
146	N/A	61.6	58.4	60
215	N/A	63.3	63.1	63.2
258	N/A	66.1	65.3	65.7
329	N/A	66.7	71.1	68.9
338	66.5	N/A	N/A	66.5
358	N/A	79.7	72.2	75.95
365	62.4	N/A	N/A	62.4

The Sydney Journal of Interdisciplinary Engineering
SJIE 1(2) X–X (2025) https://doi.org/XXXX/XXXX

Increasing Thermal Comfort: How Colour and Fabric Composition of Clothing Impacts Warmth

Angelina Khun[1], Gen Watson[1], Miriam Zalloua[1], Riyanka Sarkar[1], Anika Younus[1], Sebastion Dominguez[2], Juanita Suarez[2], Minghao Zhang[2], David Alam[1] and Gobinath Rajarathnam[*]

[1] CHNG2803/CHNG9203, School of Chemical and Biomolecular Engineering, University of Sydney, Sydney, Australia
[2]Tutor for CHNG2803/CHNG9203, School of Chemical and Biomolecular Engineering, University of Sydney, Australia
[*]Corresponding Author and Lecturer for CHNG2803/CHNG9203, School of Chemical and Biomolecular Engineering of University of Sydney, Sydney, 2006, Australia
E-mail: gobinath.rajarathnam@sydney.edu.au

Abstract

As energy costs rise and carbon reduction targets intensify, passive strategies to improve thermal comfort indoors are increasingly important. This study evaluates the heat retention performance of four commercially available beanies differing in colour, composition, and insulation type to determine which materials most effectively limit heat loss. Using a silicone heat pack as a controlled thermal source, internal and surface temperatures were measured over time to quantify thermal conductivity and infer insulation capacity. Results showed that insulated beanies, particularly the navy beanie, retained greater heat over five minutes compared to uninsulated alternatives. Although darker colours are expected to absorb and retain more heat, the navy insulated beanie conserved more heat than the black insulated beanie, indicating that colour has minimal impact under typical indoor conditions. Thermal conductivity (k) values were calculated but are only partially representative due to complex multilayered structures, air gaps, and mixed heat transfer modes. The findings suggest that material layering and structure, rather than colour or fabric composition alone, play dominant roles in thermal retention. These insights support the potential for targeted clothing choices to enhance personal warmth in low-energy domestic settings.

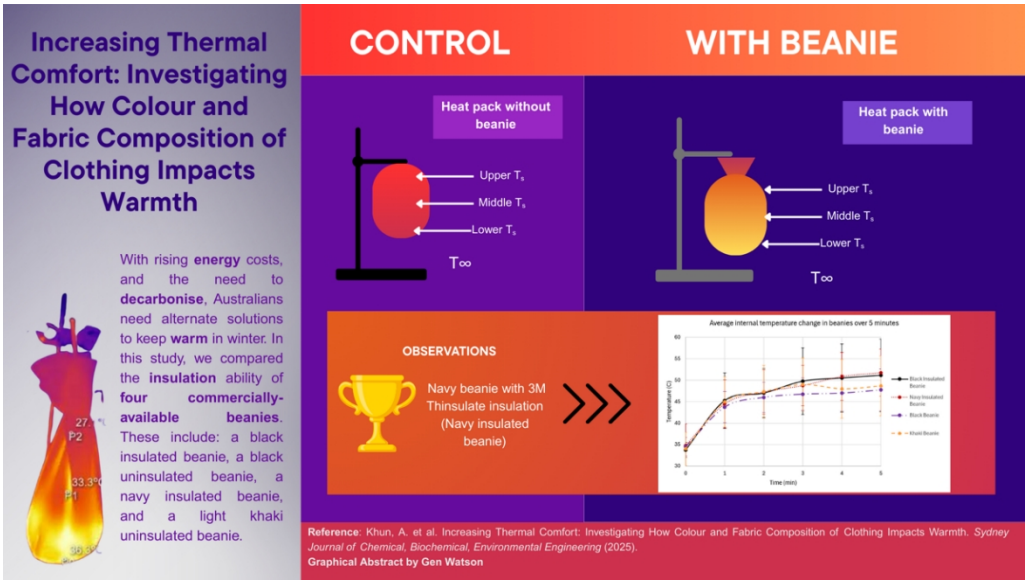

Keywords: insulation, thermal comfort, thermal conductivity, clothing materials, heat retention

1 Introduction

Many Australian homes offer limited protection from the cold, lacking the insulation and heating systems common in colder climates. This results in significant indoor heat loss during winter, often compensated for with electric heating; an increasingly expensive and carbon-intensive solution. As electricity prices rise and national decarbonisation efforts intensify, there is a growing need for low-energy strategies that maintain indoor comfort without increasing emissions[1, 2].

Clothing presents a simple yet underexplored solution [3]. By modulating heat exchange between the human body and its environment, clothing can significantly influence thermal comfort. This study investigates the thermal performance of everyday fabrics in a domestic context, with the aim of informing energy-efficient clothing choices[4]. We hypothesise that: The black insulated beanie will exhibit the highest heat conservation. Furthermore, beanies with a higher proportion of synthetic fibers (e.g., polyester) will retain more heat. These hypotheses are grounded in established heat transfer principles. Thermal conductivity (k) governs the rate of heat flow through fabric fibres, while the convective heat transfer coefficient (h) affects energy exchange at the fabric-air interface[5]. Materials such as wool and synthetics with embedded air pockets exhibit low k values, acting as thermal resistors. Multi-layered or thick fabrics further suppress convective currents, enhancing insulation. Additionally, fabric colour influences radiative heat transfer - darker colours, with higher emissivity and absorptivity, typically absorb and emit more thermal radiation than lighter-coloured ones[5].

Despite the extensive literature on fabric insulation in outdoor and extreme environments, there is limited research on the thermal performance of common garments in domestic settings[6]. This study aims to address that gap by evaluating the heat retention of four commercially available beanies differing in fabric type, colour, and insulation: a black insulated beanie, a black uninsulated beanie, a navy insulated beanie, and a khaki uninsulated beanie.

Using a controlled thermal source to simulate skin temperature, we measured the internal and surface temperatures of each beanie over a five-minute period. The results aim to inform practical, low-energy strategies for maintaining warmth indoors through clothing selection.

2. Method

2.1 Experimental Methodology

To begin the experiment, multiple silicone heat packs were placed in an oven and heated for approximately 20 minutes. After this period, the average surface temperature of the heat packs was found to be around 45°C, based on thermal camera readings taken during a control test. While the heat packs were warming, the experimental setup was assembled. A retort stand and clamp were used to hold the thermal camera in place, ensuring a consistent and stable view of the test area. A second retort stand, positioned opposite to the camera, was used to suspend each beanie during testing. The complete setup, including both stands and the camera-beanie arrangement, is shown in Fig. 1.

Once the heat packs were ready, an initial control test was conducted using a heat pack on its own. This control was placed within the view of the thermal camera, and surface temperatures were measured using the P2 Pro thermal camera app. Four surface measurements were taken every minute: the upper, middle, and lower regions of the heat pack, as well as the ambient room temperature.

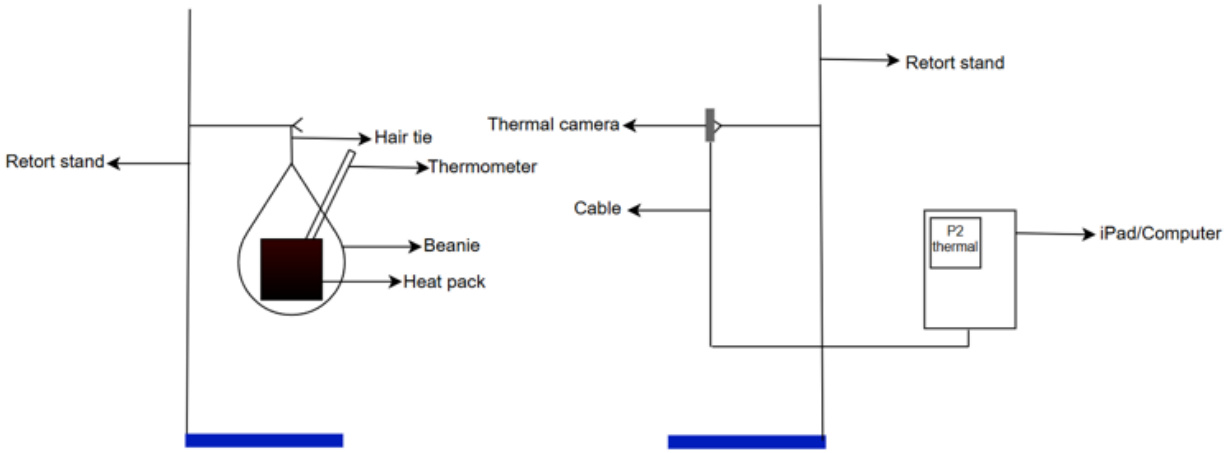

Figure 1: Diagram of experimental setup.

Next, testing began on the beanies. A freshly heated pack was inserted into the first beanie and secured with a hair tie. The beanie was clamped on the stand facing the thermal camera. A thermometer was inserted through the beanie fabric to measure internal temperature. Because the beanie was not see-through, the thermometer's exact position couldn't be checked, but care was taken to make sure it touched the heat pack each time. The same insertion method was used for all beanies to keep things consistent. Surface and internal temperatures were recorded every minute using the thermal camera and a thermometer, respectively. While measurements were taken as close to each minute as possible, slight human timing errors may have occurred.

This procedure was repeated for all four beanies: a khaki non-insulated beanie, a black non-insulated beanie, a black insulated beanie, and a navy insulated beanie. The entire experiment was performed four times, with three replicates for each beanie to ensure accuracy and repeatability.

2.2 Calculation Methodology

To analyse the results, heat loss from the pack was calculated using the formula:

$$Q = mc\Delta T \qquad (1)$$

Where m is the mass of the pack in kilograms (kg), c is its specific heat capacity in Joules per kilogram per Kelvin ($J.Kg^{-1}.K^{-1}$) , and T is the change in internal temperature over 5 minutes in Kelvin (K). This gave heat loss in Joules (J), which was then divided by 300 seconds to give power in Watts (W).

Surface area was estimated assuming the beanie-heat pack setup was roughly spherical:

$$A = 4\pi \left(r_{heatpack} + r_{beanie_{thickness}}\right)^2 \qquad (2)$$

Where A is the surface area in square meters(m^2), $r_{heatpack}$ is the radius of the heat pack in meters(m), and $r_{beanie\ thickness}$ is the radius of the beanie in meters.

Using these values, the thermal conductivity k of each beanie was calculated as:

$$k = \frac{Q \times L}{A \times \left(T_2 - T_1\right)} \qquad (3)$$

Where k is the thermal conductivity in Watts per meter kelvin ($W.m^{-1}.k^{-1}$), L is the thickness of the beanie in meters (m), T_1 is the internal temperature in Kelvin (K), and T_2 is the surface temperature in Kelvin (K).

It is assumed there is perfect thermal contact between the heat pack and the beanie throughout the experiment. For calculation purposes, the thermal camera readings are considered 100% accurate. The combined beanie and heat pack are collectively referred to as the "system" in this study.

3. Results

The objective of this report is to determine which beanie insulates heat best. This will be determined by the beanie that yields the best conduction value (a smaller k-value indicates better efficacy for use). The different colours, composition and presence of an insulating layer were the most significant factors.

3.1 Assumptions

This reaction was assumed to be in steady state such that the rate of convection and conduction occurred at equal magnitudes. Three repetitions of the experiment were performed and an average value was taken for the calculations. The thermal camera measured temperature at points labelled "P1", "P2" and "P3" as per Fig. 2. However, the average temperature for the surface temperature was the average between P2 and P3 since P1 was an inconsistent measurement. The density of the heat pack for silicone beads was assumed to be 1100kg / m3 and the heat capacity of silicone beads was assumed to be 1250 J/kg K[8] The mass of the heat pack was averaged to 540g.

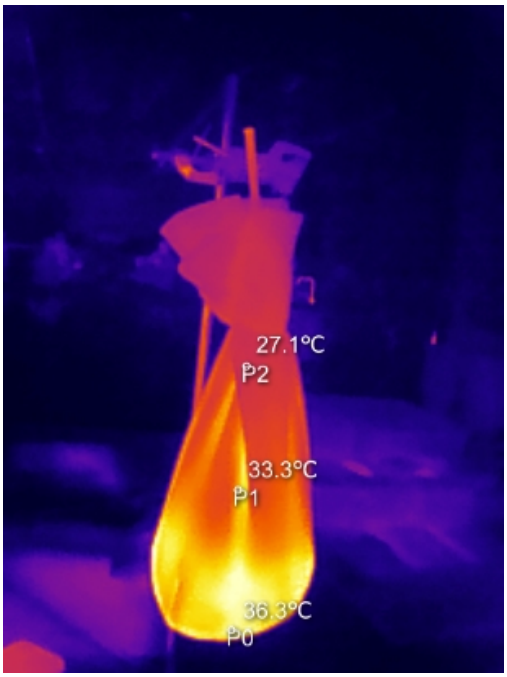

Figure 2: Thermal camera photo of experimental setup.

3.2 Conduction Results

Table 1: k value of different beanies and the individual qualities of each beanie.

	Composition	Colour	Bi-Layered	k-value (W/m·K)
1	50% Viscose 28% Polyester 22% Nylon	Black	No	0.075
2	50% Viscose 28% Polyester 22% Nylon	Light khaki	No	0.064
3	Outer: 52% Polyester 48% Acrylic Lining: 100% Polyester Filling: 61% Polypropylene (PP) 39% Polyester	Black	Yes	0.178
4	Outer: 54% Polyester 46% Acrylic Lining: 100% Polyester Filling: 61% Polypropylene (PP) 39% Polyester	Navy	Yes	0.201

Note that due to experimental error the temperature of the system increased over time, indicating energy generation. However, this is not true as there was no heat input and this most likely was a result of the exothermic reaction from the heat pack.

Conduction was calculated as it was predicted that the beanies with the smallest k values would be the greatest insulators as they limited heat transfer. This is dependent on the hot air from the heat pack conducting to the outer surface of the beanie. However, this assumes that all the beanies would experience conduction equally. This is only a valid assumption in beanie 1 and 2. For beanies 3 and 4, there were multiple layers, as per table 1. Although the polyester lining may have experienced conduction, the conducted heat was insulated by the second layer and filling as these layers were not one composite material. This could indicate that the surface temperature of beanies 3 and 4 are a greater reflection of the ambient temperature than the heat conducted by the heat pack.

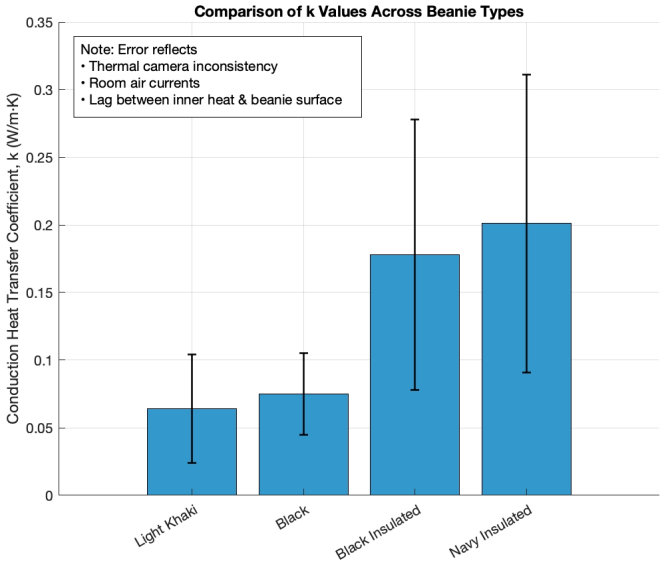

Figure 3: Bar chart of respective k -values with error bars.

Figure 3 is a graphical representation of the calculated k values and showcases the error bars for each k value. These error bars were calculated as the standard deviation for the k value of each beanie type of each repetition. Figure 3 indicates that the black beanie has the greatest replicability as the error of these calculations is smallest. These errors consider incomplete thermal contact, the air current of the rooms, the differing ambient temperatures and experimental error.

The paper's objective is to determine which beanie is most effective for heat insulation for the model 'head'. Therefore, there is a greater focus on heat retention within the beanie environment. As conduction is not a reasonable assumption for this experiment, a greater reflection of this trend is the change in temperature over the change in time.

As Figure 4 indicates, there is a steeper increasing temperature gradient for the insulated beanies in comparison to uninsulated. This solidifies previous assumptions that conduction may be an unreliable indicator within this experiment, and that the internal temperature of the heat pack may be more applicable to reflect real world conditions.

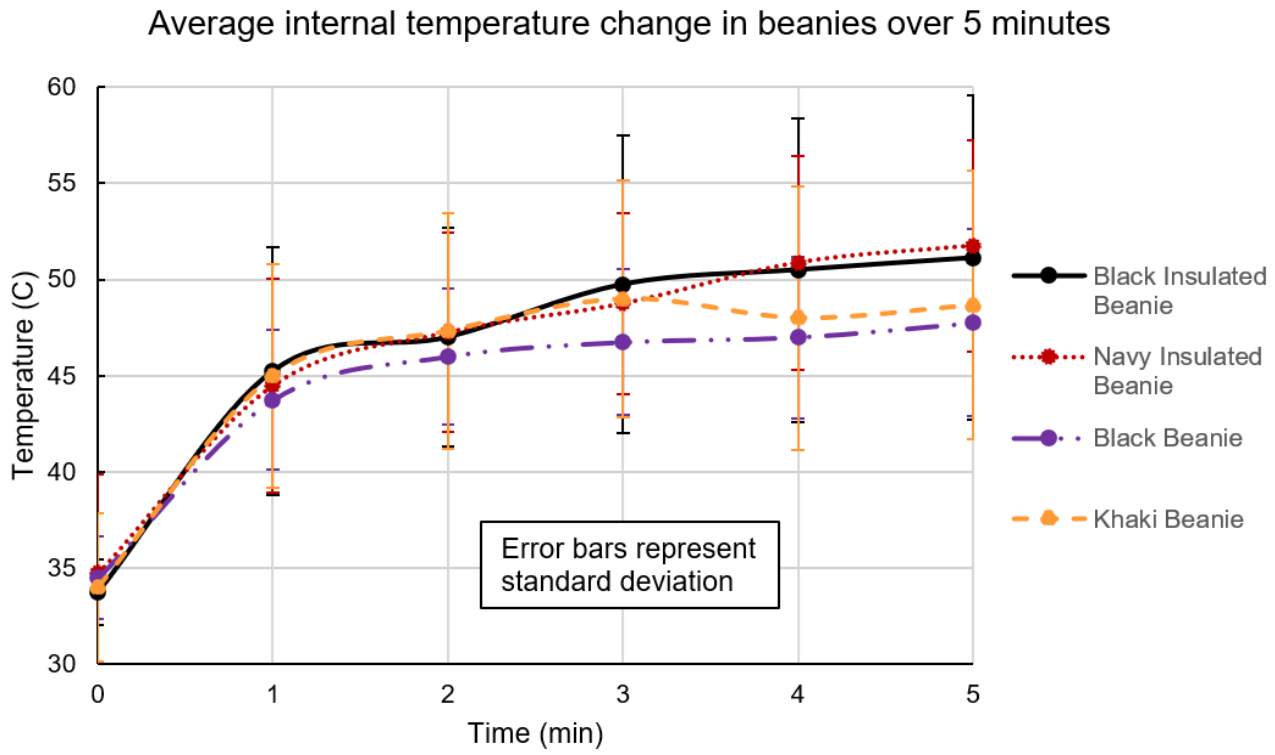

Figure 4: Internal temperature change in different beanies incorporating individual standard deviations.

3.3 Other Considerations

Interpreting the convection coefficients was also considered, however these results were not factored when considering which beanies were most effective. The convection coefficient considers the disparity between the beanie surface temperature and the ambient temperature.

However, this again assumes that the heat of the heat pack has transferred to the surface of the beanie. Biot number calculations, as found in appendix, indicate that all beanies had a Biot number far greater than 0.1. This indicates that convection dominates instead of conduction, however this is inaccurate in this scenario as thermal cameras over time indicate that some beanies had very little heat transfer from heat pack to beanie surface. Therefore, the thermal conductivity constant k is a better indicator of heat retention. For reference, the Biot number results and h-value coefficients can be viewed in appendix. The full scope of all numerical results can also be found via appendix.

4. Discussion

The purpose of this study was to compare the thermal retention capacity of four commercially available beanies under controlled laboratory conditions, using internal temperature change and thermal conductivity as comparative metrics. It was hypothesised that the black insulated beanie would be most effective in heat retention. As illustrated in Fig. 4, the insulated beanies retained heat more effectively over time compared to the uninsulated ones. The temperature drop in the uninsulated beanies was significantly faster, which indicates a lower capacity to resist heat loss. To quantify thermal performance, thermal conductivity (k) was calculated using a conduction-based approach. The black uninsulated beanie had the highest estimated value (k = -7.49 × 10-2 W/m·K), followed by the light khaki beanie (k = -6.43 × 10-2 W/m·K), both suggesting relatively poor insulation.

Although the insulated beanies showed lower thermal conductivity values navy (-20.1 × 10-2 W/m·K) and black (-17.8 × 10-2 W/m·K), these results should be interpreted with caution. Due to the internal layer of insulation creating pockets of air, the assumption of pure conduction does not apply. In such cases, the derived k-values might not represent purely conductive behaviour, but they were still included to fulfill the experimental requirement and to allow comparison under a consistent methodology. These observations underline the importance of considering the dominant heat transfer mode when interpreting calculated thermal parameters.

These results align with fundamental heat transfer principles, where materials exhibiting lower thermal conductivity typically offer higher thermal resistance. In the case of the insulated beanies, the dual-layer configuration, featuring a synthetic polyester lining beneath a knitted fabric, introduces air pockets that serve as barriers to both conductive and convective heat loss[9, 10]. While the calculated k-values

for these samples should be interpreted cautiously, their observed thermal performance is consistent with findings from similar textile studies, where microstructural layering and trapped air significantly contribute to thermal retention[11– 14]. This effect is especially relevant in cold environments, where minimizing heat dissipation is essential for preserving core body temperature[1].

Several key findings emerged. The black insulated beanie did not perform as well as the navy insulated beanie, despite both sharing identical structure, thickness and very similar composition (refer to Table 1 above). There is uncertainty as to why the black beanie didn't perform as well as predicted, perhaps due to material properties, light reflection,or experimental error. Literature indicates that darker fabrics absorb and re-radiate more infrared energy[5], but their overall effectiveness as insulators also depends on weave tightness[15], fibre density[16] and internal air trapping capability[6, 11, 14]. It is likely that the shaded environment in which the experiment was conducted resulted in an inaccurate representation of the relationship between solar radiation absorption and colour of surface. Hence, the hypothesis of the black insulated beanie retaining more heat than the navy insulated beanie was not proved in this study, as colour of the fabric may not be a major factor in the indoor environment. To sufficiently investigate the effect of fabric colour on thermal warmth, a change to the method of experimentation, for example the addition of a controlled source of light, would be required. It is relevant to note that the colour of the beanie functions more in affecting thermal absorptivity, rather than thermal resistance.

Not all findings aligned exactly with theoretical expectations. A small yet noticeable increase in internal temperature was observed during certain observations, likely stemming from the exothermic nature of the heat packs used. Since no additional energy input occurred after placement, the apparent "heat gain" can be attributed to delayed equilibration between the heat pack and the surrounding air within the beanie. This may be alleviated by implementing a short, standardised waiting period in future experiments. The temperature gradient between the heat pack and the room likely required time to stabilise. Additionally, the delay in thermometer responsiveness likely skewed early temperature readings, introducing time lag errors that propagated across the measurement interval.

The observed inconsistencies in thermal conductivity values may also result from experimental uncertainty in beanie thickness measurements. The beanie was wrapped once around the heat pack as seen in Fig. 1 and Fig. 2. This was to create a near-spherical shape and thus imitate real-life conditions. However, the compressibility of fabric and shifting of silicone beads inside the pack likely altered the radius and the contact area during setup. These variables influence the conductive path length (δ) and surface area (A), which directly affect k-value calculations via Fourier's law. In future, it is recommended to use non-contact thickness sensors and 3D thermal imaging to minimize such uncertainties.

Ambient conditions also played a significant role. The experiment was conducted over two different days, with ambient room temperature varying between 22.3°C and 24.0°C. Although this variation seems minor, even small fluctuations in T_∞ can affect convective heat loss rates, especially when low-temperature gradients exist between the beanie surface and surrounding air. A tighter controlled test environment, such as performing all experiment runs in the same day, would improve reproducibility.

It is also important to consider the interplay between insulation and heat dissipation. Thicker fabrics usually keep the body warmer, but sometimes, the materials can increase heat transfer. This can happen if the fabric traps moisture, lets air pass through or creates more surface area for heat to escape, like how fins work in cooling systems[5, 12, 13, 17]. However in this experiment this was not observed: insulated beanies consistently retained heat better, indicating minimal fin effect. This follows theory as insulation reduces critical surface area for heat transfer - thermal insulation increases as the air gap between the body and the fabric increases, though beyond a gap of about 7.5–10 mm the thermal insulation decreases because of convection effects[18]. Scenarios involving external airflow (e.g., outdoor winter wear), affect this interplay and hence warrant further exploration[3, 6]. The effect is reportedly minimised in closely woven fabrics[18]

A factor to consider is the composition and knit weave type of the beanies. Non-insulated beanies did not include acrylic (generally more thermally insulating than polyester[19]) nor PP (the insulation material between the layers), whilst the insulated beanies did not contain any viscose, which provides stretch in the knit weave of the beanie. All materials are assumed to be synthetic, but any finishes or coating are not known. The differing composition and build between insulated and non-insulated beanie fabric affects stretch and porosity[20], critical surface area, moisture absorption[19], and heat resistance [19]. Furthermore, the k-values between beanie three and four could, but not conclusively, be attributed to the 2% more polyester content in the navy beanie's outer shell. If negating the factor of colour given the assumption that the experiment was conducted with little solar radiation impact, in literature, acrylic can trap moisture whilst polyester tends to be "moisture wicking" and relatively more breathable[19]. However, some research suggests that polyester fabrics, when layered, are very effective for heat retention (due to the air pockets created)[5, 9, 20]. Of particular importance, weave type of a knit fabric greatly affects thermal insulation [21] (which decreases as moisture increases) due to capillary action of the fibres facilitating moisture absorption[9, 18]. Coated fabrics can utilise moisture

absorption qualities to consequently impact thermal insulation[18]. Literature suggests that moisture retention is one of the main factors affecting thermal conductivity of fabric[22] Due to the variety of polyester fabrics and their coatings, it would have been beneficial to understand what polyester is used to determine the effect of fabric composition and weave type on heat changes.

While this study did not provide definitive material rankings due to equipment-related variability and environmental influences, the relative comparisons between samples remain valid. Since identical methods were applied across all four beanies, consistent trends could still be observed and evaluated. Despite limitations such as potential thermometer delay and minor setup inconsistencies, the experimental arrangement was sufficiently controlled to yield meaningful insights into fabric insulation performance. The findings underscore how subtle experimental factors can influence thermal measurements and highlight the superior heat retention of insulated fabrics under the tested conditions. Future investigations could benefit from extending the observation period beyond five minutes and incorporating advanced techniques such as differential scanning calorimetry (DSC) or infrared thermography for more accurate quantification of heat flux. It is also relevant to investigate the thermal characteristics of knit fabrics made of natural materials that are not derived from petrol, such as yarn made from peat fibre[23], wool[24], or synthetic fibres combined with natural[25].

5. Conclusion

The hypothesis proposed in this study of the black insulated beanie exhibiting the highest heat conservation was only partially supported by the results of the experiment. Although the insulated beanies demonstrated superior heat retention, the black insulated beanie did not outperform the navy insulated beanie as predicted. This suggests that while insulation and fibre composition are key factors, colour was not a significant contributor to thermal retention under the indoor conditions tested. Overall, the study confirms that insulation and multi-layered construction significantly enhance thermal performance in everyday garments. However, inconsistencies in thermal conductivity calculations and internal temperature changes explained by methodological constraints such as delayed heat pack equilibrium indicate that conduction alone may not be a fully reliable indicator of insulation effectiveness in this context. Furthermore, factors such as moisture absorption and weave of the knit were not controlled or accounted for, and thus their impact upon results cannot be determined. Future experiments with refined measurement strategies and methodology, better environmental controls, and more suitable fabric samples would further isolate the influence of the factors of fabric composition and colour on thermal retention in domestic settings.

References

[1] Barlow, C. F., Daniel, L. & Baker, E. Cold homes in australia: Questioning our assumptions about prevalence. *Energy Res. Soc. Sci.* **100**, 103124, DOI: 10.1016/j.erss.2023.103124 (2023).

[2] Barik, D. *Energy from toxic organic waste for heat and power generation*. Woodhead Publishing Series In Energy (Woodhead Publishing, An imprint Elsevier, Duxford, United Kingdom, 2019).

[3] Zhao, W., Chow, D., Yan, H. & Sharples, S. Influential factors and predictive models of indoor clothing insulation of rural residents: A case study in china's cold climate zone. *Build. Environ.* **216**, 109014, DOI: 10.1016/j.buildenv.2022.109014 (2022).

[4] Ziqi, C., Jingxian, X. & Yehu, L. Heat transfer simulation in electric heating fabrics. *Energy buildings* **306**, 113917, DOI: 10.1016/j.enbuild.2024.113917 (2024).

[5] Williams, J. *Textiles for cold weather apparel* (Woodhead Publishing Ltd, 2009).

[6] Yang, L. et al. Research on the local clothing thermal insulation prediction model with different dress state of indoor occupants. *Energy Build.* **324**, 114861, DOI: 10.1016/j.enbuild.2024.114861 (2024).

[7] Incropera, F., DeWitt, D., Bergman, T. & Lavine, A. *Fundamentals of Heat and Mass Transfer* (John Wiley Sons, 2007), 6th edn.

[8] AG, W. C. Solid and liquid silicone rubber material and processing guideline.

[9] Erdumlu, N. & Saricam, C. Investigating the effect of some fabric parameters on the thermal comfort properties of flat knitted acrylic fabrics for winter wear. *Textile Res.* J. **87**, 1349–1359, DOI: 10.1177/0040517516652347 (2017).

[10] Yang, J. et al. Wearable fluidic fabric with excellent heat transfer performance for sports recovery. *Adv. Sci.* 12, DOI: 10.1002/advs.202411691 (2025).

[11] Xu, D. et al. Hump-inspired hierarchical fabric for personal thermal protection and thermal comfort management. *Adv. Funct. Mater.* **33**, DOI: 10.1002/adfm.202212626 (2023).

[12] Puszkarz, A. & Krucinska, I. The study of knitted ´ fabric thermal insulation using thermography and finite volume method. *Textile Res.* J. **87**, DOI: 10.1177/0040517516635999 (2016).

[13] Su, Y., Yang, J., Li, R., Song, G. & Li, J. Experimental study of moisture role and heat transfer in thermal insulation fabric against hot surface contact. *Int. J. Therm. Sci.* **156**, 106501, DOI: 10.1016/j.ijthermalsci.2020.106501 (2020).

[14] Dong, Z., Fang, X., Ding, Y., Cong, H. & Ma, P. Heat/moisture transfer mechanism in weft-knitted seamless fabrics. *Textile Res.* J. **94,** 1692–1702, DOI: 10.1177/00405175241236886 (2024).

[15] Wang, F., Lai, D., Shi, W. & Fu, M. Effects of fabric thickness and material on apparent 'wet' conductive thermal resistance of knitted fabric 'skin' on sweating manikins. *J. Therm.* Biol. **70**, 69–76, DOI: 10.1016/j.jtherbio.2017.03.004 (2017).

[16] Nazir, M., Shaker, K., Nawab, Y., Fazal, M. Z. & Umair, M. Investigating the effect of material and weave design on comfort properties of bilayer woven fabrics. *J. Textile Inst.* **108**, DOI: 10.1080/00405000.2016.1247616 (2016).

[17] Kim, H. A. Water/moisture vapor permeabilities and thermal wear comfort of the coolmax®/bamboo/tencel included pet and pp composite yarns and their woven fabrics. *The J. The Textile Inst.* **112**, 1–14, DOI: 10.1080/00405000.2020.1853409 (2020).

[18] Hunter, L. & Fan, J. *Improving the Comfort of Garments*, 739–761 (Woodhead Publishing, 2015).

[19] Fei, B. *High-performance fibers for textiles*, 27–58 (Woodhead Publishing, 2018).

[20] Ma, W., Cheng, L., Liu, Y., Psikuta, A. & Zhang, Y. Study on the thermo-physiological comfort properties of cotton/polyester combination yarn-based doublelayer knitted fabrics. *Textile Res.* J. **95**, 569–583, DOI: 10.1177/00405175241268802 (2025).

[21] Gong, R. & Ozgen, B. *Fabric structures: Woven, knitted, or nonwoven*, 107–131 (Woodhead Publishing, 2018).

[22] Bedek, G., Salaün, F., Martinkovska, Z., Devaux, E. & Dupont, D. Evaluation of thermal and moisture management properties on knitted fabrics and comparison with a physiological model in warm conditions. *Appl. Ergonomics* **42,** 792–800, DOI: https://doi.org/10.1016/j.apergo.2011.01.001 (2011).

[23] Mikucionien ˇ e, D., ˙ Cepukone, L. & Milašien ˇ e, D. Investigation on mechanical and thermal properties of knits from peat fibers and their combination with other natural fibers. *Textile Res.* J. **88**, 004051751770563, DOI: 10.1177/0040517517705633 (2017).

[24] Abo Elnaga, H. T. & Yahia, M. Eco-friendly materials knitting by different yarn ply for high-performance garments. *Res. J. Textile Appar.* (2023). 6/9

[25] Çil, M., Nergis, U. B. & Candan, C. An experimental study of some comfort-related properties of cottonacrylic knitted fabrics. *Textile Res.* J. **79**, 917–923 (2009). Copyright - Copyright Textile Research Institute Jul 2009; Document feature - Tables; Graphs; ; Last updated - 2024-10-04; SubjectsTermNotLitGenreText -Environmental.

Author Contribution Statements

A.K. performed calculations, extensively analysed results, created Fig. 2 and 3, Table 1, appendix and paper formatting. G.W. conceived the introduction, graphical abstract, and Fig. 3. M.Z. wrote the abstract, honed and wrote the methodology, created Fig. 1. R.S. further analysed and interpreted the results in depth, connecting to literature, in the discussion. A.Y. contributed to discussion, wrote discussion and formatted bibliography. All authors were involved in experiment methodology design and conducting the experiment, as well as reviewed and edited the manuscript. All tutors provided task direction and project assistance, and Dr. Gobinath Rajarathnam provided conceptual direction, research and writing guiding frameworks, facilitated project resources, and direct project supervision.

Competing Interests

Authors declare no competing interests.

Appendix

Appendix 1: Sample calculation using the insulated navy beanie. The mass of the heat pack was 0.54kg, estimated specific heat capacity 1250Jkg ×K, the beanie thickness was 0.008m and the radius of the heat pack as a sphere was 0.07. The below is for the navy beanie in repetition 1:

Using equation 1:

$$Q = mc\Delta T$$

$$Q = 0.54kg \times 1250 \left(\frac{J}{kg \times K}\right) \times (54 - 42)\, K$$

$$Q = 8100J$$

Heat per second over 5 minutes (300s):

$$Q = \frac{8100J}{300s} = 27W$$

Using equation 2:

$$A = 4\pi (0.07m + 0.008m)^2 = 0.076\, m^2$$

Using equation 3:

$$k = \frac{Q \times d}{A \times \Delta T} = (27W \times 0.008m) / (0.076\, m^2 \times (54 - 36.2)\, K = \frac{0.16W}{m \times k}$$

Appendix 2: Biot number results for each beanie

Beanie	Biot Number
1	2.36
2	2.55
3	3.42
4	2.39

Appendix 3: h-value results

$$h = Q / (A \times (T_{surface} - T_{ambient})$$

Where $A = 0.076\, m^2$, $T_{surface} = 32.65°C$, $T_{ambient} = 23°C$

$$h = (27W) / (0.076\, m^2 \times (32.65 - 23)\, K = 36.6 \frac{W}{m^2 \times K}$$

Beanie	Average h-value
1	76.43
2	60.77
3	76.11
4	59.9

Appendix 4: Raw results for repetitions 1-4

Repetition 1	Intial	Column1	t=5	Column2	Column3	T=0	T=54
Time	middle	bottom	middle	bottom	average		
Control (heat with no beanie)	46	47.5	38.2	41.1	39.65	47.5	41.1
Light coloured	29	32.5	29.2	33.9	31.55	39	49
black beanie	33	36.3	30.1	36.3	33.2	35	47
black beanie w insul	28.1	35	27.2	29	28.1	37	54.5
navy beanie w insul	31.2	32.9	29.1	36.2	32.65	42	54
Repetition 2	Intial		t=5				
Time	middle	bottom	middle	bottom		T=0	T=5
Control (heat with no beanie)	48.3	40.8	42.3	33.7	38	48.3	42.3
Light coloured	28.3	33.1	30	35.4	32.7	33	56
black beanie	27.2	33.3	28.3	32.9	30.6	34	56
black beanie w insul	29.4	31	33.9	31.5	32.7	34	54
navy beanie w insul	29.8	33.2	30.3	34.1	32.2	34	52
Repetition 3	Intial		t=5				
Time	middle	bottom	middle	bottom		T=0	T=5
Light coloured	27.7	29.7	26.2	30.5	28.35	30	41
black beanie	27.5	31.5	27.2	33.2	30.2	33	46
black beanie w insul	30	25.5	29.6	27.7	28.65	34	53
navy beanie w insul	27.3	35.1	27.6	32.9	30.25	33	55
Repetition 4	Intial		t=5				
Time	middle	bottom	middle	bottom		t=0	t=5
Light coloured	27.5	32.1	27.3	31	29.15	36	42
black beanie	26.8	28.5	27.2	31.5	29.35	30	46
black beanie w insul	29.8	26.7	29.1	28.7	28.9	33	37
navy beanie w insul	29.4	30.2	34.4	30.9	32.65	30	43

The Sydney Journal of Interdisciplinary Engineering
SJIE 1(2) X–X (2025) https://doi.org/XXXX/XXXX

Impact of Packaging Material on Heat Retention in Ready-to-Eat Noodle Cups

Elias Navarrete Cubillos[1], Gabriel Gutierrez Salmeron[1], Jordan McCammon[1], Samuel Stoyles[1] and Llewellyn Govender[1]; Sebastian Dominguez Flores[1], Juanita Suarez Perez[1], Minghao Zhang[1], David Alam[1] and Gobinath Rajarathnam[1]

[1] School of Chemical and Biomolecular Engineering, The University of Sydney, Sydney, Australia

E-mail: enav6196@uni.sydney.edu.au

Received 2nd May 2025
Accepted for publication xxxxxx
Published xxxxxx

Graphical Abstract

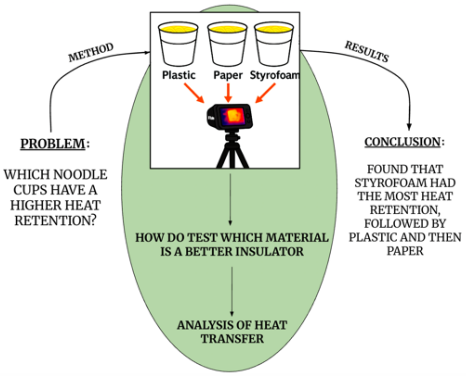

Abstract

Thermal insulation in ready-to-eat food packaging is critical for maintaining food quality and safety. This study evaluates the heat retention performance of three common instant noodle cup materials, paper, plastic, and Styrofoam, using infrared thermal imaging across two controlled experiments: one with noodle-filled cups and another with hot water only. Temperature decay was analysed using Newton's Law of Cooling and cumulative heat loss calculations. Styrofoam consistently exhibited the best insulation, showing the lowest cooling rates and least heat loss. Plastic cups provided moderate retention, while paper allowed the fastest heat dissipation. These results highlight the strong influence of material properties, particularly thermal conductivity, on passive cooling. Despite its thermal advantages, Styrofoam, an Expanded Polystyrene (EPS), presents environmental concerns, prompting the need for sustainable alternatives. This study underscores the importance of balancing performance, cost, and environmental impact in packaging design and supports further investigation into bio-based or thermally adaptive materials for future applications.

Keywords: Heat retention, Food packaging, Instant noodles, Infrared Thermal Imaging, Newton's Law of Cooling, Insulation

1. Introduction

Efficient thermal management is a fundamental consideration in modern engineering systems, influencing the performance, safety, and energy efficiency of processes across sectors. From industrial-scale reactors to household appliances and packaging, the way heat is transferred, retained, or dissipated has broad implications for material selection, system design, and user experience[1,2]. In the context of consumer goods, particularly in the food sector, heat transfer plays a central role in safety, quality, and consumer satisfaction, especially in the context of ready-to-eat meals[3,4].

As the demand for convenience foods grows globally, so too does the importance of packaging materials that can preserve temperature for a longer duration[5,6]. This is particularly relevant for ready-to-eat meals such as instant noodles, where thermal insulation impacts the eating experience and the safe handling of the food. Instant noodles are among the most widely consumed convenience foods globally, with billions of servings consumed each year[7].

Instant noodle packaging varies widely in form and material. These meals are typically packaged in single-serve containers made of diverse materials, ranging from lightweight paper cups to plastic bowls and expanded polystyrene (styrofoam) containers. Each material possesses distinct thermal properties that influence how quickly heat is lost to the environment. While manufacturers may prioritise cost-effectiveness or aesthetic appeal, thermal performance is often overlooked. This is despite its direct impact on food temperature, cooking effectiveness, and the time window in which a meal remains palatable and safe to eat.

Packaging materials vary considerably in their thermal properties. For example, polystyrene foam is known for its low thermal conductivity and is widely used in insulated containers, while paper-based packaging offers environmental advantages but generally poorer heat retention[8,9]. Plastic containers fall somewhere in between, offering moderate insulation and structural strength[10,11]. In real-world settings, these material differences could significantly alter the rate at which heat is lost from the food to the environment.

From a Chemical Engineering perspective, understanding how material properties influence heat transfer enables more informed decisions in packaging design, particularly for products requiring thermal insulation without the use of active heating. Additionally, understanding the heat retention and treatment capabilities as a design aspect of packaging materials can guide design improvements in insulation, reduce unnecessary energy loss, and enhance consumer safety[12].

Heat transfer in this context is primarily governed by conduction through the packaging wall and convection at the fluid-air and container-air interfaces, with minor contributions from radiation. The process can be quantitatively described using Fourier's Law for Conduction and Newton's Law of Cooling for convection, where the rate of temperature change can be modelled using both the former and the latter. Hence, accounts for the geometry and material properties of the container. Furthermore, the physical properties of the contents, such as water content and heat capacity, may introduce confounding effects in real-use scenarios, which require controlled comparisons to isolate the role of the container material.

Despite the ubiquity of instant noodles, only a few studies have systematically compared the thermal performance of different food packaging materials under controlled conditions, and those studies mentioned do not specifically mention instant noodles or their optimal packaging design[13–15]. This presents a critical gap in understanding how material choices influence passive thermal management, especially in single-use packaging for instant noodles.

This study investigates how packaging material affects heat retention in ready-to-eat noodle cups by comparing three commercial products made of paper (Coles Chicken Noodles), plastic (Lian Pho Bo), and styrofoam (Fantastic Noodles). Two complementary experiments were conducted: the first measured cooling rates of the complete noodle systems, while the second used hot water alone to isolate the influence of packaging material without the confounding effects of food composition. The findings aim to inform packaging design strategies in the food industry, with broader implications for industrial performance, product quality, and sustainable material selection.

2. Methods

2.1 Experimental Setup

This study investigated the effect of packaging material on heat retention in ready-to-eat noodle cups using infrared thermal imaging. Two parallel experiments were conducted:

(1) Heat retention of noodle cups filled with noodles and hot water, and
(2) Heat retention of noodle cups filled with hot water only, isolating the influence of container material.

Three types of commercially available noodle cups were selected, representing different packaging materials:

- Coles Chicken Noodles – *Paper cup*
- Fantastic Noodles – *Styrofoam cup*
- Lian Pho Bo Rice Noodles – *Plastic bowl*

Prior to testing, cups containing noodles were weighed and adjusted to achieve consistent mass across all samples, ensuring that only the independent variable was the cup material. Water was heated to approximately 80°C using a standard electric kettle and poured into each cup at 250 mL for each cup. Lids were removed to allow natural convection, and all cups were placed on insulated laboratory benches to minimise conductive heat loss through the base.

A calibrated InfiRay Pro 2 thermal imaging camera was mounted on a makeshift tripod (Retort stand and clamp) and positioned vertically above the noodle cups to maintain a consistent viewing angle. The ambient room temperature was assumed to be approximately ~23°C throughout both experiments. A schematic overview of the procedure is provided in Figure 1**.**

2.2 Materials

- Instant noodle cups (paper, plastic, styrofoam – as above)
- Boiling water (~80 °C from electric kettle)
- InfiRay Pro 2 thermal camera (USB-C connected, calibrated)
- Retort stand and clamp (camera stabilisation & backup mounting)
- Digital scale (±0.1 g precision)
- Stopwatch (manual timing control)
- Beakers and stirring rods (for uniform water transfer)

2.3 Data Collection

After adding hot water to the noodle cups, thermal images were recorded at 5-minute intervals over a 25-minute period. Each thermal image captured the surface temperature distribution across the cup and the liquid interface. Spot temperature readings were also taken using the thermal camera's built-in measurement tool, capturing the central surface temperature of each cup. Data collection was synchronised using a stopwatch, with one operator recording times and another recording temperature readings to ensure accuracy and minimise delay.

Each measurement was repeated across five trials per cup type to account for experimental variability and support statistical analysis. All data were logged in structured spreadsheets in Microsoft Excel for subsequent processing.

2.4 Data Collection

Thermal image data were processed using the InfiRay manufacturer's software, which enabled frame-by-frame review and extraction of surface temperature data. The mean surface temperature at each time point was used to generate cooling curves (temperature vs. time) for each container type.

From these curves, the rate of heat loss was assessed visually and quantitatively. Heat transfer trends were interpreted using Newton's Law of Cooling, and container material performance was compared using the initial cooling rate. Where applicable, the convective heat transfer coefficient h was estimated assuming standard thermal models, and assessed thermal gradients across the container surfaces using visual infrared patterns.

A comparative evaluation of thermal retention performance was conducted for both experiments, isolating material influence while accounting for variability due to contents and environmental conditions.

3. Results

3.1 Temperature Measurements Over Time

Two complementary experiments were conducted. In Experiment 1, noodle cups containing both noodles and hot water were tested. In Experiment 2, the cups were filled with hot water only to isolate the effect of the packaging material alone. Temperature readings were recorded over a 25-minute period at 5-minute intervals using a calibrated thermal imaging camera. The average surface temperatures from five trials per cup type are summarised in Table 1.

Table 1. Average surface temperatures (°C) for noodle cups over 25 minutes in Experiments 1 and 2.

Temperature uncertainty: ±2 °C; time uncertainty: ±0.005 min.

EXPERIMENT 1: NOODLES AND WATER				EXPERIMENT 2: WATER WIHTOUT NOODLES		
Time (min) ±0.005 (*min*)	Coles Chicken (Paper) T (℃) ± 2(℃)	Lian Pho Bo (Plastic) T (℃) ± 2(℃)	Fantastic (Styrofoam) T (℃) ± 2(℃)	Coles Chicken (Paper) T (℃) ± 2(℃)	Lian Pho Bo (Plastic) T (℃) ± 2(℃)	Fantastic (Styrofoam) T (℃) ± 2(℃)
0	80	80	80	0	80	80
5	66	69.5	72.2	5	67.2	70.8
10	56.5	62.7	67.4	10	57.9	64.1
15	49.8	56.8	63.1	15	50.6	58.3
20	45.1	51.6	59.3	20	45.2	53.4
25	41.6	47.5	55.9	25	41.1	49.4

3.2 Cooling Rate Constants

To quantify heat dissipation over time, Newton's Law of Cooling was applied (*Equation 1)*:

[1] $\frac{dT}{dt} = -k\left(T - T_{amb}\right)$

Rearranging the equation we can obtain *(Equation 2):*

[2] $ln\left(T - T_{amb}\right) = -kt + C$

In order to calculate graphically the values for the cooling rate constant k, $ln\left(T - T_{ambient}\right)$ was graphed against time for both experiments, where T_{amb} = 23℃. The slope of the linear trendline represents the cooling rate constant, k as shown in Figure 1.

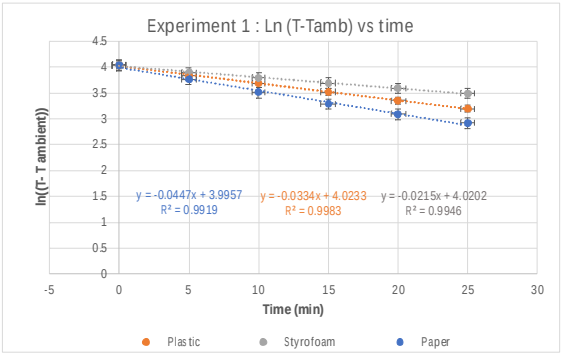

Figure 1. Cooling curves based on Newton's Law of Cooling for Experiment 1.

Logarithmic temperature differences $ln\left(T - T_{ambient}\right)$ plotted against time for three packaging materials: plastic (orange), styrofoam (grey), and paper (blue). Linear regression lines represent cooling behaviour in Experiment 1 (noodles and hot water), with slopes corresponding to the cooling constants k. Styrofoam exhibited the slowest rate of cooling, followed by plastic, with paper cooling most rapidly. Error bars represent the standard deviation from five replicates per material.

After conducting the same procedure for both Experiment 1 and 2, the following cooling constants were obtained, as shown in Table 2.

Table 2. Cooling rate constants k (min^{-1}) for paper, plastic, and Styrofoam noodle cups across Experiments 1 and 2.

EXPERIMENT N.	COLES (PAPER) $k\ (min^{-1})$ ±0.0020	Lian Pho Bo (Plastic) $k\ (min^{-1})$ ±0.0007	Fantastic (Styrofoam) $k\ (min^{-1})$ ±0.0008
1	-0.0447	-0.0334	-0.0215
2	-0.0459	-0.0306	-0.0204

Cooling constants were derived from linear regression $ln\left(T - T_{ambient}\right)$ vs. time plots, based on Newton's Law of Cooling. Experiment 1 included noodles and hot water; Experiment 2 used hot water only. Mean values are shown with standard errors: paper (±0.0020), plastic (±0.0007), styrofoam (±0.0008).

3.3 Heat Loss Quantification

Total accumulated heat loss was calculated separately through conduction and convection using the following equations ([3],[4]).

[3] $Q_{cond} = \frac{k_{material} \cdot A \cdot \left(T - T_{amb}\right)}{D}$

[4] $Q_{conv} = h \cdot A \cdot \left(T - T_{amb}\right)$

Where:

- $k_{material}$: thermal conductivity – paper (0.05), plastic (0.2), Styrofoam (0.033) $W\ /\ m \cdot K$
- h: Convective heat transfer coefficient - paper (10), plastic (12), Styrofoam (8) $W\ /\ m^2 \cdot K$
- A (Surface Area) = 0.01 m^2
- D (Diameter) = 0.002 m
- T_{amb} = 23°C

Table 3 summarises the calculated heat losses at each time point for both experiments.

Table 3. Accumulated heat loss by conduction and convection for paper, plastic, and Styrofoam noodle cups in Experiments 1 (a) and 2 (b).

(a).

EXP 1	ACCUMULATED HEAT LOSS Q (W)					
Time (min) ±0.005 (min)	$Q_{conducted}$ (PAPER) ±0.05W	$Q_{convected}$ (PAPER) ±0.02W	$Q_{conducted}$ (Plastic) ±0.2W	$Q_{convected}$ (Plastic) ±0.024W	$Q_{conducted}$ (Styrofoam) ±0.033W	$Q_{convected}$ (Styrofoam) 0.016 ± W
0	14.25	5.7	57	6.84	0.57	4.56
5	25	10	103.5	12.42	1.062	8.496
10	33.375	13.35	143.2	17.184	1.506	12.048
15	40.075	16.03	177	4.056	0.401	3.208
20	45.6	18.24	205.6	7.488	0.764	6.112
25	50.25	20.1	230.1	10.428	1.093	8.744

(b).

EXP 2	ACCUMULATED HEAT LOSS Q (W)					
Time (min) ±0.005 (min)	$Q_{conducted}$ (PAPER) ±0.05W	$Q_{convected}$ (PAPER) 0.02 ± W	$Q_{conducted}$ (Plastic) ±0.2W	$Q_{convected}$ (Plastic) ±0.024W	$Q_{conducted}$ (Styrofoam) ±0.033W	$Q_{convected}$ (Styrofoam) ±0.016W
0	14.25	5.7	57	6.84	9.405	6.84
5	25.3	10.12	104.8	12.576	17.8365	12.972
10	34.025	13.61	145.9	17.508	25.476	18.528
15	40.925	16.37	181.2	21.744	32.3565	23.532
20	46.475	18.59	211.6	25.392	38.5935	28.068
25	51	20.4	238	28.56	44.22	32.16

This table presents accumulated heat loss $Q\ (W)$ at 5-minute intervals over a 25-minute period for two conditions: Experiment 1 (a) (noodle cups with noodles and hot water, top panel) and Experiment 2 (b) (cups with hot water only, bottom panel). Heat loss was calculated separately via conduction and convection using standard thermal models and material properties. Assumed parameters include surface area $A = 0.01\ m^2$, Diameter $D = 0.002\ m$, and literature values for thermal conductivity k and convective heat transfer coefficient h. Reported uncertainties reflect propagation of error from temperature measurements and material constants.

Conductive heat loss increased linearly with time and was highest for plastic and paper containers. In contrast, Styrofoam cups exhibited markedly lower conductive losses, consistent across both noodle-containing and water-only trials seen in Figure 2.

Convective heat loss followed a similar trend, shown in Figure 3, with paper containers losing the most heat to the surrounding environment and Styrofoam the least. Plastic cups showed intermediate performance across all timepoints.

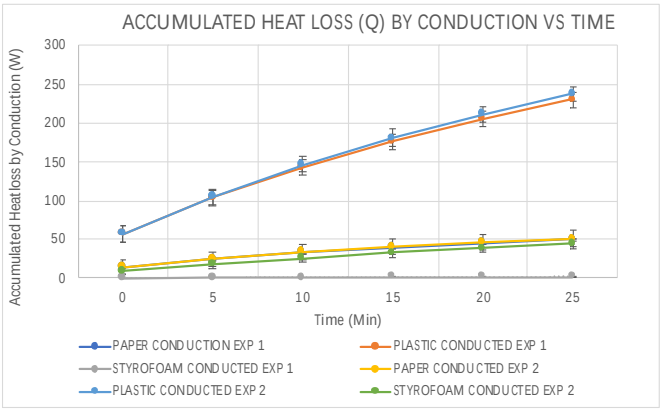

Figure 2. Accumulated heat loss by conduction over time for three packaging materials (Paper, Plastic, Styrofoam) across two experimental conditions (Experiment 1: Noodles & water, Experiment 2: Without noodles, water only).

Total conducted heat loss $Q\,(W)$ was calculated using Fourier's law for paper, plastic, and styrofoam noodle cups at 5-minute intervals. Experiment 1 (with noodles and water) and Experiment 2 (with water only) are compared. Plastic and paper cups exhibited substantially higher conductive heat loss than Styrofoam. Error bars represent uncertainty from temperature measurements and assumed material parameters.

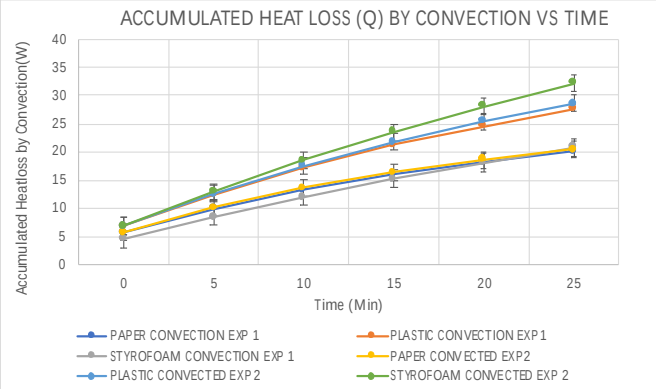

Figure 3. Accumulated heat loss by convection over time for three packaging materials (Paper, Plastic, Styrofoam) across two experimental conditions (Experiment 1: Noodles & water, Experiment 2: Without noodles, water only).

Total convective heat loss $Q\,(W)$ was calculated using Newton's law of cooling for paper, plastic, and styrofoam noodle cups at 5-minute intervals. Experiment 1 (with noodles and water) and Experiment 2 (with water only) are compared. Paper consistently showed the highest convective heat loss, while Styrofoam showed the lowest, indicating superior insulation performance. Results reflect the combined influence of surface temperature difference and estimated convective heat transfer coefficients. Error bars represent propagated uncertainty in thermal measurements and modelling assumptions.

4. Discussion

The results of both experiments confirm that packaging material plays a significant role in determining the thermal retention properties of ready-to-eat noodle cups. Across both trials, Styrofoam consistently exhibited the highest insulation performance**,** as evidenced by the lowest cooling rate constants and the smallest cumulative heat loss from both conduction and convection. These findings are consistent with prior literature that highlights the low thermal conductivity of expanded polystyrene (EPS), attributed to its porous microstructure and entrapped air pockets that inhibit heat transfer[16].

The exponential cooling behaviour observed in all materials, with R^2 above 0.998 for the fitted logarithmic models, seen in Figure 1, confirms the suitability of Newton's Law of Cooling for modelling temperature loss in this system. This agreement further validates the use of logarithmic regression to derive reliable cooling rate constants for comparative analysis.

In line with thermal conductivity data, plastic containers showed intermediate insulation, while paper cups exhibited the most rapid heat loss**.** The thermal conductivity values assumed in our calculations, 0.03 W/m·K for styrofoam, 0.2 W/m·K for plastic, and 0.05 W/m·K for paper, generally match trends reported in studies of commercial and biodegradable packaging materials[17,18]. However, it is important to note that theoretical $\boldsymbol{k}$ represents idealised or pure materials, whereas actual food containers often involve composite structures**,** such as laminated layers, wax coatings, or blended polymers**.** Real packaging may vary in wall thickness, material blends, or include multilayered structures designed to mimic biological thermoregulation, as explored in biomimetic packaging research[19]. Hence, these heterogeneities may lead to significant variation in real-world performance.

Notably, Experiment 2**,** which removed noodles and used only hot water, revealed greater differentiation in thermal performance among the containers. This outcome may reflect the fact that food content modifies heat transfer dynamics by absorbing thermal energy and limiting convective surface exposure. Previous infrared thermography studies support the observation that internal contents play a critical role in modulating heat retention[20].

From a Chemical & Environmental Engineering perspective, these results highlight the trade-off between thermal insulation and environmental sustainability. While Styrofoam demonstrated superior heat retention, its ecological footprint remains a pressing concern. Life cycle assessments have consistently shown that polystyrene contributes disproportionately to pollution and waste compared to biodegradable alternatives such as mycelium-based composites or molded pulp[21]. Although these greener materials continue to improve in durability and thermal stability**,** they still fall short of the mechanical performance achieved by petroleum-based polymers, particularly under moisture or high-temperature stress[22].

Another key consideration is food safety, particularly in relation to temperature exposure over time. Bacterial proliferation is known to peak within specific thermal windows, for example, *Escherichia coli* grows optimally between 20 °C and 45 °C, with peak replication near 37 °C[23]. Thus, the choice of packaging material has critical implications for shelf life, consumption safety, and thermal hold times. Emerging technologies such as phase change materials (PCMs) offer dynamic thermal buffering, which could help maintain temperatures outside microbial growth ranges while also enhancing thermal regulation[19].

This study, while robust in design, is subject to several limitations. First, thermal conductivity values were treated as

constant, despite the fact that many materials, especially foams, exhibit temperature-dependent thermal behaviour[24]. The assumption of a fixed k-value across a cooling range from 80 °C to ~40 °C may introduce inaccuracies in estimating actual heat loss.

Additionally, instrumentation variability may have introduced measurement error. The thermal imaging cameras were calibrated prior to use, but slight inconsistencies in angle, distance, or emissivity calibration could affect surface temperature readings. Repeat trials reduced the influence of outliers, but improvements could include automated temperature logging**,** multi-angle imaging**,** or the use of embedded thermocouples to cross-validate infrared readings.

The simplified geometric and thermal modelling also assumed uniform wall thickness and heat distribution, while real containers may have variable thickness**,** double walls**,** or hidden layers**.** Future studies could employ CT scanning or destructive cross-sectional analysis to better characterise material structure and validate modelling assumptions.

Future work should also investigate hybrid packaging materials, including those augmented with aerogels or PCMs. Aerogel-embedded composites have been shown to provide exceptional thermal resistance at minimal weight, though they currently remain cost-prohibitive for widespread food packaging use[25]. Broader studies could also include biodegradable or recyclable materials, helping industry transition away from EPS (Styrofoam) while maintaining effective thermal performance.

Overall, the findings reinforce that packaging material choice directly influences heat retention in ready-to-eat foods. While EPS (Styrofoam) continues to deliver excellent performance in short-term insulation, it raises significant environmental and regulatory concerns**.** The results of this study contribute to the growing body of work aiming to find balanced solutions that optimise thermal insulation, food safety**,** environmental responsibility, and economic feasibility**.** With the emergence of novel material systems and advanced modelling techniques, future packaging innovations will be better equipped to meet these demands across the food sector.

5. Conclusion

This study demonstrated that packaging material has a significant impact on the heat retention performance of ready-to-eat noodle cups. Through two complementary experiments, one using noodle-filled containers and the other using hot water only, we showed that Styrofoam consistently exhibited the highest thermal insulation, followed by plastic, with paper showing the most rapid heat loss. These findings directly support the research aim of evaluating how material composition affects heat transfer and highlight the dominant role of packaging properties in controlling thermal behaviour during passive cooling.

The results have clear Chemical Engineering relevance, particularly for the design of thermally efficient and cost-effective food packaging. The application of Newton's Law of Cooling and fundamental conduction/convection models allowed for the quantification of cooling rates and cumulative heat loss, confirming that EPS (Styrofoam) materials retain heat longer due to their low thermal conductivity. However, the environmental burden of polystyrene packaging presents a major trade-off. This underscores a key industry challenge: balancing thermal performance with environmental sustainability, safety, and cost.

These insights have practical implications for food safety, shelf-life management, and the development of more sustainable packaging alternatives. Material innovations such as bio-foams, molded pulp, and aerogel-enhanced composites may offer viable alternatives that reduce environmental impact while maintaining adequate thermal performance. However, these emerging materials require further testing under real-use conditions to evaluate durability and cost-effectiveness.

Future research should explore temperature-dependent material properties**,** multilayer or composite packaging systems, and the incorporation of phase change materials for active thermal regulation. Improvements in thermal measurement techniques, such as embedded sensors or multi-surface infrared capture, could reduce experimental error and provide more detailed thermal mapping. Expanding the analysis to include biodegradable materials or dynamic loading conditions (e.g. opening/closing lids) would further enhance the applicability of findings.

In summary, this work reinforces the importance of packaging material selection in food engineering applications and provides a methodological foundation for evaluating insulation performance in consumer products. Continued interdisciplinary efforts will be essential to develop packaging solutions that meet the demands of thermal efficiency, environmental responsibility, and public health.

Acknowledgements

The authors thank the University of Sydney and the CHNG2803 teaching team for providing access to thermal imaging equipment and laboratory resources. We also acknowledge the guidance provided by our lab demonstrators and tutors during the experimental sessions.

The authors used AI-assisted tools (OpenaAI's ChatGPT) for drafting support, low-level proofreading and for the editing and improvement of the graphical abstract of this Journal Article.

Authorship statement: Elias Navarrete Cubillos served as the project coordinator, assigning roles, managing deadlines, and contributing to the Introduction, Abstract, and Conclusion while providing support for Methods, Results, and Discussion. Gabriel Gutierrez Salmeron was responsible for the Results

section and contributed to proofreading and overall editing of the Journal Article. Jordan McCammon co-authored the Discussion, alongside Samuel Stoyles, who also contributed to its development. Llewellyn Govender led the preparation of the Methods section. Sebastian Dominguez Flores (Tutor) provided task direction and project assistance, and Dr. Gobinath Rajarathnam provided conceptual direction, research and writing guiding frameworks, facilitated project resources, and direct project supervision.

Appendix

Error Calculation for k values graphical analysis:

Starting from $\Delta T = \pm 2$°C from device,

$$\Delta y = \left|\frac{d}{dT} Ln(T - Tamb)\right| \cdot \Delta T = \frac{1}{T - Tamb} \cdot \Delta T$$

Where $\Delta y = erroronln(T\text{-}Tamb)$,

Once we calculate the error Δy for each measurement we then have to consider the form of the best-fitting line formula: $\Delta y = mx + b$ where the error on m would be **:**

$$\Delta m = \frac{s}{\sqrt{\sum (xi - \bar{x})}}$$

Where s is the is the standard error of the residuals:

$$\Delta s = \sqrt{\frac{1}{n-2} \sum (yi - \bar{y})^2}$$

This way we found out the error for all the values of K on the report

Error Calculation for heat flux conduction:

Defining C as a constant because there are guessed values,

$$q = C \cdot (T - Tamb)$$

$$\Delta C = \frac{k \cdot A}{d}$$

$$\Delta q = \left|\frac{dq}{dT}\right| \cdot \Delta T = \left|C \cdot \frac{d\,(T - Ta)}{dT}\right| \cdot \Delta T = C \cdot \Delta T$$

$$\Delta q = \frac{k \cdot A}{d} \cdot \Delta T$$

Repeating this calculation for both experiments calculated we computed Δq conducted.

Error Calculation for heat flux convection:

$$q = C \cdot (T - Tamb)$$

$$\Delta C = h \cdot A$$

$$\Delta q = \left|\frac{dq}{dT}\right| \cdot \Delta T = \left|C \cdot \frac{d\,(T - Ta)}{dT}\right| \cdot \Delta T = C \cdot \Delta T$$

$$\Delta q = h \cdot A \cdot \Delta T$$

Repeating this calculation for both experiments calculated we computed Δq convection .

References

1. Bramsiepe, C. *et al.* Low-cost small scale processing technologies for production applications in various environments—Mass produced factories. *Chem. Eng. Process. Process Intensif.* **51**, 32–52 (2012).

2. Tong, C. Materials-Based Solutions to Advanced Energy Systems. in *Introduction to Materials for Advanced Energy Systems* 1–86 (Springer International Publishing, Cham, 2019). doi:10.1007/978-3-319-98002-7_1.

3. Michel, M. *et al.* Benefits and challenges of food processing in the context of food systems, value chains and sustainable development goals. *Trends Food Sci. Technol.* **153**, 104703 (2024).

4. Coorey, R. *et al.* The Impact of Cooling Rate on the Safety of Food Products as Affected by Food Containers. *Compr. Rev. Food Sci. Food Saf.* **17**, 827–840 (2018).

5. Ncube, L. K., Ude, A. U., Ogunmuyiwa, E. N., Zulkifli, R. & Beas, I. N. Environmental Impact of Food Packaging Materials: A Review of Contemporary

Development from Conventional Plastics to Polylactic Acid Based Materials. *Materials* **13**, 4994 (2020).

6. Guillard, V. *et al.* The Next Generation of Sustainable Food Packaging to Preserve Our Environment in a Circular Economy Context. *Front. Nutr.* **5**, 121 (2018).
7. Park, J., Lee, J.-S., Jang, Y. A., Chung, H. R. & Kim, J. A comparison of food and nutrient intake between instant noodle consumers and non-instant noodle consumers in Korean adults. *Nutr. Res. Pract.* **5**, 443–449 (2011).
8. Deshwal, G. K., Panjagari, N. R. & Alam, T. An overview of paper and paper based food packaging materials: health safety and environmental concerns. *J. Food Sci. Technol.* **56**, 4391–4403 (2019).
9. Ghoshal, T., Parmar, P. R., Bhuyan, T. & Bandyopadhyay, D. Polystyrene Foams: Materials, Technology, and Applications. in *ACS Symposium Series* (ed. Gupta, R. K.) vol. 1439 121–141 (American Chemical Society, Washington, DC, 2023).
10. Nayanathara Thathsarani Pilapitiya, P. G. C. & Ratnayake, A. S. The world of plastic waste: A review. *Clean. Mater.* **11**, 100220 (2024).
11. Farrell, R. *et al.* The function and properties of common food packaging materials and their suitability for reusable packaging: The transition from a linear to circular economy. *Curr. Res. Green Sustain. Chem.* **9**, 100429 (2024).
12. Turan, D., M. Keukens, B. & N. J. Schifferstein, H. Food packaging technology considerations for designers: Attending to food, consumer, manufacturer, and environmental issues. *Compr. Rev. Food Sci. Food Saf.* **23**, (2024).
13. Wang, K., Yang, L. & Mariusz, K. Investigation of the effect of thermal insulation materials on packaging performance. *Packag Technol Sci* **33**, 227–236 (2020).
14. Ding, Y., Jiang, Y., Deng, Y. & Zhao, Y. Effect of packaging materials and storage temperature on water status, mechanical and thermal properties of black garlic. *Food Packag. Shelf Life* **24**, (2020).
15. Dieckmann, E., Nagy, B., Yiakoumetti, K., Sheldrick, L. & Cheeseman, C. Thermal insulation packaging for cold-chain deliveries made from feathers. *Food Packag. Shelf Life* **21**, (2019).
16. Zhou, E., Wu, J., Shen, C., Zhang, H. & Qin, G. The stable behavior of low thermal conductivity in 1T-sandwich structure with different components. *J. Appl. Phys.* **131**, 185702 (2022).
17. Asfaw, N. T., Absi, R., Labouda, B. A. & El Abbassi, I. Assessment of the thermal and mechanical properties of bio-based composite materials for thermal insulation: A review. *J. Build. Eng.* **97**, 110605 (2024).
18. Cheng, J., Gao, R., Zhu, Y. & Lin, Q. Applications of biodegradable materials in food packaging: A review. *Alex. Eng. J.* **91**, 70–83 (2024).

19. Guo, Z.-G. *et al.* Biomimetic, hierarchical-programmed gel coating for adaptive and sustainable thermal modulation. *Matter* 102057 (2025) doi:10.1016/j.matt.2025.102057.

20. Kim, K. & Feng, S. S. Thermal Mapping Using Infrared Thermography. in *Application of Thermo-Fluidic Measurement Techniques* 215–250 (Elsevier, 2016). doi:10.1016/B978-0-12-809731-1.00008-3.

21. Enarevba, D. R. & Haapala, K. R. A Comparative Life Cycle Assessment of Expanded Polystyrene and Mycelium Packaging Box Inserts. *Procedia CIRP* **116**, 654–659 (2023).

22. Liu, Y., Ma, S., Wang, F. & Wang, L. Advances in Research of Molded Pulp for Food Packaging. *J. Renew. Mater.* **11**, 3831–3846 (2023).

23. Parker, N., Schneegurt, M., Thi Tu, A.-H., Lister, P. & Forster, B. M. *Microbiology*. (OpenStax, 2016).

24. Berardi, U. The impact of aging and environmental conditions on the effective thermal conductivity of several foam materials. *Energy* **182**, 777–794 (2019).

25. Zhang, J. *et al.* Silica aerogel-PVA dough: A high internal phase composite with superior thermal insulation and gas barrier. *Compos. Sci. Technol.* **251**, 110553 (2024).

The Sydney Journal of Interdisciplinary Engineering
SJIE 1(2) X–X (2025) https://doi.org/XXXX/XXXX

Heat Transfer of Sunscreens: Investigation into the Conductive Properties of Sunscreen

Matthew De Dominicis[1], Jake Shearan[1], Aoi Miyata[1], Aryan Reddy[1], Ethan Le[1], Sebastian Dominguez Flores[1], Sebastian Dominguez Flores[1], Minghao Zhang[1], David Alam[1], Gobinath Rajarathnam[1]

[1]Chemical and Biomolecular Engineering, The University of Sydney, Sydney, Australia

E-mail: xxx@xxx.xx

Received xxxxxx
Accepted for publication xxxxxx
Published xxxxxx

Abstract

Sunscreen is a major preventative product very commonly used for protection against ultraviolet (UV) radiation and the skin cancers associated with extended exposure. There is minimal research into the conductive properties of sunscreen as the major research focus is on radiation effects, but it is still important to understand the impact of sunscreen on the body's natural heat transfer to the external environment through the skin and extremities, a necessary process to ensure homeostasis. Our research group investigated the conductive properties of sunscreens over two experiments. The first analysed the effect of increasing the thickness of sunscreen on its conductive heat transfer. The results showed that as thickness increased, heat transfer decreased and allowed us to calculate the conduction coefficient (k) for this specific sunscreen sample to be 0.43 W/mK. The second experiment analysed what the impact of combining multiple sunscreens which varied in ingredients, sun protection factor (SPF) and being water or oil based was on their heat transfer. The results allowed us to calculate the thermal conductivity constant (k) for each sunscreen and their mixtures, with Sunscreen B (Brand name Bondi Sands©) having the highest at k=1.34 W/mK, and Sunscreen A (Brand name LeTan©) the least at k=0.27 W/mK. Further, it was found that combining different sunscreens in a 1:1 ratio roughly portrayed that the conductive properties of the mixture was the average of the sunscreen's properties on their own (For example mixture AB had a conduction coefficient of k=0.70 W/mK). With an understanding of the conductive properties of sunscreen, we can see how exactly its application impacts heat transfer and evaluate if its effects in general are significant, or whether some sunscreens are better for different applications (i.e. ensuring insulative or conductive properties of different sunscreens are used for correct applications).

Keywords: *conduction, sunscreen, conductive heat flux (q''), thermal conductivity constant (k), ultraviolet (UV) radiation*

1. Introduction

1.1 Motivation and Aim

1.1.1 General problem

In Australia, sunscreen is an essential resource in providing protection against the relatively large proportion of UV radiation we experience in everyday life. It is one of the most effective preventative measures against skin cancers such as basal cell carcinoma, squamous cell carcinoma and melanoma, making it vital in ensuring the longevity of our lives. Due to this the prevalence of sunscreen use is at an all-time high, but since the focus is on its benefits in radiation prevention, there is minimal research into its conductive properties. The human body relies on heat transfer between the extremities and skin against the external environment as a way to ensure thermal homeostasis [1]. For the body's continued effective function, core temperature must

remain approximately between 36.5 to 37.5 degrees Celsius, as this allows for the correct and optimized function of enzymes and other conditions of various bodily systems.

1.1.2 Scope and objective

In this study, we researched into the conductive properties of various brands of sunscreen, with different ingredients and Sun Protection Factor (SPF) ratings. Our research was conducted over two experimental investigations with the following questions:

What is the effect of increasing the thickness of sunscreen on its conductive ability to allow heat transfer?

This allowed us to analyse the conductive properties of sunscreen as an implication to its effect on the body's heat transfer.

What is the impact of applying different types and/or a combination of different sunscreens on their heat transfer?

It is quite often that when we apply sunscreens, we use different or multiple sunscreens with different protection ratings and ingredients. This experiment analysed the different conductive properties of different brand sunscreens (Appendix M), and what the impact of applying multiple sunscreens in a mixture is on its heat transfer properties.

For both these experiments, we simulated heat transfer using a hot plate as our heat generation source and measured the temperature of our sunscreen samples over a controlled period of time using thermal imaging cameras. From this experimental data, we used theory such as Fourier's law to calculate the conductive heat transfer coefficient (k), heat flux and other conductive properties of our samples. Through the trends in the data, we analysed our research questions and discussed if the application of sunscreen has a significant impact on the body's overall heat transfer. It is important to note that there were some significant assumptions made during this investigation, primarily that were was negligible heat loss the surroundings and there was only 1D conduction. This was primarily justified through the methodology and data collected and the experimental set-up. With the measured temperature being taken directly from the hot plate and the surface of the sunscreen sample, heat flux lost to the surroundings through the sides of the sample and other dimensions would have negligible impact due to relatively small height of the samples compared to the radius, leading to minimal heat loss. This was true in both investigations.

1.2 Previous studies

There has been minimal study into the conductive properties of sunscreen as all studies predominantly analyse its UV radiation protection properties. With that said some relevant trends can be seen as a result of studying different applications (although there was more qualitative analysis rather than quantitative measurement of convection). Some relevant trends were seen in the following studies:

'*Effects of sunscreen use during exercise in the heat', T.D. Wells* – In this study, it was found that sunscreen worn in hot, dry conditions significantly increased skin temperature (i.e. less heat was transferred from the boundary between the body and bulk air) [2].

'Sunscreen Use and Sweat Production in Men and Women' J. Aburto-Corona – In this study, the application of sunscreen decreased perspiration, which could be a result of sunscreens impact on heat transfer between the body and external environment [3].

The lack of information on these conductive properties of sunscreen is part of our motivation to partake in this study, as it is important to understand the underlying effects such a commonly applied product has on maintaining health and wellbeing.

2. Methodology

2.1 General setup of the equipment used

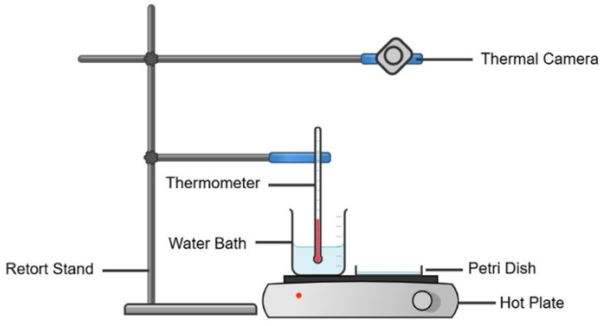

Figure 1: Experimental diagram testing varying combinations of sunscreen samples for both investigations 1 and 2.

The same experimental setup was used for throughout the investigation, which is shown in Figure 1. A thermometer was clamped to a retort stand and placed in a 50 mL beaker water bath to continually measure the temperature of the hot plate (37°C). The sunscreen sample tested was put inside petri dish case made of PET (polyethylene terephthalate) plastic with thickness of approximately 0.5mm. An InfiRay Pro 2 thermal camera was connected to a laptop via a cable and placed above the hot plate and the sunscreen surface. The thermal camera was fixed on an angle above the hot plate surface, in order to increase the reliability and the accuracy of the temperature recorded. The major challenges of this methodology involved getting consistent temperature readings from the thermal camera, due to unsteady camera angles as they were originally held by hand. This was addressed by attaching the camera to the retort stand to ensure consistent readings between measurements, improving accuracy and lowering error. Additionally, pre-mixing the sunscreen samples before application aided homogeneity of samples. More impactful challenges for the equipment and methodology that had a significant effect on the investigation have been discussed in section 3.3.2. Aside from this, the experimental set-up and methodology worked effectively.

2.2 Investigation 1: Effect of Sunscreen Thickness on Conductive Heat Flux

The petri dish was filled with sunscreen of various thicknesses. There was a total of 5 samples used with thicknesses ranging between 2 mm to 10 mm in increments of 2 mm. The thickness of the sunscreen was measured by dipping a metal plate into the petri dish, then measure the length of the plate that was covered by the sunscreen. The surface temperature of both the sunscreen and the hot plate was measured every 1 minute and up to three minutes after placing the samples on the heat plate. For each reading the temperature was recorded at three different points on the surface area for each sample, as shown in Figure 2. This was done in order to increase the reliability and account for the slight uncertainty of the thickness across the sunscreen sample.

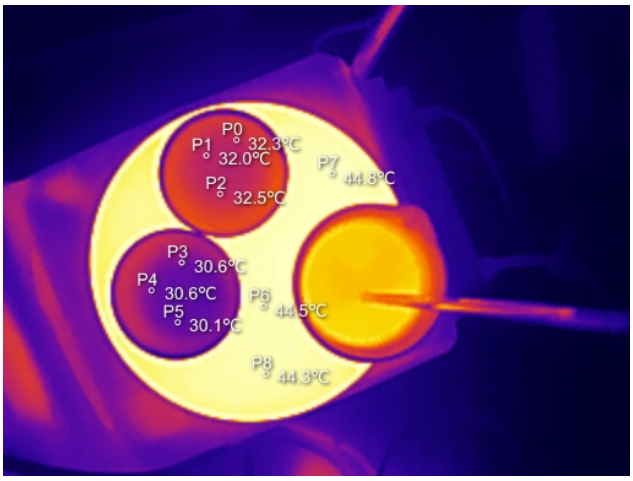

Figure 2. Screenshot of the thermal scan taken for thickness sample 6 and 8 mm, at third minute. Notice 3 measurements were done for each sample in order to account for variation of the thickness across the surface.

2.3 Investigation 2 - Effect of Sunscreen Mixture on Conductive Heat Flux

1 g of sunscreens A, B, and C were evenly distributed on separate plastic petri dishes. Mixtures AB and AC were composed of an evenly mixed 1:1 ratio of each sunscreen (0.5 g each). They were placed on the hot plate and temperatures were recorded every minute for six minutes. A temperature time plot was then produced. The overall method was very similar to the general methodology, with variations of mixture composition rather than thickness.

3. Investigation 1 - Effect of Sunscreen Thickness on Conductive Heat Flux

3.1 Hypothesis

The rate of the heat transferred from the hot plate to the surface of the sunscreen can be determined by the Fourier's law of thermal conduction for plane wall.

$$q'' = -k\frac{(T_{Plate} - T_{Surface})}{L_{(Sunscreen\ Thickness)}} \qquad \text{Eq (1)}$$

Where q'' is the conductive heat flux through the sunscreen (W/m^2), k is the thermal conductivity constant (W/mK), T_{plate} and $T_{surface}$ refer to the temperature of the heat plate and sunscreen surface respectively and L refers to the sunscreen thickness (m). As shown in Equation 1 above, the characteristic length of the plane (L) is inversely proportional to the heat flux (q"). Therefore, an increase in the thickness of the sunscreen

is expected to decrease the rate of conduction. However, it is important to mention that some simplifications have been applied to this hypothesis. Firstly, heat conduction through the plastic container was assumed to be negligible (i.e., the measurement of the heat flux assumes that the sunscreen is directly in contact with the hot plate). Under temperatures between 20°C and 80°C, the thermal conductivity (k) of PET is around 0.2 W/m·K [4]. Considering that the approximate *k* value of the sunscreen is 0.43 W/m·K, the plastic would function as an insulator. However, the thickness of the plastic is approximately 0.5 mm, which is very thin. Therefore, the assumption is made that the temperature gradient throughout the plastic container will stabilise relatively quickly, and it would not affect the overall trend in the change of heat conduction, given that the temperatures are measured every 60 seconds. The inclusion of conduction through the plastic container increases the complexity of the heat conduction estimation significantly, as the plastic container also covers the sides of the sunscreen.

The second major predicted trend is that the heat flux will decrease with time. Again, using Fourier's law of conduction (Equation 1), the heat transfer rate is proportional to the temperature difference between the surface of the hot plate and the sunscreen. With this, as natural convection is the only factor for convective heat transfer from the sunscreen to the ambient air, it is reasonable to assume that the rate of heat transfer into the sunscreen is greater than the amount going out due to convection (i.e., energy is being stored in the sunscreen over time). Therefore, it is appropriate to consider that the temperature of the sunscreen surface will increase over time, and hence the temperature difference will decrease. Consequently, the heat transfer rate will decrease over time as well.

3.2 Results

3.2.1 Calculations for k

The thermal conductivity constant for the sunscreen in the thickness investigation was found through researching current literature on the composition of general sunscreens. Current literature indicated the base of sunscreens typically consist of water and oils with other active ingredients acting as UV filters and blockers [5]. Generally, sunscreen foundations consist of approximately 50-70% water [6] and 10-30% mineral, silicone and plant-based oils, with the rest being smaller constituents and active ingredients. The thermal conductivity constants for water and generic oils can be found and from this a thermal conductivity constant was estimated by using a weighted average approach, assuming the sunscreen was 60% water, 30% oils and 10% active ingredients. Water is known to have a conductivity constant of approximately 0.61 W/mK [7] at room temperature (300K). The thermal conductivity constant of the oil mixture was estimated to be approximately 0.15 W/mK by averaging generic values of mineral, silicone and plant-based oils [8] [9] [10]. The only active ingredient specific to the sunscreen used in this investigation that had an accessible conductivity constant was octyl salicylate with a value of 0.15 W/mK [11]. From this, the generic thermal conductivity constant was calculated to be 0.43 W/mK (Appendix G). This is a fair value based upon known thermal conductivities of the key components of common sunscreens.

3.2.2 Main Results

The data collected across the five trials of thickness at three repeats indicate two major trends, with high R^2 values for all trend lines. The first is the expected behaviour of the heat flux via conduction through the sunscreen decreasing with greater thickness due to a more protective and insulated character. Analysis of experimental data as seen in Figure 3 shows that the heat flux dropped from its initial values from approximately 84.1% to 90.2% when the thickness increased from 2mm to 10mm (Appendix H). Another trend identified was that the decrease in heat flux as thickness increased seemed to taper off, resulting in diminishingly lower heat fluxes as the results stayed relatively stable beyond 6mm of thickness. Analysis shows that the heat flux drops were greatest in the 2mm to 6mm range, with drops of between 43% to 57% approximately, with the least significant thickness increments being in the 6mm to 10mm range, with heat flux drops as low as 13% (Appendix I).

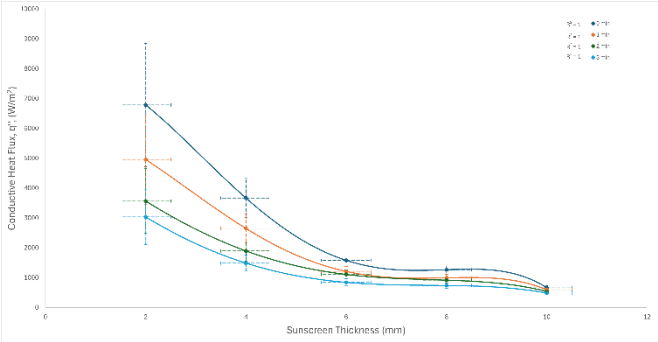

Figure 3: Graphed results of thickness investigation against conductive heat flux with error bars and uncertainty shown. The full tabulated experimental and calculated results can be found in Appendix B and C. A larger graph can be found in Appendix N.

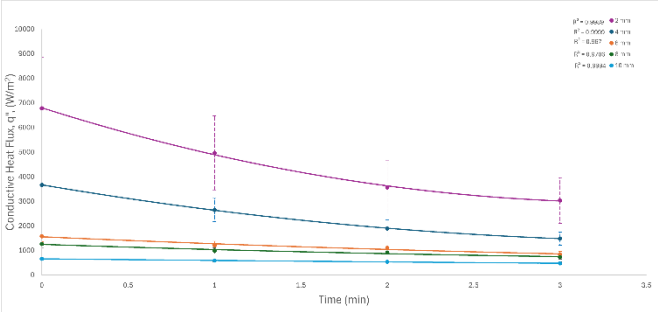

***Figure 4*: Graphed results of time against conductive heat flux with error bars and uncertainty shown. A larger graph can be found in Appendix N.**

The other major series of trends found relate to how the heat flux varied with time in this investigation. Firstly, the drop in heat flux remained relatively constant (between 90.1% to 84.1%) as thickness increased at different time periods of the investigation, indicating that the sunscreen's conductive properties were unaffected by time exposure and supports the ability of sunscreen to limit conductive heat transfer at longer periods of time. However, the difference between the heat fluxes at the same thickness greatly varied with time at smaller thicknesses, from drops of up to 59% at 2mm and 4mm to only 27% at 10mm (Appendix J). This can be best seen in Figure 4, where the largest drops in the early time periods of the investigation can be seen in the 2mm and 4mm series. This indicates that while the properties of the sunscreen samples remained relatively constant throughout the investigation period and exposure to heat transfer, the effect of initial conductive heat transfer is most significant with minimal sunscreen applied; with a greater thickness the effects of longer exposure are mostly mitigated, demonstrated by the 10mm measurements being very closely grouped by comparison. This mirrors the trends found above of increasing thickness having a diminishing effect upon decreasing conductive heat flux, with increasing the thickness also having an effect upon the effects of time exposure.

3.3 Discussion

3.3.1 Interpretation of trends.

Examining the overall trend of how the conductive heat flux decreased with increasing sunscreen thickness, this is something that is generally expected as a thicker material results in improvements to the insulative characteristics of the material and larger resistance, resulting in lower heat flux via conduction with an inverse relationship [12]. This can also be examined through Fourier's law, (Equation 1), which states that the heat flux is inversely proportional to material thickness, given all other conditions remain constant. This is quite strongly reflected in the experimental data, with the sunscreen thickness increasing by five times resulting in a heat flux decrease of approximately 80% to 90%. Another important trend found was that after 6mm, increasing the thickness had a diminishing effect on lowering the heat flux through the sunscreen. This is generally attributed to how a material may reach a point where additional layers contribute minimally to heat transfer due to the limited temperature gradient across them [13]. However, this may have also been caused by an equipment fault of poor hotplate calibration resulting in inconsistent temperature differences between trials, which is discussed in more detail below. These are important observations in terms of applying this investigation to a practical scenario and investigating the aim of this investigation, as it shows how sunscreen can be used as a protective/insulative barrier to conduction. While it is unlikely that an individual would put any more than 1mm or 2mm of sunscreen, it demonstrates the overall trend of how heat flux can be minimized by applying the correct thickness of sunscreen as well as the optimal thickness of sunscreen to minimize heat flux while using the minimum amount required. While the experimental set-up did not properly mimic human tissue or everyday conditions, it still demonstrates the underlying principles and trends that are relevant in practice.

Another major trend found was how the thermal insulation and heat flux drop remained constant with increasing thickness regardless of the time period of the investigation, indicating the conductive and thermal properties of sunscreen were unaffected by the time and thermal exposure, indicating they were able to maintain their protective characteristics over the course of the investigation. This is somewhat contradictory to known literature, as the protective qualities of sunscreen are only expected to decrease with time due to photodegradation [14] of active components and environmental wearing [15]. However, given the limited length of time exposure (three minutes) and the fact that most of these degradations are primarily related to UV radiation, the findings in this investigation are not really in conflict with known literature. This is an important finding in terms of practical applications as it suggests that sunscreen can maintain its conductive protection over longer time periods, though the limited time scope of this investigation needs to be considered. The other major trend found was that with less thin sunscreen samples, there was a far larger and impactful difference in between the start and end of the time period. This is important in terms of a practical application of this investigation as it indicates that given longer time periods of exposure, applying a thicker layer of sunscreen is more important for stronger heat flux protection.

3.3.2 Limitations and Future Work

- *Thermal Conductivity Constant*

One of the major limitations of this report was that a specific value of the thermal conductivity constant was not able to be readily accessible, and so a generic value was calculated from approximate value of major components of sunscreen. This is a significant issue as it does not allow for certainty in numerical value of heat flux and questions the accuracy and validity of the results. However, it is important to note that regardless of the value of this constant, relative comparisons are still completely valid, and numerical calculations of differences between trend lines are still applicable as simple scalar multiples.

- *Uncertainty*

Considering uncertainty, it can be seen in Appendix C and Figures 3 and 4 that there was a significant effect of uncertainty, with final fractional uncertainties between 0.11 and 0.30. Most of the results had uncertainty values of between 0.11 and 0.18 which are impactful, but still mostly acceptable, with the 2mm trial having significantly larger uncertainty due to the larger fractional uncertainty of sunscreen thickness. This resulted in a significant uncertainty for the 2mm trials, resulting in overlapping values (which can be seen in Figure 3) primarily caused by the large thickness uncertainty. While this is significant, the overall trends found are still readily apparent and repeatable. Additionally, it is important to consider how the validity of the uncertainty calculations was limited by the lack of information of the thermal conductivity constant. A value of 5% was chosen for this, through it is difficult to evaluate if this is a fair value and is important to critically examine.

- *Equipment Error and Calibration*

A problem with the equipment was with the hot plate calibration that resulted in random variation of temperatures during and between trials as the temperature probe was placed in a beaker of water. Since the heat capacity of water is significantly higher than that of sunscreen, and since there was more water in the beaker, this control beaker was far less responsive to temperature changes than the sunscreen samples, meaning that small changes in the water temperature resulted in large temperature changes in the samples. This resulted in random variation between trials at certain points lowering accuracy. This is also important in the practical application of data as it meant that the experimental set up was unable to properly mimic human tissue due to significantly higher hot plate temperature than intended (around 40^{o}C-65^{o}C rather than the intended 37^{o}C) reducing the practical applicability of this investigation.

Another problem was that it was difficult to accurately record and ensure even distribution of sunscreen in the petri dish. While parallax error was accounted for by dipping a small stick into the dish and measuring the height, the choice of measuring equipment was not ideal resulting in significant uncertainties compared to the size of the samples, increasing inaccuracy and random variation. Additionally, it was difficult to ensure even distribution of sunscreen and a piece of equipment such as a tamper could have helped to ensure even

distribution. The uneven distribution of sunscreen had a non-negligible effect resulting in variations of temperature across the sample surface. This was accounted for by taking three measurements for each individual measurement and averaging them to account for this variation. Another small point that created some systematic error came from the thickness of the petri dish. While this investigation assumed that the surface temperature of the hot plate was the temperature of the lower sunscreen, this would not be true due to some heat loss through the thickness of the base of the petri dish, leading to a small systematic error increasing the heat flux results from the true value. This is a limitation but isn't all that significant as this investigation cannot be directly applied to practical scenarios (due to the unrealistic temperatures and thicknesses) and still allows for strong comparison between trends and series. Additionally, the heat flux through the petri dish base would be insignificant compared to the sunscreen heat flux.

- *Practicality*

To improve the applicability of this investigation, the ranges of the thickness of sunscreen should be expanded to thinner values, as it is unlikely that an individual would apply more than two or so millimetres of sunscreen. Likewise, the time period could be expanded to better investigate if the conductive properties of sunscreen remain constant over longer periods that are more likely to be relevant to practical scenarios (such as up to an hour), and the experimental set-up could be more reflective of human tissue through the replacement of the petri dish with synthetic skin and tissue to mimic the thermal character of humans more accurately. In reality, there would be some form of uncontrolled convection, while in the investigation the effects of convection were minimal due to the walls of the petri dish blocking air flow. While this aided to isolate the effects of conduction, it limits the direct applicability of this investigation and convection would also have a significant effect of the behaviour and effectiveness of sunscreen. Additionally, a second thermal camera could be position horizontal to the sunscreen sample to measure the temperature gradient of the sample to gather more information on the conductive properties of the substance.

4. Investigation 2 - Effect of Different Sunscreen Material Composition and Combination on Heat Conduction.

4.1 Hypothesis

This experiment aimed to investigate the difference in heat transfer due to active ingredients of different brand sunscreens. The thermal conductivity (k) values of our sunscreens A, B, and C were 0.19, 1.34, and 0.27 respectively. It is known that mineral oils used in cosmetics, biomedicine, and food processes possess k values that range from 0.12-0.14 W/mK [8]. This is due to their physical structure, as oils contain weak intermolecular bonds that cannot absorb heat well. Studies show that starch water gels, at temperatures of 10, 50, and 80 degrees Celsius, possess k values of 0.364, 0.386, and 0.388 W/mK [18]. This demonstrates the difference in intermolecular bond strength between water and oil. It is predicted that mineral sunscreens that contain zinc oxide, such as sunscreen C, will exhibit the least heat transfer due to their low thermal conductivities. This is because of its properties as a physical blocker, forming a barrier on top of our skin to scatter and reflect UVA and UVB rays [16]. This is compared to chemical sunscreens which absorb into the skin, producing heat, rather than reflecting it [17].

4.2 Results

Table 1: Temperature increase of Sunscreens over 5 minutes

Mixture	ΔT(℃)
A	0.733
B	2.47
AB	2.17
C	0.967
AC	0.867

Table 2: Calculated K values of each individual type of Sunscreen

Sunscreen	Cp	q	K
A	2.81	2.06	0.19
B	3.10	7.65	1.34
C	2.84	2.75	0.27
AC	2.83	2.45	0.24
AB	2.97	6.43	0.70

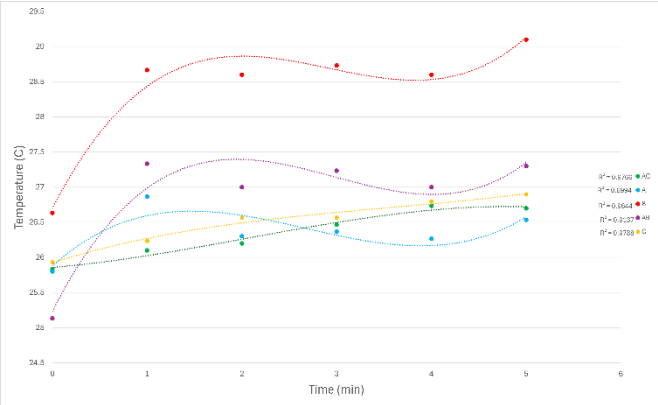

Figure 5: Average temperatures of Sunscreen mixtures over 5 mins. A larger graph can be found in Appendix N.

4.3 Discussion

4.3.1 Interpretation of results

The results collected measuring the temperature difference among mixtures of sunscreen indicated that the Sunscreen B (Bondi Sands) had the highest temperature increase of 2.47°C whereas the Sunscreen A (LeTan coconut Sunscreen) had the lowest of 0.73°C increase across 5 minutes. It was also found that the mixtures containing a 1:1 ratio of two designated sunscreens contained temperature increases that were approximately the average of their individual sunscreen tests. For example, Sunscreen A and Sunscreen C had a temperature increase of 0.73°C and 0.96°C respectively, and mixture AC was found to be 0.87°C, approximately the average of Sunscreen A and Sunscreen C's values with an error of only 2%. However, this trend was not fully consistent, as mixture AB's temperature increase was between the range of A and B but had a 35% error from the average. This observation would be mainly accounted by how uniform and how well the two sunscreens mix.

With this, there are 2 types of trends for the temperature change over time, depending on the type of sample used which are shown in Figure 5. For the sunscreen samples A, B and AB, the temperature tended to increase rapidly at the beginning, however it plateaus towards the end. For example, the surface temperature of the sunscreen for sample B had increased by 2.1℃ after 1 minute from initial temperature of 26.6℃ to 28.7℃, however the temperature fluctuates at around 28.7℃ between 1 to 5 minutes. The samples C and AC displayed a linear trend, since the temperature increased consistently throughout the experiment. This is clearly shown in the two straight lines coloured in yellow (Sample C) and green (Sample AC). This can be attributed to Fourier's law of conduction as initially the Sunscreen is around room temperature whereas the hot plate was 32°C. Thus, the first minute has the largest temperature difference between the two surfaces resulting in higher heat transfer in the system initially. In some cases, the sunscreen may not behave linearly due to the decomposition of the active ingredients within the emulsifier [21].

4.3.2 Analysis of mixtures

Instead of being evenly distributed within the emulsion, the active ingredients end up clustering, leaving gaps within the emulsion and allowing the heat to pass through unaffected. This means that at higher temperatures, the effectiveness of the sunscreen is compromised. Another possible explanation is that the mixture may not be entirely homogeneous. Some sunscreens may be more polar than others resulting in insolubility when mixing. Polar molecules tend to favour other polar molecules, hence introducing the phrase, "like dissolves like". Without an amphiphilic emulsifier, the two sunscreens simply produce a biphasic mixture with droplets of each sunscreen surrounding each other. Studies show that mixing chemical sunscreens with zinc oxide may significantly reduce its effectiveness. Research of mixing a non-mineral SPF 15 chemical sunscreen with and without zinc oxide was conducted [19]. It was found that the sunscreen with the zinc oxide reduced in effectiveness by 84.3-91.8% whilst the lone sunscreen exhibited a decrease of only 15.8%.

4.3.3 Analysis of materials and polarities

Sunscreens are generally divided into two groups being oil based, and water based. Sunscreen B mainly contains compounds such as benzyl alcohol and phenoxyethanol which are low molecular mass and polar solvents that would have better thermal conduction. Polar solvents are generally more able to transfer heat than non-polar counterparts purely due the stronger intermolecular forces allowing for effective energy transfer between molecules. Polarity can be compared through the Reichardt's ET (30) Polarity scale which compares the polarity a molecule to water [20]. The ET (30) scale of polarity is units of kcal/mol representing the energy between intermolecular bonds. However relative polarity is a ratio between waters polarity of 63.1kcal/mol (Saini) - 2023.

$$Relative\ Polarity = \frac{Polarirty_{\ molecule}}{63.1 kcal/mol} \quad \text{Eq(2)}$$

Benzyl alcohol and phenoxyethanol have relative polarities of 0.608 and 0.81. For comparison methanol which is a highly polar organic molecule has a relative polarity of 0.762 which indicates that molecules have strong hydrogen bonding allowing for more efficient heat conduction. Sunscreen A states it is water resistant, indicating the solution must mainly consist of oils to create a hydrophobic barrier. Oils are generally worse at transferring heat due to their lower densities and weak intermolecular forces. For example, Sunscreen B has Octocrylene as one of the ingredients providing the hydrophobic barrier. Since its chemical formula is $C_{24}H_{27}NO_2$ it can be assumed that its relative polarity would extremely low due being slightly higher than benzene's value of 0.009 due to majority of the molecule being nonpolar. Although all sunscreens do have common preservatives since Sunscreen C contains more nonpolar substances such as Octocrylene than Sunscreens A and B. With a lower molecular polarity, a large portion of the ingredients in Sunscreen C relies on weaker intermolecular bonds such as dispersion forces which limits the molecules' ability to have strong interactions resulting in inefficient energy transfer. Furthermore, high molecular weight molecules reduce molecular mobility, lowering thermal conductivity. Octocrylene, with a molar mass of approximately 361.5 g/mol is significantly heavier than the alcohol molar mass of 108.1 g/mol. This results in Octocrylene requiring more energy to move in a system and transfer energy than a Benzyl Alcohol molecule, resulting in less efficient conduction in comparison. Another key point is the ingredient of zinc oxide within sunscreen c. Zinc oxide is mainly used to absorb UV waves however it does have the zinc oxide do contain nanostructures which are spread across the sunscreen dispersing and limiting the heat conducted [22] explaining why it had the second lowest temperature increase.

4.3.4 Calculations for conduction coefficient

Through the ingredient descriptions of each sunscreen, their heat capacities were estimated as seen in Table 3. The ingredient descriptions mainly consisted of alcohols, oils and water as the main solvent in sunscreens. The heat capacity of oils is around 1.7J/gK and alcohols are around 2.5J/gK [23], and so these values were assumed for calculation. Combing these values with the percentage compositions of ingredients in each sunscreen, the heat capacity value was calculated. Sunscreen A contained 25% mass zinc oxide which has a heat capacity of 0.494 [24]. See Appendix E for calculations for estimated heat capacity values. The conduction coefficient was calculated using the specific heat capacity formula (Eq 3) and Fourier's Law (Eq 4):

$$q = mc\Delta T \quad \text{(Eq 3)}$$

$$q = -kA\frac{\left(T_{Plate} - T_{Surface}\right)}{L_{(Sunscreen\ Thickness)}} \quad \text{(Eq 4)}$$

Equation 2 is the specific heat capacity formula where q is defined as the energy transferred (Joules), m being the mass of the sunscreen (1g) and c representing the approximated heat capacity of each mixture. For this formula ΔT represents the temperature increase the sunscreen experienced over the 5 minutes of their respective trial. Equation 2 was equated to equation 3 being Fourier's conduction formula multiplied by Area. The hot plate temperature remained constant at 32°C to simulate the skin temperature, which is used for all calculations for *k (conduction coefficient)* for the different sunscreens. $T_{surface}$ represents the temperature of sunscreen at 5 minutes. *A* represents the total area of the sunscreen which was found considering the diameter of petri dish was 5cm. However, for these calculations' assumptions were considered to ensure values could be calculated. Minor assumptions were that the sunscreen was evenly spread among the total area of the petri dish where some areas may have had a larger thickness. The calculation method for the conduction coefficient assumes that there is only 1D conduction between the sunscreen and the hotplate. Future more in the experiment the conduction of the petri dish was assumed to be negligible considering it had a very low thickness allowing for majority of the energy to travel through the material to the sunscreen. See Appendix F for sample calculations of K.

The thermal conductivity values that were calculated in Appendix F and shown in Table 3 for the different sunscreen mixtures reveal distinct trends in heat transfer efficiency. Sunscreen B had the highest *k* value of 1.34 W/(mK), indicating the greatest thermal conductivity, consistent with its high heat absorption. In contrast, Sunscreen A exhibited the lowest conductivity suggesting stronger insulating properties which was

consistent with the temperature observations. However, the *k* values for AB and AC closely align with the average *k* value between the individual samples. AB has 8% difference, and AC has a 4% difference only. This supports the assumption that thermal conductivity behaves approximately linearly with respect to the component proportions. The mixtures contain approximately the average conduction between two different types of sunscreens.

4.3.5 Limitations and Future Work

Although the experimental results were able to display clear trends between each sunscreen mixture there were several limitations throughout the experiment that hindered the validity and accuracy of the experiment.

- *Limitations in mixing procedures*

The first limitation in the validity of the result was caused by the possible lack of through mixing of the sunscreen samples. During the experiment, the two types of the samples were weighed on a petri dish and then mixed manually using a glass rod. This may have caused uneven distribution of the samples, as it is visually difficult to determine if the samples have been completely mixed or not. Having inhomogeneous mixtures can impact the result, as the surface of the sunscreen which the temperature was measured could have had different ratio of sunscreen compared to intended ratio. As shown in the result, the greatest error value was 4% obtained by the sample AB, and most of the other results have had low values ranging between 0 to 1% (Appendix D). Based on the results, it is appropriate to consider that the sunscreen samples were mixtures sufficiently, although there are few improvements that could be implemented as a future work.

A possible improvement would be to use a centrifugal mixer into order ensure that the two samples of sunscreen have been homogenous. Additionally, the use of centrifugal mixer means that it is likely that greater amount of sunscreen would be required compared to 0.5 grams per sample (i.e. mix 10 grams of sample A and B, instead of 0.5 gram each). This would improve the validity further as using greater amounts of sunscreen to prepare testing sample would decrease the uncertainty of the mass ratio.

- *Improvements for Accuracy*

In terms of the accuracy of the experiment, this could have been improved by testing larger variations of samples for example extra for CB and possibility 33% mixture of ABC could have been conducted. As this can allow for further comparison on whether applying different mixtures of sunscreen is more or less effective than just 1 type. Additionally, the R^2 value for the A sample was far lower than all other samples, indicating a higher degree of random error.

- *Potential Improvements for Materials*

Also, the plastic petri dish is a poor conductor of heat compared to human skin, and its insulating properties likely reduced the rate of heat transfer from the hot plate to the sunscreen. As a result, the measured temperature changes may not accurately reflect how the sunscreen would behave on actual skin. To improve validity, future experiments could use synthetic skin pads or gelatine-based materials to match skin thermal properties providing a more realistic approximation of how heat flows through skin in contact with sunscreen.

5. Conclusion

5.1 Investigation 1

In conclusion, the first investigation with the aim of investigating how the thickness of sunscreen affects the conductive heat flux through the samples was successful. Clear trends were found supporting the hypothesis of an inverse relationship between thickness and heat flux, with valuable secondary trends established such as the diminishing effect of extensive thickness application and the conductive performance with prolonged exposure. While there were some limitations around the experimental equipment, literature values and uncertainty, there were still clear trends established that effectively addressed the aim of this investigation with strong applicability to a practical scenario.

5.2 Investigation 2

In conclusion, the second investigation, with the aim of understanding the impact of mixing sunscreens of different active ingredients on thermal conductivity, was successful in identifying trends in relation to thermal conductivity for both material composition and effect of

mixture. The hypothesis that that Sunscreen C would exhibit the lowest temperature change was somewhat supported. However, this does not suggest that the study did not possess several limitations which included improper and evenly distributed mixing which impacted the ratio of sunscreen at certain spots, small sample sizes and a possible three-way mixture, and the use of a petri dish which fails to mimic human skin in its ability to conduct heat due to its insulating properties.

5.3 Summary

In conclusion, this investigation was successful in finding characteristics that influence the conductive heat flux and heat transfer through different sunscreens, investigating both the effect of sample thickness, their compositional makeup and the effect of mixing different sunscreens. Identifying and improving some experimental limitations, such as assumptions of negligible heat loss to the surroundings, 1D conduction and limited convection could improve experimental accuracy and reliability in additional studies. Further improvements to the investigation would focus on improving the direct applicability of data to practical scenarios.

Acknowledgements

Thank you to the University of Sydney for providing their equipment and laboratory facilities for the investigation, as well as the lab team for their assistance. Furthermore, thank you to Gobinath Rajarathnam and Minghao Zhang for their assistance during the laboratory and continous feedback

References

[1] Koop, L. and Tadi, P. (2023) *Physiology, Heat Loss* [Preprint]. Available at: https://www.ncbi.nlm.nih.gov/books/NBK541107/.

[2] Wells, T.D., Jessup, G.T. and Langlotz, K.S. (2016) 'Effects of sunscreen use during exercise in the heat', *The Physician and Sportsmedicine*, pp. 132–142. Available at: https://www.tandfonline.com/doi/abs/10.1080/00913847.1984.11701879.

[3] Aburto-Corona, J. and Aragón-Vargas 1, L. (2016) *Sunscreen Use and Sweat Production in Men and Women* [Preprint]. doi:10.4085/1062-6050-51.11.01.

[4] Lopes, C. and Felisberti, M. (2004) *Thermal conductivity of PET/(LDPE/AI) composites determined by MDSC* [Preprint]. doi:https://doi.org/10.1016/j.polymertesting.2004.01.013.

[5] Salih, H., Psomadakis, C. and George, S.M. (2024) 'Sunscreens: A narrative review', *Skin Health and Disease*, 4(6). doi:10.1002/ski2.432.

[6] Lademann, J., Fluhr, J.W. and Meinke, M.C. (2020) 'Characterization of sunscreens: Determination of the SPF', *Practical Aspects of Cosmetic Testing*, pp. 197–205. doi:10.1007/978-3-030-44967-4_18.

[7] Ramirez, M. (1994) Standard reference data for the thermal conductivity of water, Standard Reference Data for the Thermal Conductivity of Water. Available at: https://srd.nist.gov/jpcrdreprint/1.555963.pdf (Accessed: 01 May 2025).

[8] *Thermal conductivity measurement of mineral oil with MP-V* (2024) *Thermtest*. Available at: https://thermtest.com/application/thermal-conductivity-of-mineral-oil (Accessed: 09 May 2025).

[9] Michael (2024) *Silicone oil thermal conductivity guide: Dakenchem, Electronic Chemicals Supplier Daken Chem*. Available at: https://www.dakenchem.com/silicone-oil-thermal-conductivity-guide/ (Accessed: 09 May 2025).

[10] *List of thermal conductivities* (2025) *Wikipedia*. Available at: https://en.wikipedia.org/wiki/List_of_thermal_conductivities (Accessed: 09 May 2025).

[11] *Octisalate* (no date) *Octisalate - an overview | ScienceDirect Topics*. Available at: https://www.sciencedirect.com/topics/medicine-and-dentistry/octisalate#:~:text=Octisalate%20(Octyl%20Salicylate),be%20used%20in%20higher%20concentrations. (Accessed: 09 May 2025).

[12] *The physics classroom tutorial* (no date) *The Physics Classroom*. Available at: https://www.physicsclassroom.com/class/thermalP/u18l1f.cfm (Accessed: 09 May 2025).

[13] Zhang, B. *et al.* (2025) 'Investigating the distribution of heat transfer in a thick-walled functionally graded cylindrical shell under heat flux', *Journal of Engineering and Applied Science*, 72(1). doi:10.1186/s44147-024-00571-y.

[14] Serpone, N. (2021) 'Sunscreens and their usefulness: Have we made any progress in the last two decades?', *Photochemical & Photobiological Sciences*, 20(2), pp. 189–244. doi:10.1007/s43630-021-00013-1.

[15] Rajan, R. (2024) 'Sunscreen challenges: Stability, systemic absorption, and environmental concerns', *Sunscreens for Skin of Color*, pp. 283–310. doi:10.1007/978-981-97-3195-4_11.

[16] Tiege Hanley (2020) *Pros and cons of Zinc Oxide Sunscreen*. Available at: https://www.tiege.com/blogs/news/zinc-oxide-sunscreen-3-pros-and-cons (Accessed: 09 May 2025).

[17] HealthPartners (2025) *Best sunscreen ingredients and which ones to avoid, HealthPartners Blog*. Available at: https://www.healthpartners.com/blog/sunscreen-ingredients-to-avoid/ (Accessed: 09 May 2025).

[18] Morley, M.J. and Miles, C.A. (1997) 'Modelling the thermal conductivity of starch-water gels', *Journal of Food Engineering*, 33(1–2), pp. 1–14. doi:10.1016/s0260-8774(97)00043-5.

[19] Kaplan, C. (2021) *Mixing certain sunscreens might weaken Sun Protection*. Available at: https://www.scimex.org/newsfeed/mixing-certain-sunscreens-might-weaken-sun-protection (Accessed: 09 May 2025).

[20] Cataldo, F. (2022) 'Application of reichardt's solvent polarity scale (ET(30)) in the selection of bonding agents for composite solid rocket propellants', *Liquids*, 2(4), pp. 289–302. doi:10.3390/liquids2040017.

[21] Leydon, A. (2020) *The Effect of SPF 50 when left in Different Tmperatures*. Available at: https://www.oliphantscienceawards.com.au/files/3534_107-011_leydon_report_watermark.pdf (Accessed: 09 May 2025).

[22] Wang, Qian *et al.* (2022) 'Shell/core structure zinc oxide/iron oxide: A new sunscreen material against Blue Light', *Materials Letters*, 322, p. 132529. doi:10.1016/j.matlet.2022.132529.

[23] *Table of Heat Capacities* (no date) *Table of heat capacities of various liquids*. Available at: https://miriam-english.org/files/table_heat_capacity.html (Accessed: 09 May 2025).

[24] (No date) *Zinc oxide, zno, cubic*. Available at: https://www.matweb.com/search/datasheet.aspx?matguid=173a8f1e7cec4ce7af5dc3b90d10f756 (Accessed: 09 May 2025).

Appendix

Appendix A: Sample valculations for Investigation 1:

Note that all sample calculations shown are for the 0 minute, 2mm trial 1:

- Heat flux:

$$q'' = -k\frac{dT}{dx} = -0.43\,\frac{W}{mK}\cdot\frac{66.5^{o}C - 35.4^{o}C}{0.002\,m} = 6690\,W$$

The values of the three repeats were then averaged for the tabulated value.

- Uncertainty for heat flux:

$$\frac{\delta T_h}{T_h} + \frac{\delta T_c}{T_c} + \frac{\delta x}{x} + \frac{\delta k}{k} = \frac{0.1^{o}C}{66.5^{o}C} + \frac{0.1^{o}C}{35.4^{o}C} + \frac{0.0005}{0.002} + 0.05 = 0.304$$

The uncertainty for the average heat flux for each trial was calculated through the sum of square errors merhod:

$$\sqrt{\frac{\sum\left(\frac{\delta q''}{q''}\right)^2}{3}} = \sqrt{\frac{(0.30)^2 + (0.30)^2 + (0.30)^2}{3}} = 0.30$$

From this the absolute uncertainty of the final value was found:

$$\delta q''_{avg} \frac{\delta q''_{avg}}{q''_{avg}} \cdot q''_{avg}\ 0.30 \cdot 6790\,W = \pm\ 2070\,W$$

Appendix B: Full table of experimental and calcualted results for Investigation 1:

		Temperature (ºC)			
Thickness (mm)		**0 min**	**1 min**	**2 min**	**3 min**
2	Trial 1	35.4	39.1	40.7	40.1
	Plate	66.5	60.3	57.5	54.7
	Trial 2	35.5	38.4	42.3	40
	Plate	66.5	60.4	57.4	54.8
	Trial 3	33.8	34.2	39.5	41.8
	Plate	66.4	60.2	57.4	54.8
4	Trial 1	32.7	33.7	39.9	40.6
	Plate	66.5	60.3	57.5	54.7
	Trial 2	32.5	37.1	39.9	41.3
	Plate	66.5	60.4	57.4	54.8
	Trial 3	31.8	36.1	39.5	40.8
	Plate	66.4	60.2	57.4	54.8
6	Trial 1	27.8	30.2	30.4	32.2
	Plate	50	47.7	45.9	44
	Trial 2	27.9	30.2	30.2	32.1
	Plate	50	46.3	45.8	44
	Trial 3	28.1	30.6	30.5	32.5
	Plate	50.1	47.8	45.9	44.2
8	Trial 1	26.3	28.8	28.9	30.6
	Plate	50	47.7	45.9	44
	Trial 2	26.4	28.7	28.8	30.5
	Plate	50	46.3	45.8	44
	Trial 3	26.6	28.6	28.6	29.8
	Plate	50.1	47.8	45.9	44.2
10	Trial 1	27	26.8	27.8	28.2
	Plate	42.7	40.7	40.2	39.2
	Trial 2	26.9	26.4	27.5	27.7
	Plate	42.4	40.1	40.2	39
	Trial 3	27.1	26.7	27.4	27.4
	Plate	42.4	40.8	40.1	38.9

Thickness (mm)		Heat Flux, q'', through the suncreen (W/mK)			
		0 min	1 min	2 min	3 min
2	Trial 1	6687	4558	3612	3139
	Trial 2	6665	4730	3247	3182
	Trial 3	7009	5590	3849	2795
	Average	6787	4959	3569	3039
4	Trial 1	3634	2860	1892	1516
	Trial 2	3655	2505	1881	1451
	Trial 3	3720	2591	1924	1505
	Average	3669	2652	1899	1491
6	Trial 1	1591	1254	1111	846
	Trial 2	1584	1154	1118	853
	Trial 3	1577	1233	1104	839
	Average	1584	1214	1111	846
8	Trial 1	1274	1016	914	720
	Trial 2	1269	946	914	726
	Trial 3	1263	1032	930	774
	Average	1269	998	919	740

10	Trial 1	675	598	533	473
	Trial 2	667	589	546	486
	Trial 3	658	606	546	495
	Average	667	598	542	484

Appendix C: Full table of calculated fractional uncertinty and asbsolute uncertainty for Investigation 1:

		Heat Transfer , q, through the suncreen (W)			
Thickness (mm)		0 min	1 min	2 min	3 min
2	Trial 1	0.30	0.30	0.30	0.30
	Trial 2	0.30	0.30	0.30	0.30
	Trial 3	0.30	0.30	0.30	0.30
	Average	0.30	0.30	0.30	0.30
4	Trial 1	0.18	0.18	0.18	0.18
	Trial 2	0.18	0.18	0.18	0.18
	Trial 3	0.18	0.18	0.18	0.18
	Average	0.18	0.18	0.18	0.18
6	Trial 1	0.14	0.14	0.14	0.14

	Trial 2	0.14	0.14	0.14	0.14
	Trial 3	0.14	0.14	0.14	0.14
	Average	0.14	0.14	0.14	0.14
8	Trial 1	0.12	0.12	0.12	0.12
	Trial 2	0.12	0.12	0.12	0.12
	Trial 3	0.12	0.12	0.12	0.12
	Average	0.12	0.12	0.12	0.12
10	Trial 1	0.11	0.11	0.11	0.11
	Trial 2	0.11	0.11	0.11	0.11
	Trial 3	0.11	0.11	0.11	0.11
	Average	0.11	0.11	0.11	0.11

Absolute Uncertainty (W/mK)				
Thickness	**0min**	**1min**	**2min**	**3min**
2	2066	1509	1086	925
4	659	476	340	267
6	220	168	154	117
8	150	118	109	87
10	70.7	63.5	57.5	51.4

Appendix D: Absolute and percentage errors of inestigation 2

Mixture	Time(min)	0	1	2	3	4	5
A	Absolute error	1.136	0.569	0.300	0.208	0.503	0.379
	percentage error	4%	2%	1%	1%	2%	1%
B	Absolute error	0.379	0.404	0.436	0.289	0.265	0.100
	percentage error	1%	1%	2%	1%	1%	0%

AB	Absolute error	0.416	0.850	0.964	1.097	0.872	0.781
	percentage error	2%	3%	4%	4%	3%	3%
C	Absolute error	0.306	0.404	0.153	0.058	*0.173*	0.200
	percentage error	1%	2%	1%	0%	1%	1%
AC	Absolute error	0.153	0.300	0.100	0.115	0.058	0.100
	percentage error	1%	1%	0%	0%	0%	0%

Appendix E: Compostion and Heat capacity assumptions

Sunscreen	Compostion	Cp
A	40% water, 45% oil ,15% alchohols	2.81
B	50% water 30% oils 20% alchols	3.10
C	25% Zinc Oxide., 50% water 25% alchols	2.84
AB	50% A and 50% B	2.83
AC	50% A and 50% C	2.97

Sample calculation

$$C\,p_A = 0\,.\,4 \times 4\,.\,18 + 0\,.\,15 \times 2\,.\,5 + 0\,.\,45 \times 1\,.\,7 = 2\,.\,81$$

Appendix F: Sample calculation of k value in investigation 2

$$q_B = 1g\ \times 3\,.\,1J\ /\ g \cdot K \times (29\,.\,1 - 26\,.\,63)℃\ = 7\,.\,65J$$

$$7\,.\,65J = -\,k\left(0\,.\,02\,5^2\,\pi\right)\frac{(29\,.\,1 - 32)}{0\,.\,001}\,k = 1\,.\,34W\ /\ (m \cdot K)$$

Appendix G: Calculation of the k value in investigation 1:

$$k\ =\ \frac{0\,.\,61\,\frac{W}{mK}}{60} + \frac{0\,.\,15\,\frac{W}{mK}}{30} + \frac{0\,.\,15\,\frac{W}{mK}}{10} = 0\,.\,43\ \frac{W}{mK}$$

Appendix H: % Drop in Heat flux with Increasing Thickness from 2mm to 10mm and Sample Calculation

Time	**% Drop in Heat flux with Increasing Thickness from 2mm to 10mm**
0 min	90.2%
1 min	87.9%
2 min	84.8%
3 min	84.1%

Sample Calculation: $\frac{q''_{2mm,\,0min} - q''_{10mm,\,0min}}{q''_{2mm,\,0min}} = \frac{6787\,\frac{W}{mK} - 667\,\frac{W}{mK}}{6787\,\frac{W}{mK}} = 90\,.\,2\%$

Appendix I: % Drop in Heat flux with Increasing Thickness in 2mm Increments and Sample Calculation

	% Drop in Heat flux with Increasing Thickness in 2mm Increments			
Thickness Step	**0 min**	**1 min**	**2 min**	**3 min**

2mm to 4mm	45.9%	46.5%	46.8%	50.9%
4mm to 6 mm	56.8%	54.2%	41.5%	43.3%
6mm to 8mm	19.9%	17.8%	17.3%	12.5%
8mm to 10mm	47.5%	40.1%	41.1%	34.5%

Sample Calculation: $\frac{\ddot{q}_{2mm,\,0min} - \ddot{q}_{2mm,\,3min}}{\ddot{q}_{2mm,\,0min}} = \frac{6787\,\frac{W}{mK} - 3669\,\frac{W}{mK}}{6787\,\frac{W}{mK}} = 45.9\%$

Appendix J: % Drop in Heat flux with Increasing Time at Set Thickness and Sample Calculation

Thickness	% Drop in Heat flux with Increasing Time at Set Thickness
2mm	55.2%
4mm	59.4%
6mm	46.6%
8mm	41.7%
10mm	27.3%

Sample Calculation: $\frac{\ddot{q}_{2mm,\,0min} - \ddot{q}_{2mm,\,3min}}{\ddot{q}_{2mm,\,0min}} = \frac{6787\,\frac{W}{mK} - 3039\,\frac{W}{mK}}{6787\,\frac{W}{mK}} = 55.2\%$

Appendix K: Raw results of Tempreture increases of sunscreen mixtures over 5 mineutes

	Time (min)					
Mixture	0	1	2	3	4	5
A	27.1	27.5	26.6	26.6	26.8	26.8
A	25	26.4	26	26.2	25.8	26.1
A	25.3	26.7	26.3	26.3	26.2	26.7
B	26.2	28.2	28.1	28.4	28.3	29
B	26.9	28.9	28.8	28.9	28.7	29.2
B	26.8	28.9	28.9	28.9	28.8	29.1
AB	25	26.7	26.3	26.6	26.4	26.8
AB	24.8	27	26.6	26.6	26.6	26.9
AB	25.6	28.3	28.1	28.5	28	28.2
C	26	26.3	26.6	26.6	26.9	27.1
C	26.2	26.6	26.7	26.6	26.9	26.9
C	25.6	25.8	26.4	26.5	26.6	26.7
AC	25.7	25.8	26.2	26.6	26.8	26.8
AC	26	26.4	26.1	26.4	26.7	26.7
AC	25.8	26.1	26.3	26.4	26.7	26.6

Appendix L: Average Results of Appendix K

Mixture	0	1	2	3	4	5
A	25.8	26.86667	26.3	26.36666667	26.26667	26.53333

B	26.63333333	28.66667	28.6	28.73333333	28.6	29.1
AB	25.13333333	27.33333	27	27.23333333	27	27.3
C	25.93333333	26.23333	26.56666667	26.56666667	26.8	26.9
AC	25.83333333	26.1	26.2	26.46666667	26.73333	26.7

Appendix M: Investigation 2 conduction coefficient (K) values of each sunscreen mixtures.

Sunscreen	Cp	q	K
A	2.81	2.06	0.19
B	3.10	7.65	1.34
C	2.84	2.75	0.27
AC	2.83	2.45	0.24
AB	2.97	6.43	0.70

Appendix M: Sunscreens used in Investigation 2

Sunscreen A (Letan coconut suncream 15spf) https://www.chemistwarehouse.com.au/buy/64759/le-tan-spf-15-coconut-sunscreen-lotion-125ml

Sunscreen B (Bondi sands 50spf) https://incidecoder.com/products/bondi-sands-sunscreen-lotion-face-spf50

Sunscreen C (Banna boat baby zinc spf 50) https://www.chemistwarehouse.com.au/buy/131277/banana-boat-baby-zinc-spf-50-100g

Appendix N: Larger Graphs of Figures 3, 4 and 5

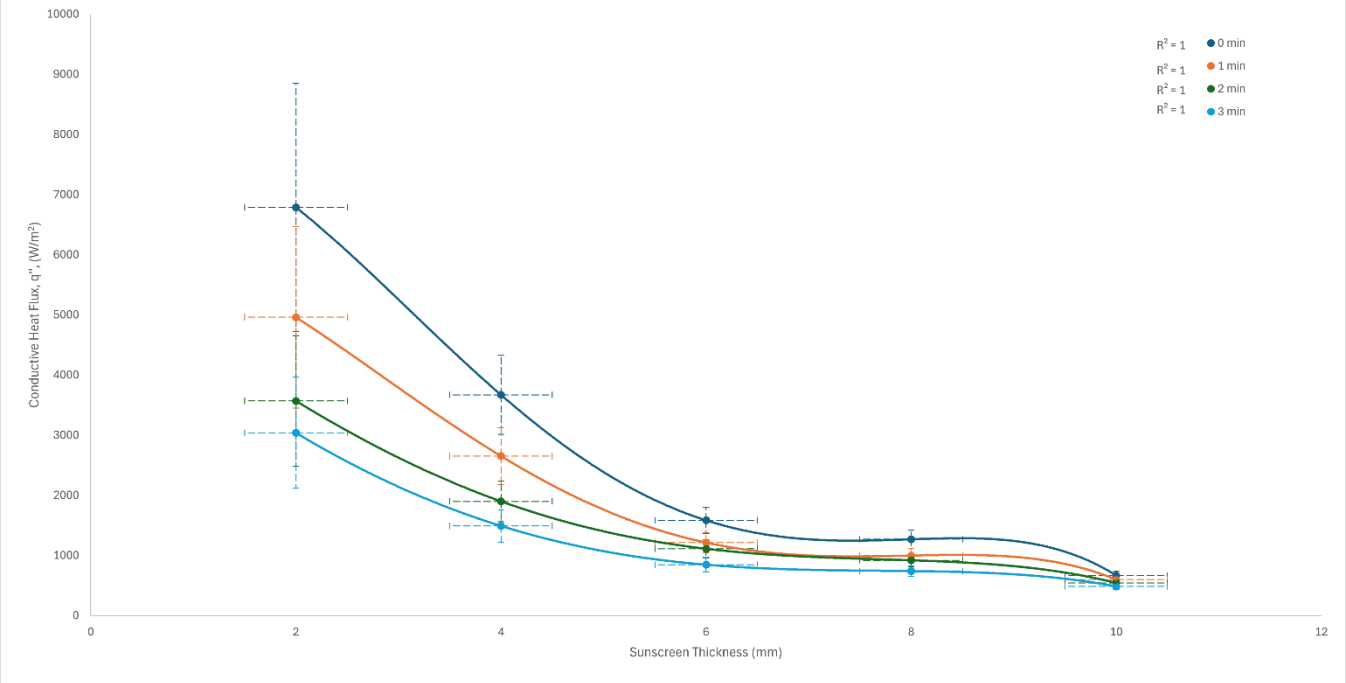

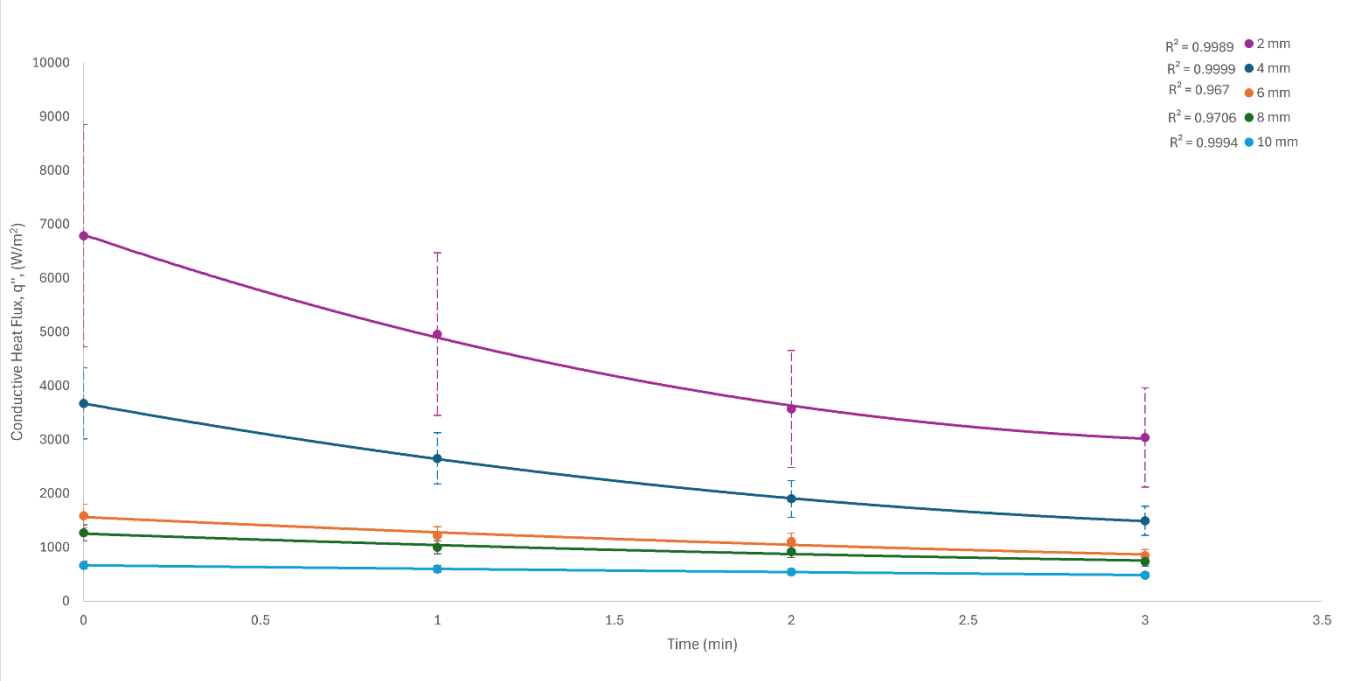
R² = 0.9989 2 mm
R² = 0.9999 4 mm
R² = 0.967 6 mm
R² = 0.9706 8 mm
R² = 0.9994 10 mm
Conductive Heat Flux, q'', (W/m²)
Time (min)

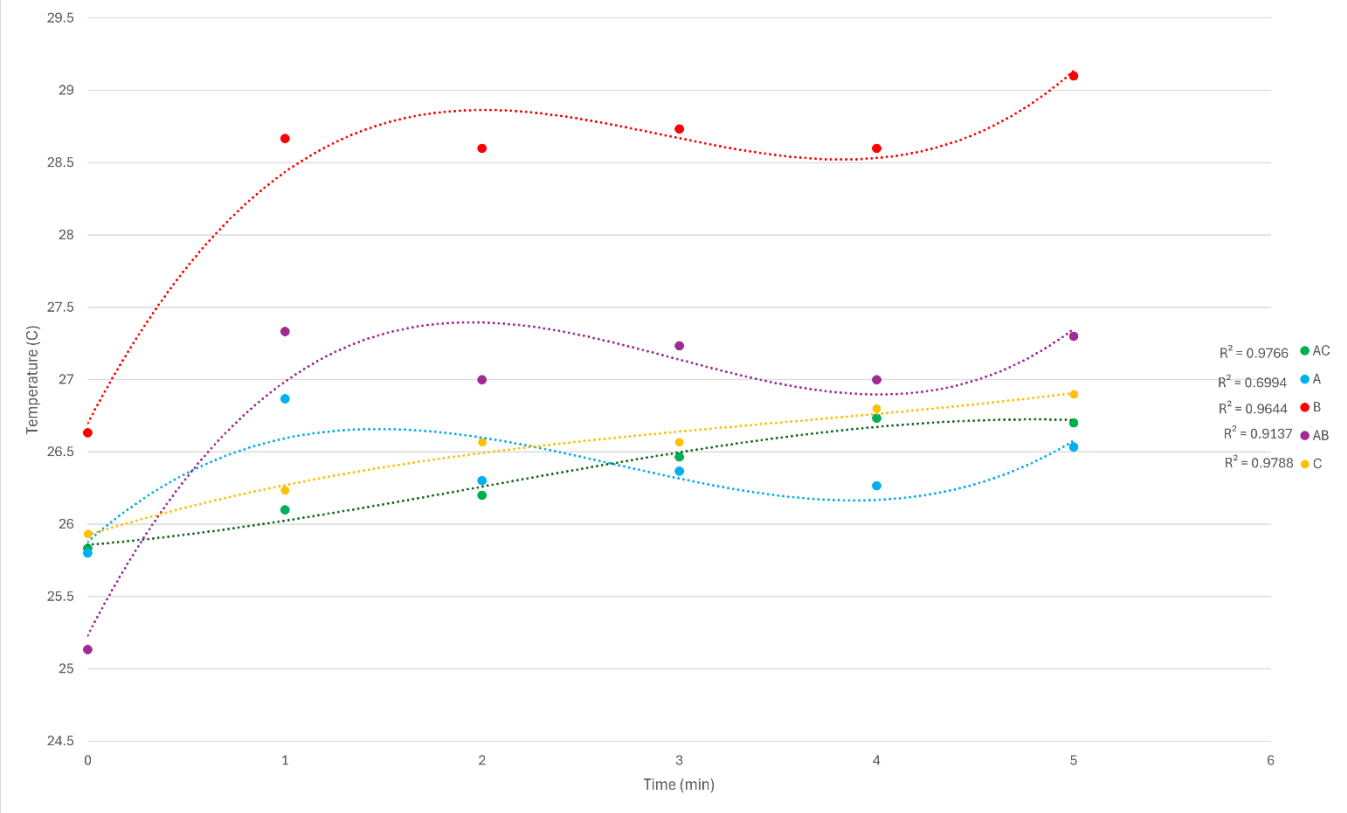
R² = 0.9766 AC
R² = 0.6994 A
R² = 0.9644 B
R² = 0.9137 AB
R² = 0.9788 C
Temperature (C)
Time (min)

SJIE 1(2) X–X (2025) https://doi.org/XXXX/XXXX

Thermal Behaviour of Vegetable Oils: Influence of Viscosity, Composition, and Convection

Lachlan Grieg[1],Owen O'Carroll[1], Nicholas Leak[1], Harry Rickard[1], and Matthew Stout[1], Sebastian Dominguez Flores, Juanita[1], Suarez Perez[1], Minghao Zhang[1], David Alam[1], Gobinath Rajarathnam[1]

[1] School of Chemical and Biomolecular Engineering, The University of Sydney, Sydney, Australia

Graphical Abstract

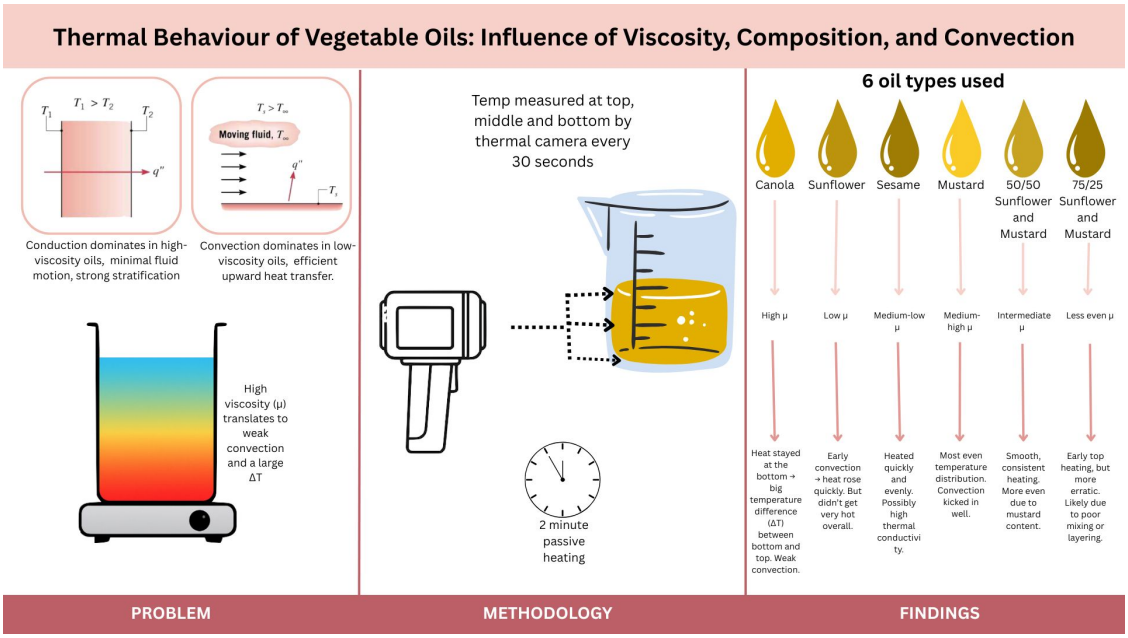

Abstract

Understanding the thermal behaviour of different vegetable oils when exposed to heat is important in contexts ranging from thermal processing to cooking. This experiment investigated temperature variation in Canola, Sunflower, Sesame, and Mustard oils, as well as sunflower - mustard blends, during a two-minute passive heating process. To observe how heat is transferred through the fluid, temperatures were recorded at the bottom, middle, and top of each sample. Results showed that viscosity was the dominant factor influencing heat distribution. Canola, the most viscous oil, developed the strongest temperature gradients, while mustard oil heated more uniformly due to lower viscosity, allowing stronger convection currents. Sunflower and sesame oils produced intermediate results, with sesame showing relatively fast heat transfer. The oil blends displayed heating patterns between those of the pure oils, with higher sunflower content leading to faster and more efficient top heating. Despite variability associated with timing, mixing precision, and equipment inconsistencies, our results aligned with expected physical properties. These results demonstrate how relatively simple heat profiling can offer valuable insights into thermal and fluid behaviour.

Keywords: Heat transfer, convection, viscosity, vegetable oils, thermal stratification, fluid properties.

1. Introduction

Heat is transported through liquids by two interconnected mechanisms. Conduction is the transfer of heat through a material caused by the movement of energy between nearby molecules[1]. Convection transports heat by the bulk motion of the fluid. Warmer, lighter regions rise while cooler, denser regions sink, setting up a circulating flow that redistributes energy[2]. In practice the two mechanisms coexist: conduction controls the microscopic transfer between adjacent fluid layers, but once buoyancy forces overcome viscous resistance, fluid motion begins, forming natural convection currents that speed up heat transfer through the fluid[3].

Thermal conductivity(k) controls how quickly heat spreads through a fluid when the fluid itself is not moving[4]. In refined sunflower, rapeseed and palm oils, *k*, falls from ≈ 0.167 W m⁻¹ K⁻¹ at 20 °C to ≈ 0.137 W m⁻¹ K⁻¹ at 230 °C, so a hotter fryer or transformer tank must rely increasingly on convective motion to move the same amount of heat[5]. Specific heat determines the thermal energy storage capacity: adiabatic scanning calorimetry shows that c_p of vegetable oils rises almost linearly with temperature and is higher in monounsaturated oils, allowing them to absorb more energy per degree than polyunsaturated oils[6]. When convection is free to develop, it often dominates overall transfer. In deep-fat frying using canola, corn, palm, and soybean oils, the surface heat transfer coefficient (*h*) decreased almost linearly as viscosity increased. Oil degradation, which raises viscosity, reduced *h* by up to 30% under the same conditions[7]. These examples underline that *k*, c_p and buoyancy-driven flow jointly dictate how rapidly and uniformly heat can be removed or supplied in industrial and culinary equipment.

Vegetable oils are important in high-temperature cooking. Their flash points around 250 °C, non-toxic nature and flavour neutrality make them the ideal choice for frying and roasting. Interest is also growing in them as bio-derived thermal fluids**.** Solar cookers and domestic sensible-heat storage pots use sunflower, palm or blended oils as sustainable substitutes for synthetic thermal oils, due to lower cost and ready biodegradability[8]. Laboratory 3-ω hot-wire measurements confirm that these fluids retain acceptable conductivity up to 250 °C and can be tailored via fatty-acid composition or nanoparticle additives for specialised cooling, quenching or lubrication services[5].

This study investigates how composition impacts heat transfer by measuring vertical temperature stratification in six oils; canola, sunflower, sesame, mustard and two sunflower–mustard blends, heated from below. By logging temperatures at the base, mid-height and surface for two minutes, we quantify the residual change in temperature (ΔT) across the beaker. A small ΔT indicates strong natural convection, whereas a large ΔT signals conduction-dominated, stratified behaviour. By comparing pure and blended oils under the same heating conditions, we can identify how viscosity, density, and fatty acid composition affect natural convection

1.1 Key Parameters

Viscosity (μ): the main influence on convection. In frying studies, a 70 % rise in μ drove a proportional fall in *h*, a ($|r| \approx 0.96$), illustrating how even modest thickening, whether from low-temperature choice or oxidative ageing can suppress circulation and elevate hot-spot temperatures[7].
Density (ρ) & thermal expansion (β): together are the forces behind natural convection. Oils richer in unsaturated chains are slightly less dense and possess larger β, yielding higher Rayleigh numbers and earlier transition to convection.
Thermal conductivity (k) & specific heat (c_p): determine, respectively, controls how fast heat spreads through a fluid and how much energy the fluid can store as its temperature increases. Both vary systematically with degree of saturation, *k* decreasing and c_p increasing as temperature rises[5,6].
Chemical composition: fatty-acid chain length and unsaturation impact all the above. Quench-cooling data show that lower-saturation (thus lower-μ) oils wet hot surfaces faster, while high-saturation oils may partially solidify at room temperature, virtually eliminating convection[9].
By comparing temperature profiles, this experiment identifies which aspects of oil composition, like viscosity or density have the strongest effect on convective heat transfer, a question with direct implications for food engineering, renewable heat storage and bio-based thermal-fluid design.

1.2 *Key Equations*

1. Fourier's Law of Conduction (Describes heat transfer by conduction):
$$q = -k\frac{dT}{dx}$$
Where k = thermal conductivity(W/mK), q = heat flux (W/m^2), dTdx = temperature gradient[1]
2. Heat transfer equation:
$$q = m\, c_p\, \Delta T$$
3. Newton's Law of Cooling (Convective Heat Transfer)
$$q = hA(T_s - T_\infty)$$
Where h = heat transfer coefficient (W/m^{2}K), influenced by viscosity, A = surface area, T_s= surface temperature, T_∞ = fluid temperature[2]
4. Rayleigh Number (Predicts the strength of natural convection):
$$Ra = \frac{g\beta\Delta T\, L^3}{v\alpha} = \frac{g\beta\Delta T\, L^3\, \rho^2\, c_p}{\mu k}$$
Viscosity enters here via: v=, kinematic viscosity, lower μ (dynamic viscosity) translates to higher Ra and hence stronger convection.[10]
5. Thermal Diffusivity
$$\alpha = \frac{k}{\rho\, c_p}$$
Which demonstrates how fast a material responds to

heating[11]

2. Methods

2.1 Experimental Setup

Given our experiment aimed to analyse convection of heat through different types of oil, our experimental setup aimed to measure the heat of oil at three points against time. To achieve this, 100mL beakers were filled to the 50mL graduation with the respective oils, whereby the three points could be measured to maintain simplicity at 0mL (the base of convection), 25mL and 50mL. Furthermore, a hot plate was installed beneath the beaker to heat the oil. The hot plate used was temperature probe based thus its heating was in accordance with the heat of the liquid used mostly for maintaining an elevated heat of liquid. Additionally, a thermal camera was installed horizontally to the hotplate's base using a retort stand. The thermal camera intended to observe and measure the heat at the desired measurement zones (bottom - 0mL, middle - 25mL, top - 50mL). Finally, the oils to be measured were, canola oil, sunflower oil, sesame oil, mustard oil and a 50/50 by volume blend of sunflower-mustard oil and a 75/25 by volume blend of sunflower-mustard oil (75% being sunflower oil). A diagram of this experimental setup is shown below.

Figure 1 *- Experimental setup:*

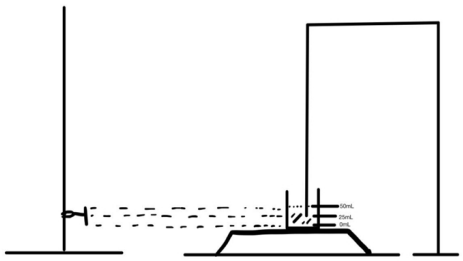

2.2 Data Collection Procedure

1. A 100 mL beaker was filled with 50 ml of canola oil.
2. Beaker was placed on the heating plate with the temperature probe submerged in the oil, not touching the base.
3. The thermal camera's capture points were set on the computer software at the base of the beaker, the 25 mL and 50 mL graduation line.
4. The temperature of the oil was recorded at all thermal camera capture points every 30 seconds for 2 minutes including the initial temperatures.
5. Steps 1-4 were repeated five times with the canola oil
6. Steps 1-5 were repeated with the other oils.
7. Once individual oils testing was completed, steps 2-5 were carried out with 50 mL of 1:1 sunflower-mustard oil blend and again for 50 mL of a 3:1 ratio of sunflower-mustard oil blend.
8. When blended mixtures were tested, observation of homogeneity was visually assessed and recorded.

2.3 Sources of Experimental Error

To assess the reliability of the results, errors were grouped into human error, equipment-related error and experimental design limitations. While these factors caused some inconsistencies, the overall trends remained fairly consistent with expected thermal behaviour.

Human Error

Accurately starting and recording time points was difficult across trials, especially when we often had to reposition the beaker or thermal camera. A Delay of a few seconds was common at the beginning of each trial. The 50 mL oil volumes were estimated by eye in 100 mL beakers, leading to small variations in fluid height. Parallax error may have also affected meniscus readings, resulting in slight volume errors. Additionally, creating 50/50 or 75/25 oil blends without pipettes also created decent variability, which could influence heating behaviour due to differences in viscosity and density between oils.

Equipment Error

The hotplate operated based on internal oil temperature targets instead of hot plate surface temperature, which caused significant variation between trials , with some beakers starting to heat on a surface over 200°C and others around 60°C. Slight changes in thermal camera positioning may have skewed results, particularly at the bottom of the beaker where reflected heat affected readings. In some cases, early measurements were delayed due to the time required to select bottom, middle, and top zones on the thermal camera interface.

Experimental Design Limitations

Mixtures were not stirred during heating to allow for natural convection and temperature gradient formation. As a result, the heavier oils like mustard may have settled unevenly, causing localised differences in heating. Even when they were pre-mixed, density and viscosity differences between oils could have led to stratification during heating.

3. Results and Discussion

3.1 Temperature Profiles of Pure Oils

The temperature profile of pure oils was examined at various height intervals (bottom, middle, top) in order to analyse key factors of heat transfer such as viscosity, thermal conductivity and specific heat capacity. All these factors influence heating behaviour, in particular the ratio between conduction and convection, and which factor is dominating heat transfer. This notion was evident in the results where intriguing discoveries were made.

Figure 2 highlights the temperature increase, and thus heat transfer through the height of sesame oil over the course of 2 minutes. Among all the pure oils tested, sesame oil consistently reached the greatest final temperature across all levels (bottom: 95.74°C, middle: 65.42°C, top: 51.9°C). This finding suggests that sesame oil has a higher thermal conductivity, enabling a faster rate of energy transfer. Alternatively, it may also indicate a lower specific heat capacity, allowing the oil to heat up quicker per unit of energy. Additionally, the consistent rise of each level's temperature as opposed to a more asymptotic nature is indicative that convection-based heat transfer was likely developed in the later stages of the experiment. Thus, initially, when the oil was still, before convection currents influenced oil movement, conduction from the base layer of the oil was relatively efficient in heating vertically upwards.

Figure 2 *- Temperature over time for sesame oil & sunflower oil:*

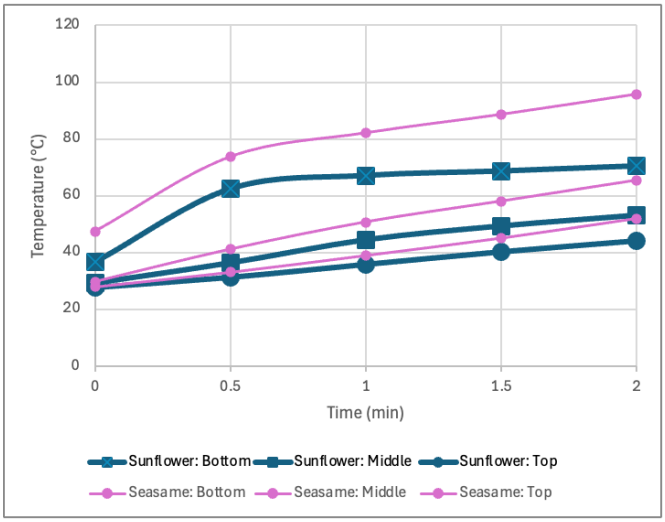

Conversely, sunflower oil displayed a high level of early convection compared to other oils due to its relatively lower viscosity. Figure 2 showcases the highest rate of temperature increase in the top layer in the earlier stages of heating, indicating the early onset of convection compared to other pure oils. This is likely due to sunflower's lower viscosity compared to sesame oil for example, and thereby, fluid motion is initiated sooner allowing for greater heat distribution upwards. However, despite the early onset of convection, this oil did not reach particularly high temperatures after the 2 minutes of elapsed time, suggesting sunflower oil may have a lower thermal conductivity. This intriguing finding conveys the essential distinction between high rates of convection, and total heat absorbed. Although natural convection is driven primarily by temperature-induced density gradients, the ability for heat to transfer through the oil (i.e., thermal conductivity) ultimately granting the formation of these convection currents. In sunflower oil, fluid motion is initiated earlier due to its lower viscosity, facilitating vertical heat transfer despite the total thermal energy absorbed being relatively low.

Mustard oil had the most uniform and efficient heat transfer and distribution, exhibiting the second highest overall temperature. Additionally mustard oil's final temperature difference between the bottom level and top level is relatively small, and thus this more uniform heating profile is indicative of consistent and effective convection currents throughout the oil after the onset of convection. Although Mustard oil is considered to be the most viscous of the 4 pure oils studied, its performance suggests that once convection was initiated in the fluid, convection dominated in heat transfer, significantly contributing.

Figure 3 *- Temperature over time for mustard oil & canola oil:*

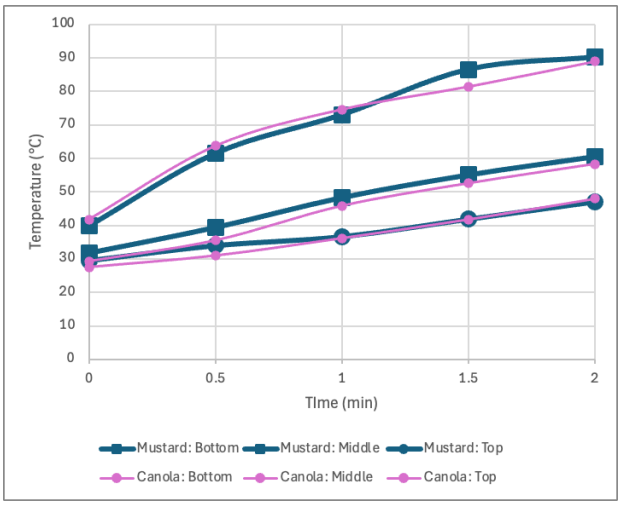

It is evident in our findings that viscosity is a key driver for convection performance. However there are other thermal properties which play a crucial role. It is important to state that based on the experimental data, it can be concluded that viscosity of the oils significantly impacts the onset and efficiency of convection, but not necessarily their overall performance in heat transfer. For example, figure 3 represents the temperature profile for canola oil. It can be deduced that despite canola oils' relatively lower viscosity compared to other oils, temperatures across all levels were particularly low over the 2 minutes. This observation is indicative that other thermal properties such as thermal conductivity and specific heat capacity heavily impact overall heat transfer, and the fluids ability to develop strong convection currents and

transfer heat, despite the perceived advantage of a less viscous liquid.

As fluids heat, density gradients are created, governing density driven convection as the fluid begins to circulate. A fluid with a low thermal conductivity may struggle to create these steep temperature gradients necessary for density based convection. In a similar context, a high specific heat value would suggest poor convection too given the innate requirement in this context for a greater energy input to reach the same increase in temperature. Given this insight, it can be taken that an oil such as mustard oil, which is comparably more viscous than canola oil, may outperform canola oil (or a less viscous oil) in the possibility that either its thermal conductivity is higher, and/or its specific heat capacity is lower.

3.2 Temperature Profiles of Oil Blends

Figure 4 presents the temperature profiles of the two sunflower-mustard oil blends (50/50, 75/25). Both blends experienced a similar final temperature at the top level of the beaker, highlighting a likely comparable overall capacity for heat transfer performance. However, a few nuances can be explored in how these blends heated and reached their final temperatures. The 50/50 blend experienced a steadier, more gradual and linear temperature increase, while conversely the 75/25 blend suggested a slightly fast heating at the top layer compared to the 50/50 blend. Additionally the 75/25 mix showcases greater variations through lower levels too. These findings suggest that the 50/50 blend facilitated greater heat retention and uniform conduction, likely due to a greater quantity of mustard oil, and therefore more favourable thermal conductivity properties. Furthermore, the 75/25 mix experienced greater convection early on due to sunflower oil's lower viscosity. It can additionally be noted that the heat transfer process in the 75/25 mix (more sunflower oil) can be described as less consistent and efficient.

Figure 4 *- Temperature over time for 50/50 sunflower-mustard oil and 75/25 sunflower-mustard oil:*

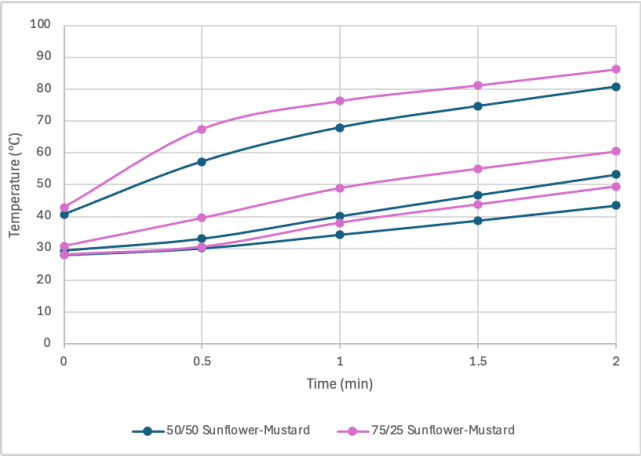

As the oil blends were mixed by hand in the experiment, there is a level of human error, and more so natural propensity for the oil to be ineffectively mixed (due to differences in viscosity, density etc). Thus, despite our best efforts to physically mix the oils, differing densities and viscosities cause the mixture to behave not as a single, homogeneous fluid. Therefore, temporary layering in the oil or incomplete mixing may have been involved, and thus causing thermal stratification and distinct (or not distinct) density layers/regions, with the denser mustard oil settling to the bottom, and vice versa with sunflower oil. This can cause local regions in the beaker where thermal properties are altered (conduction dominating in some regions and convection in others). Overall, it can be concluded that errors with layering and inconsistent miscibility, leading to thermal stratification may have contributed to inconsistencies observed in the 75/25 blend's temperature profile.

Localised convection currents likely impacted uniform heating and convection onset timing. As discussed, sunflower oil experienced convection currents early on. Hence, the 75/25 oil mix would have experienced more early convection currents. However, these currents were likely formed locally in convection cells, especially near the bottom where viscosity was lowest (highest temperature), and lacked the ability to circulate upwards promoting heat transfer. Conversely, in the 50/50 blend, while the more viscous mustard oil created a higher resistance to motion initially, this blend likely developed stronger convection currents, properly transporting and transferring heat upwards through the oil blend, due to greater heat accumulation in the mustard-oil base (denser), and thus creating more drastic density gradients for convection to be thereby facilitated. This notion is represented in figure 4 where the 50/50 mix, while exhibiting lower temperatures at each level, displays a smoother, more consistent heating trend.

3.3 h-values for Oils/Oil Blends

Figure 5 identifies the heat transfer coefficient (h), for pure oils as well as oil blends, insightfully quantifying the efficiency of heat transfer between the heated plate and the oil via convection. Consistent with transient natural convection, h decreases asymptotically as the thermal boundary layer thickens and the temperature difference between the hot surface and the bulk oil shrinks, weakening buoyancy-driven flow (lower density gradient) and reducing heat flux per unit temperature, hence balancing convection and conduction towards a steady-state condition.

Derivation of h-values are sourced from equating equation 2 (heat transfer equation), and equation 3 (Newton's law of cooling):

$$q = m\,c_p\,\Delta T, \qquad q = hA(T_s - T_\infty)$$
$$m\,c_p\,\Delta T = hA(T_s - T_\infty)$$

Figure 5 *- Convection heat-transfer coefficients plot:*

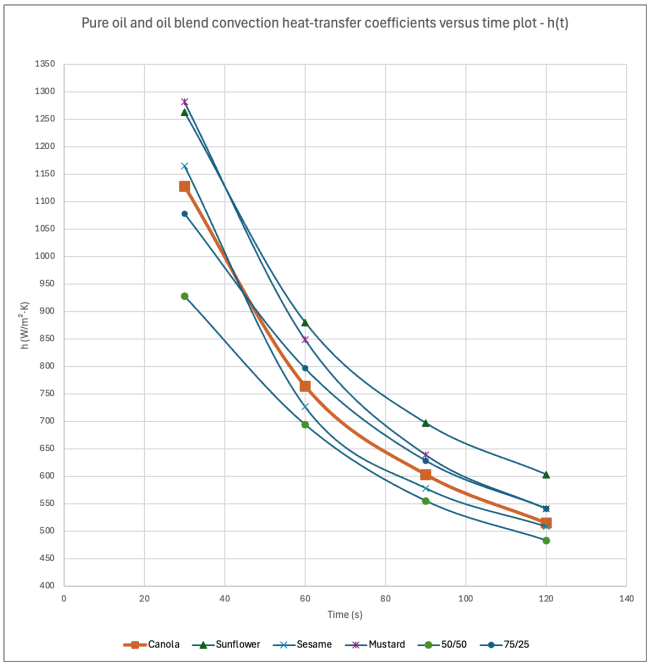

Findings of the convective heat transfer coefficient (h) and trends seen in figure 5 reinforce experimental findings in sections 3.1 and 3.2. Calculation of the convection coefficient values for the mustard oil blend found that initially heat transfer by convection occurred in a large magnitude due to the large temperature disparity between the solution and the heating mantle. As the temperature became more uniform throughout the solution and the density differences driving natural convection weakened, less convection occurred and the convection coefficient value decayed. The nonlinearity of the graph can be explained by the solution beginning to approach steady state conditions, with the h value decreasing until the heating effects and the cooling from the external surroundings balance and h reaches a stable level. Figure 5 shows a fast initial drop in h meaning that initial heat exchange in the system is efficient, providing evidence that the mustard and sunflower oil mixture is a viable option for thermal energy storage systems as it quickly absorbs heat and effectively retains and slowly releases it.

3.4 Key Influencing Factors

Several fluid properties influenced the heating behaviour observed in the experiment. These include viscosity, thermal conductivity, convection strength, and the formation of density gradients. Table 1 outlines the key factors in order of importance based on the experimental results.

Figure 6, Table 1 - Ranked Factors affecting heat transfer in oils

Factor	**Effect on heat transfer**	**Observed impact**
Viscosity	Affects how easily convection currents form. Higher viscosity slows down fluid motion.	Canola oil showed strong stratification, while mustard oil heated more evenly.
Convection strength	Circulates heat from the bottom to the top once a temperature gradient forms	Mustard and sunflower oils showed earlier or stronger convection compared to canola.
Thermal conductivity	Determines how well heat moves through the fluid.	Sesame oil heated up faster and more evenly than others, suggesting better conductivity.
Specific heat capacity	Oils with higher specific heat require more energy to heat up.	Sunflower oil heated slowly overall despite early convection.
Mixing and stratification	Uneven mixing can cause localised layering and inconsistent heating.	75/25 blend had more variation, likely due to incomplete mixing or separation.
Initial surface temperature	Hotplate control affected how much energy was delivered early in the experiment.	Some trials (e.g. sesame oil) had high starting temperatures at the base due to heat retention.

While not all results were perfectly consistent, most trends generally matched what would be expected from each oil's physical properties. Canola, the most viscous, showed delayed and weak convection, with heat staying mostly at the bottom. Mustard, although viscous, heated more evenly once convection had started, possibly due to a lower specific heat

or stronger fluid circulation. The sesame oil consistently reached high temperatures at all levels which suggests better internal heat transfer, likely due to higher thermal conductivity. Furthermore, the sunflower oil, which had low viscosity, showed signs of early convection but lower overall heating, suggesting that lower conductivity limited how much energy the fluid retained.

A lot of the differences between how the oils heated up can be explained using heat transfer principles. The first concept is the **Rayleigh number**, which tells us when natural convection is likely to kick in. It depends on factors such as viscosity and the temperature difference across the fluid. Oils like mustard and sunflower are less viscous, so they're more likely to start circulating earlier which was reflected in our results, with both showing early signs of convection and more even heating compared to thicker oils like canola, where the heat mostly stayed near the bottom.

Similarly, the **Biot number** helps explain how heat moves inside the fluid compared to how it interacts with outside air. Oils like canola, which developed strong internal temperature gradients and slow top heating, likely had higher Biot numbers, meaning that their internal resistance to heat flow was dominant. However, sesame likely had a lower Biot number which allowed for more even internal heating.

The blended oils also showed these patterns to some extent, with the 50/50 mix showing steady and consistent heating, while the 75/25 mix heated faster at the top but was less uniform overall. This could be due to uneven mixing, or slight stratification caused by differences in density or viscosities between the two oils.

3.5 Real-World Relevance

The thermal behaviour of vegetable oils plays a crucial role in both culinary applications and industrial process design. In the kitchen, oils with higher specific heat capacities can absorb and retain heat more efficiently, offering better temperature stability during cooking processes such as frying or sautéing. The main implications of heat retention and absorption in vegetable oils apply to the quality and safety of food preparation, highlighting the essentiality of understanding of chemical properties in vegetable oils specifically. In industrial settings, particularly within process engineering, the thermal conductivity and heat capacity of oils influence their suitability as heat transfer fluids in systems such as biofuel production, lubrication, and thermal storage. Understanding these properties is therefore essential for optimizing heat management, ensuring process consistency, and maintaining system efficiency.

The thermal stability of cooking oils is crucial for food safety and product quality control especially during processes that require high temperatures or an even heat distribution. Since the specific heat capacity of a stationary fluid directly impacts how its temperature changes over time, its value provides a myriad of implications for how the fluid behaves chemically under different thermal conditions. For culinary applications, these behaviours can influence the quality of the product and the safety of its consumption, in the case of vegetable oils, using an oil that is not able to suitably adjust to high temperatures results in the production of harmful chemicals and smoke. Selecting an oil that is suitable for its respective use is crucial to avoid this, and thus knowledge of the oils ability to absorb and retain heat is required. As seen in the data collected throughout this report a range of vegetable oils interact differently with temperature due to their ability to conduct heat, with oils with higher specific heats taking longer to heat up but retaining the heat for longer, and oils with low specific heats increasing in temperature at a faster rate. The heat transfer coefficient also influences the oils thermal properties, with oils like sesame and canola having lower h values and therefore lower heat exchange initially. This information allows culinary experts to determine the suitability of vegetable and other types of oils when using them for their practice, for instance, oils with higher specific heats retain heat for longer and therefore affect how evenly food can be cooked or seared. Other applications involve the oil's stability at a certain heat which is critical in deep frying, or preventing substantial temperature swings when food is added to the hot oil. Overall, knowledge of an oil's thermal properties can hold significant influence in their application in a culinary context.

Vegetable oils have gained increasing attention as alternative heat storage and heat transfer fluids in industrial applications such as their use in chemical reactors or thermal energy storage systems. The specific heats and heat transfer coefficients of the oils plays a critical role in their suitability for these applications, as it is often required that the oil be a viable means of transferring or retaining heat effectively. Oils with higher h values initially with steady decreases in h as they heat up are suitable for thermal energy systems due to their ability to quickly absorb heat and retain it for extended periods of time, this study found that sunflower and mustard oils match this criteria the most effectively. Sunflower oils have recently been integrated into the energy space with their use in solar thermal systems. In a comparative study that tested the viability for sunflower oil and water for a solar collector, sunflower oil was found to dissipate heat at a faster rate (0.462°C/min)[11] while also being heated more efficiently (12.4%)[11] when flowing through the system compared to waters 0.292°C/min[11] and 9.9%[11] respectively, making it a great option for efficient energy collection. This is partly due to the oil's lower heat capacity which enables it to absorb and dissipate heat at a faster rate than that of other fluids. Vegetable oils also offer sustainability advantages, as they are biodegradable and have a significantly lower environmental impact surrounding their production process. Thus vegetable oils provide a promising look into future solutions for energy storage that are cost efficient and stable for the long term.

An additional consideration is the phenomenon of stratified heating, where uneven temperature distribution occurs within a fluid body. This is especially relevant in large-scale operations, where inadequate mixing or poor thermal conductivity can lead to localized overheating or under processing. Thermal stratification is highly relevant in the utilisation of vegetable oils in thermal energy storage (TES) systems, as the formation of distinct temperature layers can enhance their efficiency as maintaining thermal stratification enables better temperature control and energy efficiency. Sunflower is another apt candidate for TES systems as upon testing it showed many valuable thermal properties, such as minimal thermal degradation until about 400°C [12], additionally, sunflower offered many similar characteristics to that of other thermal oils making it a viable option due to its wide availability and relatively cheap production costs. The use of vegetable oils in TES systems becomes particularly advantageous at higher storage temperatures, as oils maintain stable thermal properties while water is limited by its boiling point, making it necessary to undergo additional costs to ensure the storage vessel is pressurised and fitted with stratification devices to ensure optimal heat distribution. Overall, sunflower oil particularly and other vegetable oils provide a viable solution to maintaining optimal stratification in TES systems due to their thermal characteristics.

4. Conclusion

Within our experiment five different oils were used as well as oil blends to determine their convection profiles and their convective heat transfer coefficient. Sesame oil reached the highest temperatures and heated the fastest, reflecting its high conductivity and/or low specific heat capacity, whilst sunflower oil had high convective heat transfer potentially due to low viscosity whilst having a low temperature increase. This finding suggested lower conductivity whereby convective forces dominated. Mustard oil had the most uniform temperature distribution once density/convection currents developed. Finally, canola oil's strong stratification can be attributed to its high viscosity. Furthermore, the 50/50 blend had a relatively smooth heating whilst maintaining moderate responsiveness hence effective convection. In comparison, the 75/25 blend warmed quickly but unevenly amongst the thermal camera capture points. This was likely due to partial layering (nonhomogeneity) and thermal stratification. The convective transfer coefficient (h) decreased asymptotically as the thermal boundary layer thickened, reflecting transient heating natural convection.

Through our experiment, it is suggested that heat-transfer of oils in any industry as well as culinary applications engineering strategies should control mixing to maintain homogeneity within the oils and disrupt boundary layering. Moreover, engineers can consider finned surfaces to accelerate convection of oils to increase area limited by the beaker base. Additionally, our results made evident the changes oil blends can have convective heat transfer by manipulating physical attributes such a viscosity or density. Hence, implementing more complex blends based on these attributes can accelerate heating and thereby increase energy efficiency.

Acknowledgements

The authors thank the University of Sydney School of Chemical and Biomolecular Engineering for giving us access to laboratory facilities and equipment. We would also like to acknowledge the support of the teaching staff and laboratory technicians for their assistance during our experiment.

References

[1]1. Pekař, L. *Introduction to heat exchangers*. In *Advanced Analytic and Control Techniques for Thermal Systems with Heat Exchangers* (ed. Pekař, L.) 3–20 (Academic Press, 2020)

[2]. Sokolova, I. *Temperature Regulation*. In *Encyclopedia of Ecology* 2nd edn (ed. Fath, B.) 633–639 (Elsevier, 2019).

[3] NZIFST. Heat transfer theory. New Zealand Institute of Food Science & Technology.]https://nzifst.org.nz/resources/unitoperations/httrtheory6.htm (accessed 15 Apr 2025).

[4] Van Krevelen, D. W. & Te Nijenhuis, K. *Transport of Thermal Energy*. In *Properties of Polymers* 4th edn (eds Van Krevelen, D. W. & Te Nijenhuis, K.) 645–653 (Elsevier, 2009).

[5] Hoffmann, J.-F. et al. Temperature dependence of thermal conductivity of vegetable oils for use in concentrated solar power plants, measured by 3ω hot wire method. *Int. J. Therm. Sci.* 107, 105–110 (2016).

[6] Contreras-Gallegos, E. *et al.* Specific heat of vegetable oils as a function of temperature obtained by adiabatic scanning calorimetry. *J. Therm. Anal. Calorim.* 128, 135–143 (2017).

[7] Miller, K.S., Singh, R. & Farkas, B. Viscosity and heat transfer coefficients for canola, corn, palm and soybean oil. *J. Food Process. Preserv.* 18, 461–472 (2007).

[8] Abedigamba, O.P., Mndeme, S.F., Mawire, A. & Rukaaya, M. Heat utilization characteristics of two sensible heat storage vegetable oils for domestic applications. *Sustainability* 15, 6825 (2023).

[9] de Souza, E.C. *et al.* Heat transfer coefficient characterization of vegetable oils. Presented at the 18th IFHTSE Congress, Rio de Janeiro, Brazil (2010).

[10] Zeneli, M., Nikolopoulos, A., Karellas, S. & Nikolopoulos, N. *Numerical methods for solid–liquid phase-change problems*. In *Ultra-High Temperature Thermal Energy Storage, Transfer and Conversion* (ed. Datas, A.) 165–199 (Woodhead Publishing, 2021).

[11] Zanganeh, J., Moghtaderi, B. & Ishida, H. Combustion and flame spread on fuel-soaked porous solids. *Prog. Energy Combust. Sci.* **39**, 320–339 (2013)

[11] Mahavar, S., Kuldeep, P. K. & Mawire, A. Study of sunflower oil for heat transfer and storage applications. Scientific African 28, e02653 (2025)
[12] Mawire, A. Performance of Sunflower Oil as a sensible heat storage medium for domestic applications. Journal of Energy Storage 5, 1–9 (2016).

[13] Lugolole, R. et al. Experimental analyses of sensible heat thermal energy storage systems during discharging. Sustainable Energy Technologies and Assessments 35, 117–130 (2019).

[14] Santos, J. C. O. et al. Comparative study of specific heat capacities of some vegetable oils obtained by DSC and microwave oven. Journal of Thermal Analysis and Calorimetry 79, 283–287 (2005).

[15] Ashmore, M., Katlego, L., Robert, L., Denis, O. & Karidewa, N. Thermal Stratification Performance of a Packed Bed Latent Heat Storage System during Charging. E3S Web of Conferences 64, 03001 (2018).

[16] Fasina, O. O., & Colley, Z. (2008). Viscosity and Specific Heat of Vegetable Oils as a Function of Temperature: 35°C to 180°C. International Journal of Food Properties, 11(4), 738–746.

[17] Kahwaji, S., & White, M. A. (2019). Edible Oils as Practical Phase Change Materials for Thermal Energy Storage. Applied Sciences, 9(8), 1627.

[18] Oyirwoth P. Abedigamba, Frank S. Mndeme, Ashmore Mawire, Indra Bahadur, Thermo-physical properties and thermal energy storage performance of two vegetable oils, Journal of Energy Storage, Volume 61, 2023, 106774, ISSN 2352-152X.

SJIE 1(2) X–X (2025) https://doi.org/XXXX/XXXX

Evaluating Infrared Camera Performance in Detecting Moving Heat Signatures

Alysha Whitehouse[1], Bertie Lynch[1], George Ing[1], Samara Jirsa[1], Tom Waugh[1], Sebastian Dominguez Flores[1], Sebastian Dominguez Flores[1], Minghao Zhang[1], David Alam[1], Gobinath Rajarathnam[1]

School of Chemical and Biomolecular Engineering, The University of Sydney, Australia

Graphical Abstract

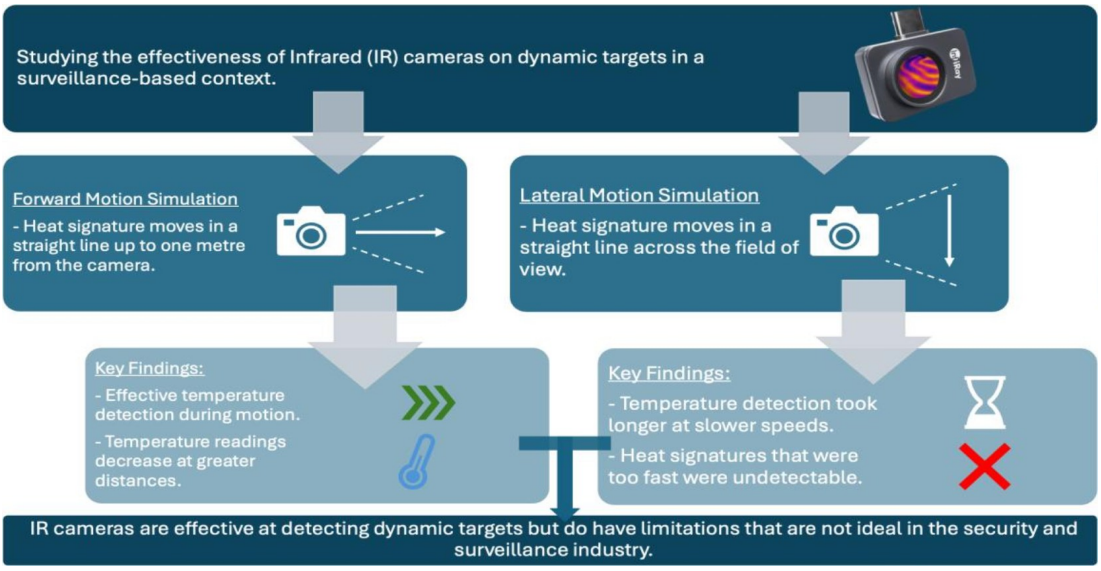

Abstract

The development and widespread adoption of infrared (IR) cameras, capable of detecting static and dynamic heat signatures, have enabled the creation of advanced security and surveillance systems. While most of the current research into the effectiveness of IR cameras in security-based settings involves the use of static heat signatures, an understanding of how these cameras perform on dynamic targets is also vital as moving heat signatures are ubiquitous in real-world scenarios. This study aims to determine the efficacy of IR cameras on a heat signature in a range of different motions to justify or challenge their prevalent use in commercial and residential surveillance systems. In this research, both forward motion and lateral motion setups were used consisting of a one-meter straight path, in-line with the IR camera, and a 70 cm straight path, facing the IR camera side-on, respectively. Both experimental setups tested the heat signatures moving at multiple speeds. This study found in the forward motion test that the IR camera was accurate in observing the temperature of the heat signature, however, greater distances between the heat signature and the camera resulted in lower temperature recordings. The lateral motion test found the sense time for the heat signature increased as its speed decreased, and that there is a speed great enough at which the heat signature remains undetected by the IR camera. Consequently, this research has confirmed that limitations do exist in IR camera surveillance technology, meaning that while significantly effective, these systems cannot be completely relied upon.

Keywords: infrared camera, heat signatures, dynamic targets, security, surveillance, forward motion, lateral motion.

1. Introduction

1.1 Motivation

Heat transfer is defined as the movement of thermal energy, in the form of heat, between physical systems with different temperatures. This transfer can occur through three primary mechanisms: conduction, which involves molecular agitation within a material without any bulk motion of the substance; convection, the transfer through the movement of fluid or gas currents between bodies; and radiation, the transfer of energy through electromagnetic waves, which does not require a physical medium (Biosystems Heat and Mass Transfer - ScienceDirect, n.d.). All these modes of transfer operate under the same fundamental principle — the tendency toward thermodynamic equilibrium — whereby two objects at initially different temperatures in thermal contact will eventually reach the same temperature (Heat Transfer, n.d.). Subsequently, heat transfer from one body to another affects the temperature of each object and thereby alters the infrared (IR) radiation emitted, also known as the 'heat signature' (Thermal Sensors - Department of Informatics, n.d.). This heat exchange impacts not only the thermal state of each object but also the intensity of the emitted infrared radiation (Infrared Radiation - an Overview | ScienceDirect Topics, n.d.). Such radiation can be converted into visible images that depict the spatial distribution of temperature differences in a scene observed by a thermal (IR) camera (Havens & Sharp, 2016). These IR cameras operate similarly to visible light (VIS) cameras: electromagnetic radiation from objects passes through a lens system (and possibly additional optical components) before forming an image of the object on a detector (Vollmer, 2021). Originally developed as surveillance and night vision tools for military use (Gade & Moeslund, 2014), thermal cameras have since been commercialised due to decreased manufacturing costs and technological advancements, now serving broader applications in sectors such as agriculture, building inspection, gas detection, and other fields related to heat energy and air conditioning (Krišto, 2016). However, while thermal cameras are widely used in these static diagnostic applications, their effectiveness in dynamic surveillance scenarios—particularly for detecting and measuring the heat signature and temperature of moving objects—remains insufficiently explored. This article aims to assess how effectively thermal surveillance cameras can detect and measure a radiating moving object's heat signature and temperature.

1.2 Literature Review

Detection of humans is the first step in many surveillance applications, and as such, general-purpose systems should be robust. For wide-area surveillance and tracking applications, Leykin and Hammoud (2016) describe a tracking framework that integrates colour and thermal imagery using a Bayesian approach based on particle filtering. In their method, each object (human) is represented by a bounding box location and a 2D colour histogram, allowing for robust tracking across varying conditions (Bhusal, n.d.). Similarly, Zin et al. (2007) proposed a system for human detection, based on the extraction of the head region, and Davis and Sharma (2004) proposed a detection system that uses background subtraction, gradient information, watershed algorithm and A* search to robustly extract the silhouettes

Although prior research demonstrates the potential of combining thermal and visual data for robust tracking, few studies isolate and evaluate the standalone performance of thermal cameras in detecting moving radiating objects, revealing a gap that this research aims to address.

2. Experimental Method

2.1 Forward Motion Procedure

To assess the thermal signature generated during forward motion, a one-metre straight-line path was marked on a flat surface in a location that allowed unobstructed movement of the heat pack. The InfiRay thermal imaging camera was positioned 23 cm laterally from the zero point and angled such that the entire interval remained within the field of view throughout each trial. This distance ensured complete visibility of the heat pack at both the starting and ending positions. The heat pack, heated to approximately 50 °C, was aligned so that its centre coincided with the zero point. It was then moved smoothly along the path until its centre reached the one-metre mark. This motion was executed over three fixed durations: 10, 5, and 2.5 seconds, with three separate trials conducted for each time interval to ensure repeatability.

Before recording, the camera's point temperature tool was configured to track maximum and minimum temperatures in each frame. This tool was adjusted to monitor the area occupied by the heat pack across the path while avoiding background interference. While continuous recording was possible, individual recordings were taken for each trial to simplify data management and to allow the exclusion of inaccurately timed or inconsistent runs.

2.2 Lateral Motion Procedure

The camera was fixed in a side-on position to ensure the entire heat pack remained completely visible as it moved across a 70 cm path perpendicular to the camera's field of view. The camera was located 1.1 meters away from the centre of the heat packs traverse path. Eight sense points were designated at 10 cm intervals along this path, including the start and end positions, using the camera's point temperature function to enable consistent spatial temperature measurements. The midpoint sense point (P3) was selected for detailed analysis due to its central location and relatively stable background temperature. A temperature spike at P3 was defined as a frame-to-frame increase exceeding 3°C, surpassing the

cameras reported ±2°C margin of error and sufficiently capturing the reported temperature increases.

Three-time metrics were recorded: point cross time, the duration for the heat pack to fully traverse P3; sense time, the delay between crossing P3 and the onset of the temperature spike; and total cross time, the time taken to traverse the entire 70 cm path.

To minimise thermal interference from handling, the heat pack was moved using a thin hook attached to a loop on its tag, ensuring all operator contact remained outside the camera's field of view. Trials were performed at six discrete total cross times between 10 seconds and approximately 0.35 seconds.

2.3 Lateral Motion Analysis Method

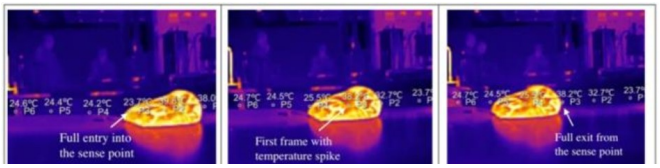

Figure 1 – Diagram of showing how the lateral motion recordings were analysed to gain meaningful data.

The analysis of the lateral motion videos aimed to quantify and explicate the camera's response delay in detecting temperature changes under motion. The individual frames of each of the relevant recordings were extracted and indexed numerically (e.g. Frame_0001 has frame number 1). For each run at each speed, three particular frame numbers were of interest (Figure 1):

- $Frame_{entry}$, the first frame where the sense point was fully positioned over the object
- $Frame_{spike}$, the first frame displaying a temperature spike at the sense point
- $Frame_{exit}$, the first frame when the object had fully passed the sense point

The camera had a reported frame rate of 25Hz. Two key time-based metrics, the sense time and the point cross time, could therefore be calculated as:

$$Sen\square\ \square\square\square e = \frac{1}{25} \times (\square r \square\square\square_{\square\square e} - \square r \square\square\square_{e\ \square\square}) \; Poin$$

$$t\ \square ro\square\ \square\square\square e = \frac{1}{25} \times (Fr\square m\square_{exit} - \square r \square\square\square_{(\square\square\square\square\square)})$$

These values describe the time between the object passing through the sense point and the thermal sensor registering temperature spike, and the duration the object remained over the sense point.

3. Results and Discussion

3.1 Forward Motion

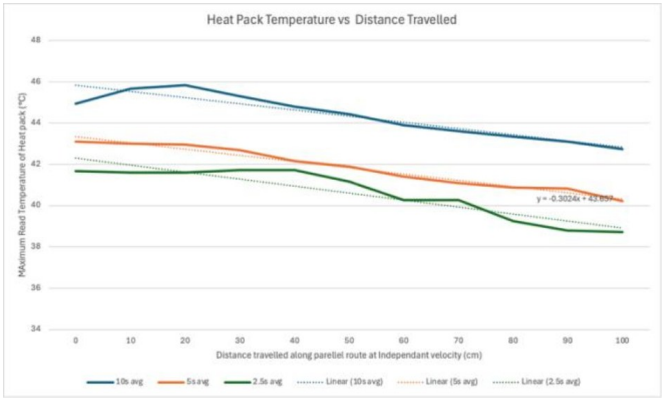

Figure 2 – Graph of the distance travelled by the heat signature against the maximum recorded temperature.

Note that data was collected sequentially, beginning with the 10 second intervals and without replacing the heat pack from any of the nine runs (three repeats of three intervals). As both the 0cm and 100cm points were taken with the pack at a standstill (velocity of 0), the disparity between temperature values is associated with the pack gradually losing energy to its surroundings between runs rather than the velocity during the pack's movement affecting the accuracy of the reading. For each time interval, the heat pack at the end of the 100cm interval read approximately 2.5 degrees cooler than it did at the beginning. The equation for this trend is shown by the equation in Figure 2, this equation was modelled upon the 5s interval runs as it fitted the linear trend the most tightly. Given that the camera was situated a further 23cm away from the zero-centimetre point of the interval, theoretically a room temperature reading of 20° C would be achieved at a certain distance:

$$Y = -0.3024x + 43.657$$

$$X = \frac{20 - 43.657}{-0.3024}$$

$$= 78.23 + 2.3$$

$$= 805.308 \text{ cm}$$

Excel treats x as the number of points taken, which in this case were every decimetre, such that the 23cm extra is an additional 2.3 dm. Extrapolating this trend back to the camera suggests that the temperature of the heat pack for while the five second interval data was collected would've been:

$$Y = -0.3024(-2.3) + 43.657$$

$$Y = 44.35252$$

The existence of this trend suggests that there is a specific distance at which the camera operates most effectively. Having an object of controlled temperature would have been useful for identifying the distance at which the camera operated most accurately. A physical thermometer would not work as effectively because there would be no way to easily to identify the warmest sections of the packs surface as the camera does.

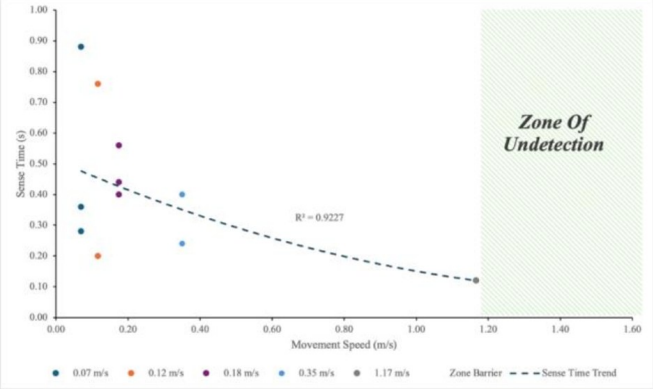

Figure 3 – Graph of movement velocity against sense time.

3.2 Lateral Motion

Figure 3 shows that for lateral object movement speed less than 1.17m/s, the camera sensed a temperature change more quickly as the object's velocity increased. Beyond this speed, the sense point did not record a temperature spike at all, indicating a complete failure of detection. This zone, defined as the zone of 'undetection', constitutes the speed above which our heated object went undetected by our sense point.

This relationship of faster speeds resulting in lower detection times is unexpected. Theoretically, as the slower moving object remains within each pixel's field of view for a longer duration, it was expected for the camera to accumulate more thermal signal to record a stronger and more stable temperature reading. In contrast, a fast-moving object may not give the sensor enough time detect and respond if only present for 1-2 frames. Hence the most logical explanation for this unexpected relationship is that when the heat object moved quickly across the cameras field of view, it may have caused an abrupt spike in infrared radiation which was more noticeable to the camera than lower speed runs as the ratio of signal to background noise was increased.

The median sense time for all successful detections was 0.37s. Significant variability however was seen across runs, particularly at lower speeds. Standard deviation in sense time was highest for the two slowest speeds (0.07m/s and 0.12m/s) at 0.326 and 0.323, respectively, with corresponding relative standard deviations (RSDs) of 64% and 84%. Faster successfully detected runs exhibited less variability, with runs at speeds 0.18m/s and 0.35m/s reporting RSDs of 18% and 27%. This shows that slower movement speed not only resulted in higher sense time but also greater absolute and relative sense time variation. This variation can be attributed to fluctuations in object emissivity, ambient thermal noise, and possible inconsistencies in object trajectory relative to the sensors focal point during the experiment.

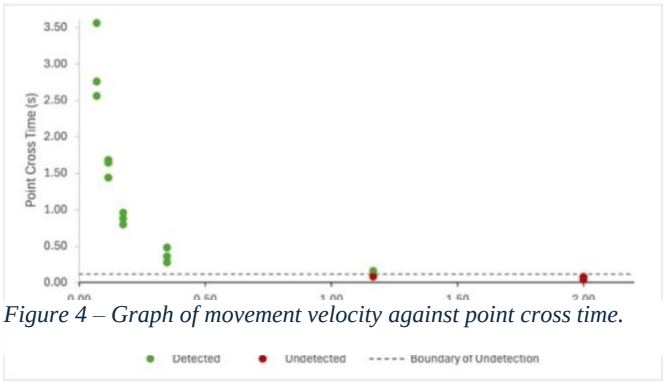

Figure 4 – Graph of movement velocity against point cross time.

The boundary of 'undetection', as seen in Figure 4, represents the boundary point cross time at which no object crossing in lesser time was detected by our camera. The minimum time the camera took to sense a temperatures spike was 0.12 seconds (3 frames after object crossed the sense point). This is the point at which our previously consistent trend of greater motion speed corresponding to lower sense times abruptly fails, and no temperature spike at all is recorded.

The presence of this boundary suggests that a heated object can pass through the cameras frame without setting off a temperature spike at high enough speeds. Consequently, systems that rely on detecting a temperature spike to set off a trigger, may fail to register a fast-moving heated object, despite its presence in the frame. Our data suggested that any object crossing the sense point in less than 0.12 seconds (3 frames) avoided causing a temperature spike in the sense point and therefore avoided detection. This may be due to the inability for the IR radiation emitted by the object to accumulate significantly within the sensor's thermal detection threshold within its brief exposure period.

These findings are highly pertinent for industrial applications. A camera set to detect a heated object (intruder, wild animal etc) may fail if the heated object is not detected by the camera's sense point and thus doesn't set off a trigger.

xxxx-xxxx/xx/xxxxxx

Table 1 – Speed required for different sized objects to avoid detection at a distance of 1.1 meters and detection boundary of 0.12 seconds.

Object (Length)	Speed Required to Avoid Detection (*m/s*)	Speed Required to Avoid Detection (*km/h*)
Heat Bag (0.2m)	1.8	6.6
Human (0.4m)	3.6	13
Large Dog (0.7m)	6.4	23
Car (4.9m)	45	160

Table 1 displays the speed required of various everyday heated objects to avoid detection by our thermal camera at a distance of 1.1 metres. This highlights an important overlooked limitation of detection that must be considered in industrial application

3.3 Combined Interpretation and Implications

Both the forward and lateral motion experiments demonstrated the importance of motion speed and direction in influencing infrared camera thermal detection. The experiment was limited in that there was little empirical analysis into the interaction of these two effects.

In the lateral experiment, the threshold speed for undetection was found to be 1.17m/s at a fixed camera distance of 1.1m. Beyond this speed, no temperature spike was observed. However, it is likely that this boundary is not only affected by object size, but also the object's distance from the camera. However, it is likely that this boundary is not only affected by object size, but also the object's distance from the camera.

Firstly, a distant object occupies fewer pixels in the camera's field of view. Consequently, at the same physical speed, a distant object traverses each pixel faster, thus reducing its likelihood of detection. This means more distant objects may can avoid detection even at lower speeds than those observed at 1.1m. In effect, the objects in Table 1, positioned greater than 1.1m away from the camera, would be capable of avoiding detection at even lower speeds.

Secondly, as illustrated in the forward motion experiment, thermal signatures at a distance becomes increasingly diffuse relative to the background. It was calculated that our heat pack would fail to register a distinct signature at a distance of 805.308cm. This limiting distance, calculated above for our heat pack, is relative to the size of the 2D projection of the object in question. At this limiting distance an object would go undetected regardless of lateral motion.

Together, these findings suggest that for a given object size and temperature there exists a two-dimensional detection boundary, defined by both distance and speed. If an object stays below this boundary, in either dimension, it can avoid detection. This offers a valuable framework for describing thermal camera limitations in surveillance applications and beyond.

4. Conclusion

The research undertaken provides insight into the effectiveness of IR cameras detecting objects in motion, especially in a security and surveillance context. Through tests simulating forward motion, it was found that the IR camera was effective in tracking the location and measuring the temperature of the heat signature in motion. However, it was discovered that the recorded temperature experienced a gradual, but significant decrease as the distance between the IR camera and heat signature increased. On average, a 2.5 °C decrease in temperature was recorded 1m further away from the camera. The tests simulating lateral motion measured the sensing time of temperature spikes due to the heat signature and found in all cases that a temperature difference was detected, it took a minimum of 3 frames (i.e. 0.12s) for a change to be recorded. This test also concluded that, contrary to the hypothesis, a faster moving heat signature resulted in a smaller temperature spike sensing time by the IR camera. Most notably, the lateral test confirmed the existence of a critical speed beyond which the IR camera could no longer detect the heat signature. This threshold was determined to be greater than 1.17m/s. As a result, IR cameras were found to be a generally effective security tool but have notable limitations in detecting dynamic heat signatures. To improve the reliability of such systems, optimal camera positioning should be considered, as the closer a heat signature is, the greater the temperature spike recorded by the camera will be. Also, avoiding lateral movement of heat signatures relative to the sensor increases the likelihood of detecting fast-moving objects. This limitation can also be addressed by deploying additional cameras focused on the same area. Finally, while this study measured the effectiveness of InfiRay cameras, other thermal camera brands on the market such as Hikmicro and FLIR, may perform better with dynamic heat signatures or possess greater framerates. A future comparison of different cameras in security settings would prove a worthwhile study.

xxxx-xxxx/xx/xxxxxx

References

Bhusal, S. (n.d.). Object Detection and Tracking in Wide Area Surveillance Using Thermal Imagery. https://doi.org/10.34917/8220085

Biosystems heat and mass transfer—ScienceDirect. (n.d.). ScienceDirect. Retrieved May 25, 2025, from https://www.sciencedirect.com/science/article/abs/pii/B9780128037799000030

Cansiz, A. (2018). 4.14 Electromechanical energy conversion. In I. Dincer (Ed.), Comprehensive Energy Systems (pp. 598–635). Elsevier. https://doi.org/10.1016/B978-0-12-809597-3.00425-9

Conduction heat transfer—An overview | ScienceDirect Topics. (n.d.). ScienceDirect. Retrieved May 23, 2025, from https://www.sciencedirect.com/topics/engineering/conduction-heat-transfer

Davis, J. W., & Sharma, V. (2004). Robust detection of people in thermal imagery. Proceedings of the 17th International Conference on Pattern Recognition.

Gade, R., & Moeslund, T. B. (2014). Thermal cameras and applications: A survey. Machine Vision and Applications, 25(1), 245–262. https://doi.org/10.1007/s00138-013-0570-5

Havens, K. J., & Sharp, E. J. (2016). Chapter 8—Imager selection. In K. J. Havens & E. J. Sharp (Eds.), Thermal Imaging Techniques to Survey and Monitor Animals in the Wild (pp. 121–141). Academic Press. https://doi.org/10.1016/B978-0-12-803384-5.00008-7

Heat transfer. (n.d.). NASA Glenn Research Center. Retrieved May 24, 2025, from https://www.grc.nasa.gov/www/k-12/airplane/heat.html

Ibrahim, S. (2016). A comprehensive review on intelligent surveillance systems. Engineering Science and Technology, an International Journal, 19(1), 22–31. https://doi.org/10.1016/j.jestch.2016.05.004

Infrared radiation—An overview | ScienceDirect Topics. (n.d.). ScienceDirect. Retrieved May 24–25, 2025, from https://www.sciencedirect.com/topics/physics-and-astronomy/infrared-radiation

Krišto, M. (2016). Review of methods for the surveillance and access control using the thermal imaging system. Review of Innovation and Competitiveness: A Journal of Economic and Social Research, 2(4), 71–91. https://doi.org/10.32728/ric.2016.24/5

Leykin, A., & Hammoud, R. (2006, June). Robust multi-pedestrian tracking in thermal-visible surveillance videos. In 2006 IEEE Computer Society Conference on Computer Vision and Pattern Recognition (CVPR) – Workshops (p. 136).

Mamat, H. (2019). Nanofluids: Thermal conductivity and applications. In Reference Module in Materials Science and Materials Engineering. Elsevier. https://doi.org/10.1016/B978-0-12-803581-8.11569-3

Thermal cameras and applications: A survey | Machine Vision and Applications. (n.d.). SpringerLink. Retrieved May 25, 2025, from https://link.springer.com/article/10.1007/s00138-013-0570-5

Thermal sensors—Department of Informatics. (n.d.). University of Oslo. Retrieved May 25, 2025, from https://www.mn.uio.no/ifi/english/research/projects/mecs/sensing/thermal-sensors

Vollmer, M. (2021). Infrared thermal imaging. In K. Ikeuchi (Ed.), Computer Vision: A Reference Guide (pp. 666–670). Springer International Publishing. https://doi.org/10.1007/978-3-030-63416-2_844

Zhao, J., & Cheung, S. C. S. (2009). Human segmentation by fusing visible-light and thermal imagery. IEEE 12th International Conference on Computer Vision Workshops.

Zin, T. T., Takahashi, H., & Hama, H. (2007). Robust person detection using far infrared camera for image fusion. Second International Conference on Innovative Computing, Information and Control.

Characteristics of Construction Materials: Thermal Expansion and Cooling Behaviours

Chloe Norman, Zachary Simmons, Sally Webster, Madeleine Ly and Anne-Mari Sigmundstad-Callahan

Chemical and Biomolecular Engineering, University of Sydney, Sydney, Australia

Graphical Abstract

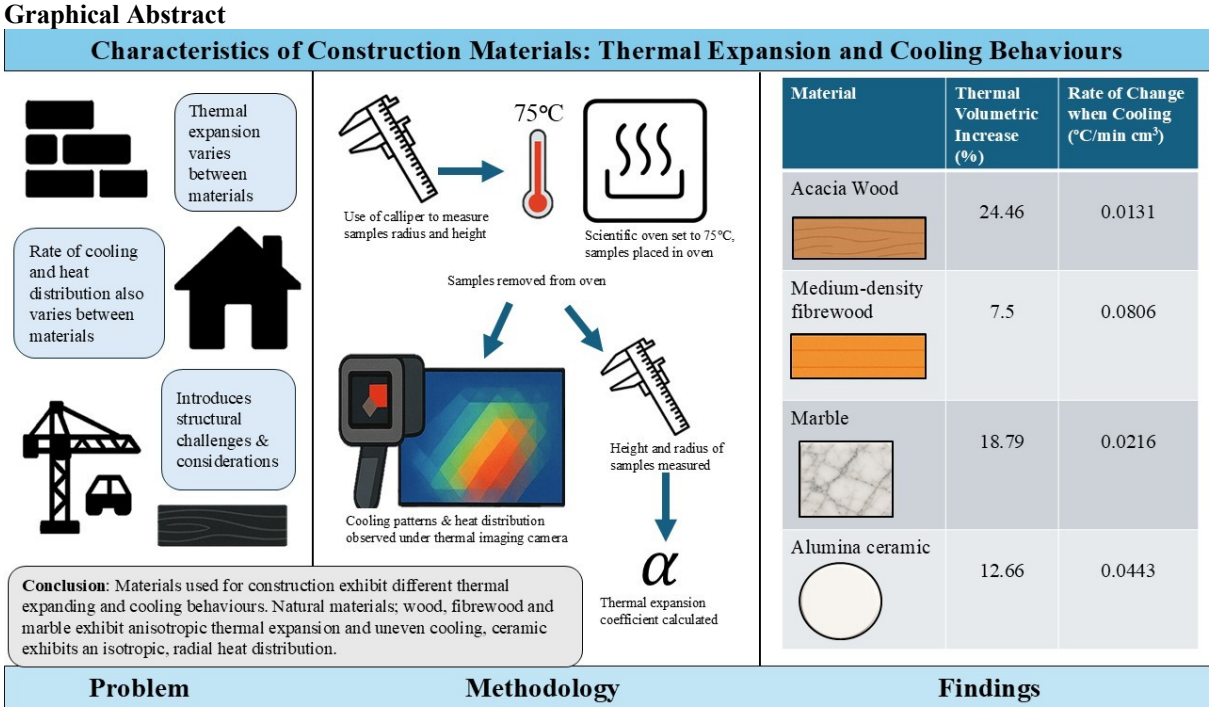

Abstract

Thermal expansion has been an issue that led to multiple challenges in fields such as transport and construction for many years. Accounting for this is an essential component of selection and usage of many materials, with the degree of uniformity to which materials expand is a centrepiece in designing products. The usage of a heat visualisation cameras allows for accurate mapping of the distribution of heat within a material and identify the uniformity of cooling and suggest the presence of uneven thermal expansions, the source of thermal stresses.

Experimental testing allowed for the modelling and analysis of isotropic and anisotropic expansion, whereby wood was found to have the highest coefficient of thermal expansion (α), indicating that when exposed to temperature variations, the change in atomic length was the largest in this material. However, experimental and theoretical α values had significant discrepancy, pointing to inaccuracy due to hygroscopic behaviour of samples and other errors. Material choice for industrial and construction applications is directly dependent on the thermal characteristics and behaviour of the material. The experiment found that Wood had the highest heat retention rate, therefore useful for insulation and structural applications. Further, the fibreboard had the lowest retention and highest rate of cooling, indicating its usefulness in rapid cooling situations and temperature stabilisation.

Keywords: Coefficient of Thermal Expansion, Isotropic, Anisotropic, Heat distribution, Homogenous

1. Introduction

Thermal expansion is the tendency of a material change in size in response to temperature changes, whereby in most cases increased temperatures induce a dimensional expansion and decreased temperature results in a dimensional contraction of a given substance. In solids this phenomenon occurs through the solid-state lattice arrangement of particles and the interatomic anharmonic potential[1] of a substance. From collision theory, as temperatures rise, thermal energy supplied causes an increase in kinetic energy, resulting in increased particle vibrations and average interatomic separation[2].

Thermal expansion of solids can be observed in respect to length, area, and volume, whereby either uniform expansion (isotropic expansion) or direction dependent expansion (anisotropic expansion) occurs. The linear thermal expansion coefficient (α_l) quantifies the degree at which a solid's respective lengths due to temperature changes. This coefficient can also be considered in terms of volume and area changes. The formula for α_l is seen below.

$$\alpha = \frac{1}{L_{initial}} \cdot \frac{dL}{dt}$$

Furthermore, observations of the heat distribution along the surface of a material as it cools is useful for identifying the usage of various materials in different contexts. Non-uniform thermal cooling can be a result of anisotropic crystalline structures or a nonhomogeneous material composition, which can lead to significant thermal stresses within a material due to variations in thermal expansion along different directions. This theory plays an essential role in many fields such as construction where thermal stresses can be highly hazardous and compounded when materials are under external stresses. Furthermore, electronics rely on consistent uniform crystalline structures for repeatability and reliability as well as dissipating heat efficiently and quickly. This naturally extends to a quantitative analysis of the volumetric ability of a material to lose heat rather than a qualitative analysis of distribution. This essential in deciding appropriate materials in heating and cooling applications such as insulation within constructions. Using a thermal camera has the advantage of analysing a map of the heat and thus the uniformity or lack of temperature within a material.

2. Methods

Experimental testing sought to quantitatively measure thermal expansion and rates of cooling for circular samples of wood, marble, ceramic, and medium density fibreboard. This was achieved through measuring the difference in diameter and height of the samples once reaching 75°C. Once this occurred, thermal cameras were then employed to measure heat loss throughout each sample, with measurements been taken over a 10-minute period. Prior to heating, measurements of the diameter and height of the 4 different materials were taken using a calliper to optimise accuracy.

The procedure involved heating the samples in a laboratory oven to 75°C, this was done at the same time to ensure reliable and uniform thermal exposure for all 16 samples. However, this was somewhat limited by the oven set up, whereby some samples were placed at the top of the oven and some at the bottom, which would have impacted the consistency of heat flux applied to each sample. Once the oven had been consistently at the desired temperature for fifteen minutes, each sample had its dimensions measured using the same calliper, this was used to quantify any thermal-induced expansion. Once all 16 samples had their dimensions measured and back up to the desired temperature, further testing was used to focus on cooling tendency and heat distribution. The experimental set up used can be seen in figure 1.

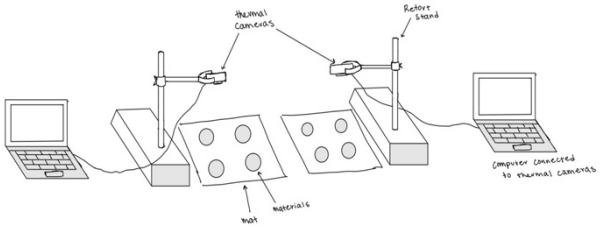

Figure 1: *Scientific drawings of experimental set up and equipment used*

To assess the distribution of thermal energy during cooling and heat loss, measurements were recorded at 1-minute intervals over a 10-minute duration through the thermal camera. The experimental setup can be seen in figure 1, whereby the thermal camera was placed vertically above the samples held by a clamp to ensure a consistent field of view. Specific temperature readings were taken for each sample, whereby measurements were taken at the centre, around the circumference, and across the radius. The data collected consisted of multiple temperature readings as well as a photo of the overall temperature distribution. These measurements provided a time-resolved data set of heat loss across each material surface and provided qualitative evidence of the differing ways heat travelled through each medium.

All the data collected in the experiment was then analytically studied, through various statistical methods, to draw accurate and reliable conclusions. The raw data of such can be found in the appendix,

and notable graphs and tables will be found further in the report.

3. Results and Discussion

3.1 Thermal Expansion

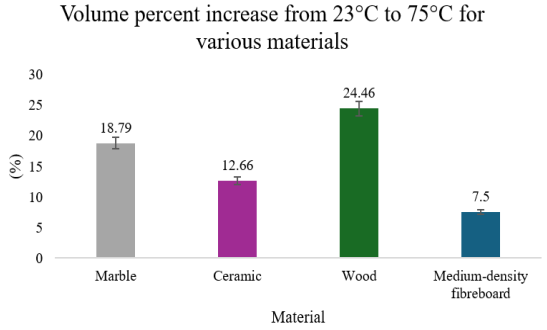

***Figure 2**: Bar graph for percentage volume increase of four tested materials when heated to 75°C*

Volume was defined as $V = \pi r^2 h$, assuming perfect cylindrical shape and uniform expansion across each material's radius and height. The results indicate that wood has the highest volume change from room temperature to 75°*C*), with marble then ceramic, and medium-density fibreboard experienced the lowest degree of expansion. The extent to which different materials thermally expand is dependent on atomic structure and intermolecular forces as well as material homogeneity.[3]

Thermal expansion varies between materials primarily as a result of increased particle separation, either due to increased bond length between atoms or cell wall swelling. The coefficient of thermal expansion is a material-specific property quantification of this, indicating the extent to which different materials expand or contract at the same temperature, in this situation it has been defined as the fractional increase in length per unit rise in temperature[4].

$$\alpha = \frac{\Delta L}{L_{initial} \times \Delta T} \quad (1)$$

Table 1: Comparison of calculated linear thermal expansion coefficients from experimental procedure versus theoretical linear thermal expansion coefficients[5]

Material	*ΔL*	*ΔT*	*α (Experimental)*	*α (Theoretical)*	*Percentage Difference*
	m	***°C***	***°C^{-1}***	***°C^{-1}***	***(%)***
Marble	0.00257	52	0.000486	0.0000141	3350
Ceramic	0.00250	52	0.000465	0.0000081	5640
Wood	0.00252	52	0.000483	0.00003	1510
Medium-density fibreboard	0.00248	52	0.000478	0.0000003	160000

Example calculation for marble length expansion 75°C

$$\alpha = \frac{0.00257}{0.102 \times 52} = 0.000486/^{o}c$$

3.1.1 Uncertainty

It should be acknowledged that the experimental procedure does hold potential uncertainty. A calliper was used to measure the radius and height, which had a resolution limit of 0.01mm and hence a measurement of 1mm has an uncertainty of +/-0.005mm. This corresponds to a percentage uncertainty of 0.5%, which is reasonably small and unlikely to pose any significant uncertainty in recorded data. However, since the small scale of the measurements, uncertainty is higher than in a larger scale situation. Further to this, potential human error could have arisen from inaccurate calliper placement, whereby the calliper was not in the centre of the circular objects nor consistently in the same position for each measurement. The laboratory oven used is regularly calibrated to ensure that the internal temperature matches that displayed, however the potential for this inconsistency remains as the experimental procedure did not use a thermometer to confirm internal temperature of the oven or the material. Furthermore, humidity was not controlled therefore a constant moisture content was not achieved in the conditions of which the samples were being tested. This resulted in some samples having a higher moisture content and therefore hygroscopic behaviour which reduces accuracy and reliability of the calculated expansion coefficient.

3.1.2 Material composition & purity

The materials used; acacia wood, alumina ceramic, marble and medium-density fibrewood, cannot definitively said to be of 100% purity as this was not tested prior to experimental procedure. While materials of high purity and isotropic structure typically exhibit a relatively uniform thermal expansion due to consistent atomic bonding and vibrational energy, impurities or amorphous components—such as lignin and other structural proteins in wood—can disrupt this uniformity, influencing thermal expansion behaviour beyond just structural considerations. Impurities can often result in anisotropic thermal properties, whereby the thermal conductivity differs in various directions[6], producing a non-uniform profile or a thermal expansion coefficient inconsistent with theory. This is particularly true for wood samples, such as the acacia wood used in this procedure, where typically smaller samples are not fully representative of the behaviour of engineered timber products at larger scales due to the present of annual rings or the stacking arrangement of wood planks[7]. This theory is a plausible explanation for the wood's deviation from the theoretical value of 0.00003 (m/m×°*C*) by 15.09 times. Further to this, typically marble samples are primarily composed of 90-99% calcite,

$CaCO_3$, as well as dolomite and serpentine[8]. The 33 times difference between marbles' theoretical coefficient 0.0000141 ($m/m\times°C$) and the experimental coefficient suggests variation from assumed purity levels; likely the material was composed of materials in high quantities other than calcite such as quart or resins. The same can be said for the alumina, Al_2O_3, ceramic and medium-density fibreboard, considering they deviated by 56 and 159 times, respectively, from the theoretical quantity. However, considering the small scales of the coefficients, that the absolution magnitude of the deviations appears larger than they physically area.

Wood and marble were found to have the largest thermal expansion coefficient in the x direction (length of the sample) with values around 0.00003 and 0.000141 respectively. These are higher than the coefficient for medium-density fibreboard due to the presence of pores within the fibreboard, diluting the volumetric change as the pores somewhat hide this. This is due to the particles expanding into the pores of the material before out of the original dimensions. The readings taken within the lab of volume through measuring length is not reflective of the actual volume of the fibreboard itself, as this formula assumed porosity was not apparent within the solid. As such, volumetric displacement would give a higher accuracy measurement and thermal expansion coefficient, however, this is not applicable in large scaler industry and is not a feasible process in this way.

The significant discrepancy between theoretical and experimental α values can be primarily attributed to high moisture content trapped within the materials, otherwise known as hygroscopic behaviour, which can be exacerbated in high humidity environments. Hygroscopic materials will experience distortion of dimensional and thermal properties, such as the coefficient of thermal expansion, heat capacity and volume. The effect moisture content has directly depended on the composition of the material, specifically the difference between the cellulous wood and the non-cellulous other samples. Wood does not have a constant equilibrium moisture content, whereby water within the material can be free and in the cell cavities or bound and within the cells themselves, as such the evaporation of water particles into pressure increasing gases does not occur. Instead, the rate of cell wall swelling increases with moisture content by 5-25% until the fibre saturation point occurs, where after this point the rate significantly declines due to capillary condensation[7]. As such, wood has the highest α value and volumetric expansion yet the lowest discrepancy between the experimental and theoretical ones.

Furthermore, studies suggest that during thermal cycling, the process of stressing and relaxing the material, cause changes to the microstructures of the material which as more cycles are perform stabilise out. This influences properties such as the thermal expansion coefficient which would be expected to deviate significantly from the tested values during an initial cycle.[9] If many cycles were performed, the thermal properties should converge to those found in literature as the nanostructures within the material begin to reach a more stable state due to the constant stress and relaxation[10].

For certain porous or hygroscopic materials, rising temperatures causes the kinetic energy of trapped water molecules within the material to increase. As the energy of particles rise, they spread out more and water undergoes a phase change from the liquid to gaseous state, generating internal pressure forces within the pores of the material and leading to expansion. This occurs to a greater extent in materials with a high moisture content and low porosity, as there is no open spaces for this gas to occupy This occurrence within the measurements lead to the significant overestimation of the expansion coefficient, as this is not due to atomic vibration which thermal expansion is defied by, rather pressure driven volumetric change. As such, it can be assumed the experimental coefficient combines this as well as atomic vibration. The effect of this was largest in the fibreboard, whereby despite its porosity, it can be assumed that it had a high moisture content which caused the largest discrepancy between its actual and experimental α value.

Conversely, the manufactured fibreboard is characteristically dimensionally stable[11] when exposed to most moderate ranging temperatures such as general temperature cycles throughout the year. However, it is very sensitive to moisture and moisture induced swelling occurs, this theory supports the assumption that the fibreboard was significantly moist, accounting for the largest difference between actual and experimental results, whereby the results calculated were distorted by dimensional and volumetric expansion. Similarly, ceramics also have a low thermal expansion and exhibited moisture-related expansion in the same way that fibreboard did, just to a lower extent

3.1.3 Anisotropic vs Isotropic

Materials tend to respond differently when exposed to high temperature environments, whereby the expansion and general material properties may be considered anisotropic or isotropic. Isotropic expansion describes a material in which has a constant linear thermal expansion coefficient (α) in terms of cylindrical coordinates z, r, and theta, resulting in a uniform percentage increase in height, width, and depth. On the other hand, anisotropic describes a non-constant thermal expansion coefficient, resulting in an uneven shape distortion when exposed to thermal energy. The isotropic or

anisotropic tendency of a material is constant regardless of thermal quantity analysed, that is if a material has anisotropic expansion, it will also have anisotropic thermal conductivity due to differing structure characteristics[12]. However, if the material is non-homogenous, such as wood or marble, then it can be highly dependent on the sample tested and exhibit significant disparities.

Natural materials tend to be anisotropic, with Wood, Medium-density fibreboard, and Marble all found to have anisotropic expansion due to differing α values between the height and length (width) seen in appendix tables 4 and 5, a phenomenon in which aligns with preexisting thermodynamic theory. The diverging coefficients arise from differing crystallographic orientations within the material, specifically whereby grains of material are elongated or stretched in each direction[13]. As such, the experimental findings can be seen in table 2, whereby the coefficient differed between the height and length expansion, with the height expansion (in the z direction) coefficient be 10 times greater than that of length.

Wood and marble are therefore more responsive to thermal increases, and the extent at which atomic vibrations accumulate under these conditions is greater than those of ceramic and fibreboard. For both materials, due to their anisotropic nature, expansion for wood occurs to a larger extent on the transverse plane (normal to the grain)[7] and for marble it occurs along the grain.[14] Therefore, the magnetite and direction of thermal expansion is influenced by the specific shape and lattice preferred orientation of the material, which is not consistent across the general categories of wood and marble.[15] Resultingly, this tendency depends on the specific type or wood, or marble used and cannot be generalised as such. This increases stresses in some points, generating weak points which can undermine structural integrity. To account for and control this, this theory can be used to inform engineering decisions on where best to add structural support mechanisms when using these as building materials.

Alumina ceramic (Al_2O_3) on large scales is isotropic[16] due to the lattice composition of the compound, with the hexagonal packing and atomic structure facilitating the relatively equal expansion along all directions in a plane. On a molecular scale, individual grains may be considered anisotropic, however for most materials on a large scale these differences cancel each other out and the material is isotropic in bulk.[13] This is the case for construction and large-scale applications of ceramics. As such, the α found should theoretically be the same and the material isothermal, however this was not found in experimental investigation, with the calculated values differing significantly. This raises the potentially errors which existed in the experiment, impacting the validity and reliability of readings, overall reducing the accuracy. A uniform material is often desired as it follows theory for isotropic homogenous materials, making it easier to predict the response under changing thermal conditions. Resultingly, these materials are often used for high temperature situations due to the uniform temperature distribution minimising thermal stresses and optimising material lifespan.

4. Cooling

Analysis of the chronological cooling of materials using the thermal cameras allows for the visualisation and analysis of heat distribution over time. This is useful for the identification and analysis of the uniformity, or lack of, of the cooling of the material. Figure 3 (below) demonstrates this sequential cooling and photos at equal time intervals of each material cooling.

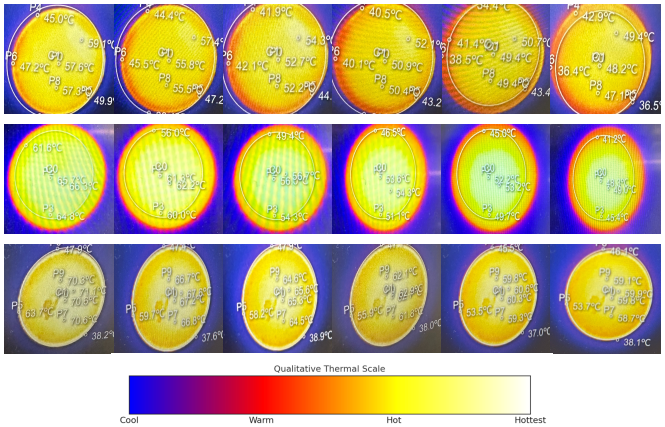

Figure 3: *Infrared images of cooling of plates of wood (row 1), ceramic (row 2) and marble (row 3) at regular time intervals of 1 minute from time = 0 to time = 5 with scale bar*

Figure 3 indicates that each material has an initial non-uniform distribution in the xy-plane. This is likely due to the slight variations in airflow patterns within the oven and non-uniform cooling during transportation from the oven to thermal camera. A possible resolution to this would be to increase the time that the materials were left in the oven. Irrespective of this, theoretically if the materials are isotropic (thus their conductivities are constant in every direction), their temperature should reach a radial distribution due to maximisation of entropy achievable in this radially symmetric configuration.[17] This is apparent for the ceramic in row 2 which shows that as time progresses the distribution (initially non-uniform) approaches a more radial distribution with the highest temperature in the middle which diffuses outwards by Fourier's law.

$$q = -k\nabla T.$$

Whilst often Fourier's law assumes symmetry in the radial direction around the midline, this is what is being analysed in this experiment thus the analysis is of 2D conduction in a non-steady

state. This radial distribution characteristic of a uniform material is however not present in the wood and marble distributions which as seen in wood has an area in the top right corner across the whole-time evolution that is consistently hotter than the centre and in marble has a section in the bottom left that is consistently cooler than its surroundings.

If isotropic, this irregularity in the heat distribution should vary but due to its presence amongst the whole time series, it indicates the non-constant conduction coefficient of the materials and thus the anisotropic nature of the material and its cooling. This is expected of materials such as wood which are uniform often in the direction of the grain but non-uniform across the grain, an orthotropic material, symmetrical in 2 planes.[18] Furthermore, the nonuniformity of wood is due to natural growth patterns which can vary on the environment that the tree is grown making each piece of wood have a non-uniform distribution.

Marble is formed when calcite (limestone) is under high pressure and temperature in which the calcite crystals dissolve and reform to produce the much denser marble. In this recrystallisation, any impurities within the calcite can produce heterogeneities within the marble evident within marble's characteristic grains where the rock has a differing mineral composition and crystalline structure.[19] This results in the material not only being anisotropic but also non-homogenous and thus a non-uniform heat distribution indicating reasoning as to the deviation from the radial heat distribution. Just as wood has grain boundaries, so does marble and these barriers alter heat transfer due to the differing compositions between the two sides of the boundary and the associated conduction coefficients.[20]

The cooling of cork was not analysed due to its rapid cooling because of its small volume. This caused the cork to hold minimal thermal energy, and its rapid cooling saw no clear pattern emerge thus minimal analysis of the distribution of the heat could be performed. In examining the heat retention of these materials, over the course of 10 minutes, the marble lost an average of 19.55ºC and the ceramic lost 24.25ºC. The wood and cork which the experiments were run for 9 minutes due to time constraints showed an average loss of 14.75ºC and 22.55ºC respectively. All four materials showed a linear cooling trend as shown in figure 4 below.

Marble, wood and ceramic all showed strong linear relationships and were still in the process of cooling down however, the cork had less of a linear relationship. As observed in the experiment, cork was the smallest and thinnest material and had the largest change in temperature in the first minute. As can be seen in the graph, the cooling starts to slow as the temperature approaches room temp, creating a more characteristic cooling curve. This suggests that while cork quickly releases heat initially, it stabilises at a slower rate as it approaches ambient conditions. From these trends in figure 4 ceramic cooled the fastest followed by cork while marble and wood retaining heat better. In observing varying relationships, a common graph used in the regression of cooling data would be an exponential model. This was done as can be seen in figure 5.

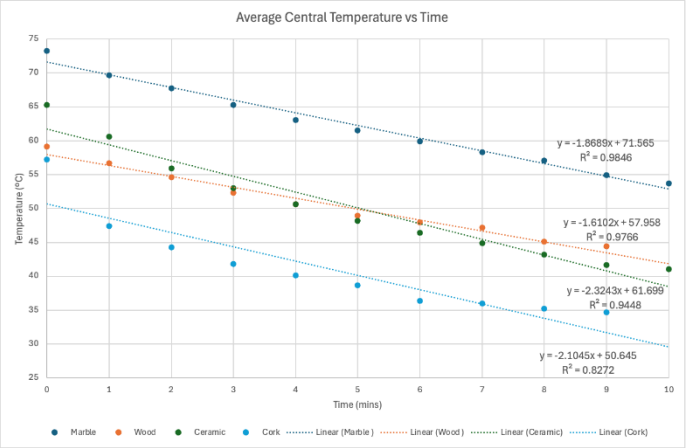

***Figure 4**: Linear Regressions for cooling data*

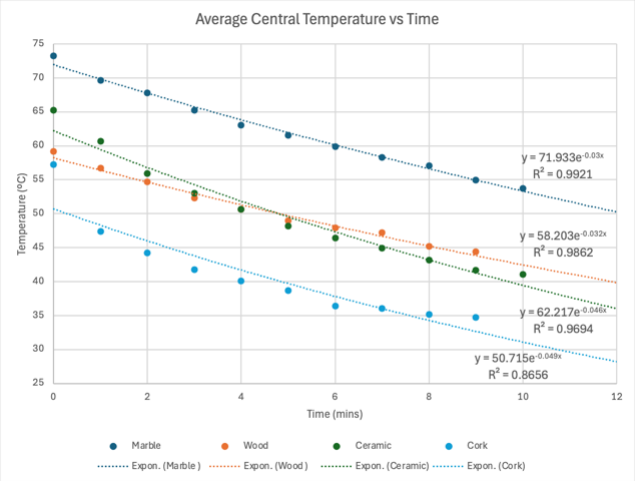

***Figure 5**: Exponential Regressions for cooling data*

As can be observed in the R^2 values, the exponential regressions seem to fit the data better than the linear regressions, however the graphs still do not appear to be characteristic of a typical exponential cooling curve. This is because after 10 minutes had elapsed, the materials were still undergoing cooling and had not yet reached the recorded room temperature of 23ºC. If the experiment were to continue until room temperature was reached, it is likely the cooling curves would fit an exponential graph very well. Since the materials differed slightly in size and volume for a more accurate comparison, the values for rate of change of temperature over time per unit volume can be found in table 2 below.

Table 2: Cooling Rates

Material	*Raw sample volume (cm^3)*	*Rate of change per unit volume ($^oC/min\ cm^3$)*
Wood	122.8	0.0131
Marble	86.7	0.0216
Ceramic	52.5	0.0443
Cork	26.1	0.0806

As seen in table 2, wood retains heat better than the other materials while cork retains heat the worst. Even though ceramic had the greatest temperature loss, when considering the volumes of each sample of material, the cork lost the fastest. This reflects how each material has varying thermal properties which are influenced by factors such as their surface area, density and specific heat capacity. For example, ceramic, despite having the greatest overall temperature loss, had a higher volumetric cooling rate, highlighting its lower thermal mass relative to its volume.

These findings can be applied to material selections in real world applications as they have practical implications where the ability to retain or dissipate heat is important in efficiency and performance. In construction, materials like wood are often favoured for interior structures and insulating elements due to its higher heat retention while ceramics are used where rapid cooling is needed such as in cooking surfaces and some heat exchangers. Likewise, cork's ability to cook quickly would be advantageous in applications that require effective insulation or a quicker temperature stabilisation. These fundamental thermal behaviours are important considerations for designing energy-efficient systems and selecting appropriate materials for specific thermal management needs.

4. Practical and Industrial Applications

Within construction, materials are often under high levels of tensile and sheer stress and thus must be able to handle these forces. On top of this, the natural cycle of the day as well as other factors such as the environment, geographical location, climate and proximity to heat sources such as furnaces exposes materials to different temperatures. Unequal distribution of heat within a material creates thermal stresses along the temperature gradient due to unequal thermal expansion.[21] In larger buildings, due to the larger load on the structure, it is essential to minimise the temperature gradient and distribute the heat in a uniform manner to decrease the thermal stresses on the materials.

As such, isotropy and homogeneity are often ideal cases as this allows for reliable predictions based on thermodynamic theory for homogenous materials whereby there is a uniform temperature gradient, and thus uniform thermal stress applied in all directions. For anisotropic materials, the thermal stress and structural fatigue must be correlated to the nonuniformity of the material, as such this makes it an unreliable construction material as these nonuniformities may vary between samples of materials due to an often lack of homogeneity. Due to expansion in different crystallographic direction and uneven atomic spacing, materials with both high thermal expansion coefficients and significant anisotropy are often unsuitable for usse in precision electrical applications, as dimensional changes can induce stress, misalignment, or changes in electrical performance due to geometry-dependent energy transfer limitations

Thermal cycling is often used to test thermal and structural integrity, determining the suitability of the given specimen for its intended purpose. The experimental procedure conducted one round of this cycling at a small temperature range; however, these tests can accumulate to 500 plus cycles. In industry these tests involve placing the material in oxygenated environments and exposing it to extreme thermal cycles of significantly high and low temperatures.[22] Furthermore, the effect of UV and air humidity can also be tested in similar stimulations[23] to give a comprehensive overview of the response of a given material. This intense testing procedure is vital in forming engineers of the durability, stability, bonding performance, and thermal responsiveness of differing materials. For anisotropic materials on a molecular level, each individual cycle creates microscopic damage at the grain boundary, and due to the anisotropic nature of many materials as well as their uneven grain distribution, some boundaries are more damaged than others. The extent of damage is directly proportional to the size of the temperature differences in the cycle, therefore more damage occurs on a seasonal basis as opposed to day to day.[24] Studies found that for marble, permanent expansion of certain types occurred by 0.2% (in volume) after exposure to 50 thermal cycles[24]

This is important to understand for marble as it is often used for historic restorations of art as well as small-scale construction within residential and commercial buildings. The diurnal heating of marble can cause large temperature differences in which literature indicates that these cycles can widen grain boundaries and produce sub-surface fractures due to the stresses induced in the non-symmetrical heat distribution reducing the structural integrity of the marble.[25] This suggests the minimisation of the usage of large slabs or marble that will have a large temperature gradient and elucidates the usage of thermal visualisation for historic marble sites to identify internal fractures and weak points within the stone's internal structure.

Wood's high thermal expansion and orthotropic properties are important considerations within its usage in construction. Its high thermal expansion which when used with other materials with varying thermal expansion coefficients can

have the same effect of varying temperatures within a material as it produces areas of differing thermal expansions causing stress on the materials. The mismatching of thermal expansion coefficients is central to the warping, delamination and fractures of materials that can cause a severe decrease in structural integrity of materials and a core consideration within all applications where varying materials are used especially for high load bearing situations.[26] These results highlight the usage of expansion joints within construction that allow for this natural expansion[27] of the wood without incurring stress between pieces of wood by allowing for the natural expansion of the wood. Furthermore, the observed variations of temperature along grain boundaries (similar to the marble) indicate that for many purposes the wood grain must be aligned in order to minimise thermal stresses amongst the material.

Contrary to the wood and marble, ceramic's uniform heat distribution in the analysed plane due to its isotropic crystalline structure. This supports its usage in high temperature systems where its ability to evenly distribute temperature reduces the probability of crystal deformation and fissures forming in these situations such as kilns and electronics. For applications such as electronics where precision and repeatability are essential, the use of the ceramic's homogeneity is highly advantageous due to its predictability and explains their resurgence in the technological age.[28]

The low expansion of cork sees its use where gasket integrity is essential such as sealing wines where the possibility of intense cycles of expansion and contraction due to temperature fluctuations pose serious risks to the structural integrity of the glass especially as the bottle ages. Due to the small volume of the supplied cork and it being highly composed of air, the cooling phase was too fast for the time gaps, and it was difficult to observe any specific patterns within the cork however this may be quite advantageous as an insulator where air has a high thermal resistance to conduction and especially within a cultural shift towards more 'green' materials it may see the more widespread and frequency use of cork.[29]

5. Conclusion

The report analyses the heating up and associated thermal expansion as well as the cooling down due to convection and the associated distribution of heat in various materials. It was found that materials such as marble, wood and the cork (medium-density fibreboard) exhibited anisotropic expansion, a result of their natural origins causing their nanoscopic structures to be non-uniform. There was a significant deviation of the calculated thermal expansion coefficients between the experiment and literature which is likely due to the expansion of trapped water within the materials and it being the first time the materials are thermally cycled in which it is expected that these values deviate from literature. It is suggested that for future investigations, rather performing a single cycle, the materials are thermally cycled, and the thermal expansion is analysed per thermal cycle. Furthermore, it should be analysed if post heating and cooling the materials return to their initial volumes to see if the heating process caused plastic deformation and from this whether the trapped water had irreversible effects. During the cooling it was found that similarly to thermal expansion, the 'natural' materials had a non-uniform heat distribution due to their structural anisotropy where the ceramic, comprised of alumina, had a radial heat distribution due to its crystalline structure which is isotropic and homogeneity of material supporting its use in high-temperature applications requiring dimensional stability. It was found, which aligns with theory, that an exponential function fitting the cooling data the best compared to linear models. These insights are essential to material selection within real world applications such as construction and electronics.

References

[1] Drebushchak, V. A. Thermal expansion of solids: review on theories. *Journal of Thermal Analysis and Calorimetry* **142**, 1097–1113 (2020).

[2] Callister, W. D. *Materials Science and Engineering*. (Wiley, 2019).

[3] Why do different materials have different thermal expansion rates? | TutorChase. *www.tutorchase.com* https://www.tutorchase.com/answers/igcse/physics/why-do-different-materials-have-different-thermal-expansion-rates.

[4] Thermal Analysis Labs. What is coefficient of thermal expansion (CTE)? how do I measure it? *C-Therm* (2018). Available at: https://ctherm.com/resources/newsroom/blog/coefficient-of-thermal-expansion/. (Accessed: 7th May 2025)

[5] The Engineering Toolbox. Coefficients of Linear Thermal Expansion. *Engineeringtoolbox.com* https://www.engineeringtoolbox.com/linear-expansion-coefficients-d_95.html (2019).

[6] Thermal Properties of Solids: Conductivity and Expansion | Solubility of Things. *Solubilityofthings.com* https://www.solubilityofthings.com/thermal-properties-solids-conductivity-and-expansion (2025).

[7] Chiniforush, A. A., Akbarnezhad, A., Valipour, H. & Malekmohammadi, S. Moisture and

temperature induced swelling/shrinkage of softwood and hardwood glulam and LVL: An experimental study. *Construction and Building Materials* **207**, 70–83 (2019).

[8] Wahab, G. M. A., Gouda, M. & Ibrahim, G. Study of physical and mechanical properties for some of Eastern Desert dimension marble and granite utilized in building decoration. *Ain Shams Engineering Journal* **10**, 907–915 (2019).

[9] Chen, G., Xiu, Z., Yang, W., Jiang, L. & Wu, G. Effect of thermal-cooling cycle treatment on thermal expansion behavior of particulate reinforced aluminum matrix composites. *Transactions of Nonferrous Metals Society of China* **20**, 2143–2147 (2010).

[10] Coulibaly, J. B., Shah, M. & Loria. Thermal cycling effects on the structure and physical properties of granular materials. *Granular Matter* **22**, (2020).

[11] Australian Wood Panels Association Incorporated. *Facts about Particleboard and MDF*. (2008).

[12] Su, S., Chen, J. & Zhang, C. Study on Performance of Anisotropic Materials of Thermal Conductivity. *The Open Civil Engineering Journal* **5**, 168–172 (2011).

[13] Nondestructive Evaluation Physics : Materials. *www.nde-ed.org* https://www.nde-ed.org/Physics/Materials/Structure/solidification.xhtml.

[14] Weiss, T., Siegesmund, S. & Fuller, E. R. Thermal degradation of marble: indications from finite-element modelling. *Building and Environment* **38**, 1251–1260 (2003).

[15] Zeisig, A., Siegesmund, S. & Weiss, T. Thermal expansion and its control on the durability of marbles. *Geological Society London Special Publications* **205**, 65–80 (2002).

[16] Liu, D. *et al.* Fabrication of strong and tough alumina ceramic with isotropic textured microstructure at low temperature. *Journal of Materials Research and Technology* **24**, 5159–5164 (2023).

[17] Carrillo, J. A., S. Hittmeir, B. Volzone & Yao, Y. Nonlinear aggregation-diffusion equations: radial symmetry and long time asymptotics. *Inventiones mathematicae* **218**, 889–977 (2019).

[18] Md. Sazedul Islam *et al.* Composite materials: Concept, recent advancements, and applications. *Elsevier eBooks* 1–43 (2022) doi:https://doi.org/10.1016/b978-0-323-85155-8.00011-x.

[19] King, H. M. Marble: Metamorphic Rock: Pictures, Definition, Properties. *Geology.com* https://geology.com/rocks/marble.shtml?utm.

[20] Karaca, Z., Hacımustafaoğlu, R. & Gökçe, M. V. Grain properties, grain-boundary interactions and their effects on the characteristics of marbles used as building stones. *Construction and Building Materials* **93**, 166–171 (2015).

[21] Bofang, Z. Thermal Stresses in Fixed Slab or Free Slab. *Elsevier eBooks* 121–142 (2013) doi:https://doi.org/10.1016/b978-0-12-407723-2.00007-5.

[22] Thermal Shock vs. Thermal Cycling Test: Understanding the Different Types of Reliability and Accelerated Life Testing. *MPI Thermal* https://mpi-thermal.com/blog/thermal-shock-vs-thermal-cycling-test/ (2024).

[23] Key Parameters in Designing Thermal Cycling Tests. *MRC Lab* https://www.mrclab.com/key-parameters-in-designing-thermal-cycling-tests-for-specific-applications.

[24] Logan, J. M. Laboratory and case studies of thermal cycling and stored strain on the stability of selected marbles. *Environmental Geology* **46**, (2004).

[25] Goudie, A. S. & Viles, H. A. The Thermal Degradation of Marble. *School of Geography and the Environment, University of Oxford, United Kingdom* (2000).

[26] Carlson, R. O., Glascock, H. H., Webster, H. F. & Neugebauer, C. A. Thermal Expansion Mismatch in Electronic Packaging. *MRS Proceedings* **40**, (1984).

[27] Gustafsson, J. & Myhrberg, J. Expansion Joints in timber bridges - Mechanical behavior under external loading. (2020).

[28] Treccani, L. & Meder, F. *Surface-Functionalized Ceramics*. *Wiley eBooks* (Wiley, 2022). doi:https://doi.org/10.1002/9783527698042.

[29] Gil, L. Cork Composites: A Review. *Materials* **2**, 776–789 (2009).

Appendix

Table 3: Dimensions of materials at room temperature (23(ºC/C)

	diameter (m)	*height (m)*	*volume (m^3)*
Marble	0.102	0.0107	8.67E-05
ceramic	0.104	0.00622	5.25E-05

wood	0.100	0.0155	0.
cork	0.0996	0.00335	2.

4	0.000450	0.000417	0.000503	0.000349
Avg.:	0.000461	0.000414	0.000502	0.000348

Example calculation for marble sample at 75ºC:

$$V = \pi r^2 h$$

$$V = \pi(\frac{0.127}{2})^2 0.0369 = 0.00471 m^3$$

Table 4: Diameter of materials at (75ºC)

diameter (75 ºC) (mm)	*marble*	*ceramic*	*wood*	*cork*
1	0.127	0.129	0.125	0.124
2	0.128	0.129	0.126	0.124
3	0.128	0.129	0.126	0.124
4	0.126	0.129	0.125	0.125
Avg.:	0.127	0.129	0.125	0.124

Table 5: Height of materials at (75ºC)

Height (75 ºC) (mm)	*marble*	*ceramic*	*wood*	*cork*
1	0.0369	0.0318	0.0402	0.0286
2	0.0356	0.0321	0.0409	0.0287
3	0.0365	0.0316	0.0405	0.0286
4	0.0360	0.0320	0.0408	0.0287
Avg.:	0.0362	0.031	0.0406	0.0286

Table 6: Volume of materials at (75ºC)

Volume (75 ºC) (mm)	*marble*	*ceramic*	*wood*	*cork*
1	0.000471	0.000413	0.000491	0.000347
2	0.000456	0.000418	0.000510	0.000348
3	0.000468	0.000410	0.000503	0.000347

Table 7: Experimental thermal expansion coefficient calculation

Material	*Initial length*	*Final Length*	*Temperature Change*	*Linear thermal expansion coefficient*
	m	*m*	*ºC*	*ºC^{-1}*
Marble	0.102	0.127	52	0.00486
ceramic	0.104	0.129	52	0.00465
wood	0.100	0.125	52	0.00483
cork	0.0996	0.124	52	0.00478

Example calculation for marble:

$$\alpha = \frac{\Delta L}{L_{initial} \times \Delta T}$$

$$= \frac{0.127-0.102}{0.102\times(75-23)} = 0.00486/\ ºC$$